The Mechanics and Influence of the Foot-Ground Interaction During Bipedal Walking

Alexandra Georgiana Hammerberg

A dissertation

submitted in partial fulfillment of the

requirements for the degree of

Doctor of Philosophy

University of Washington

2021

Reading Committee:

Patricia Ann Kramer, Chair

Steven Goodreau

Darryl Holman

Program Authorized to Offer Degree:

Anthropology

University of Washington

Abstract

The Mechanics and Influence of the Foot-Ground Interaction During Bipedal Walking

Alexandra Georgiana Hammerberg

Chair of the Supervisory Committee:
Dr. Patricia Ann Kramer, PhD
Department of Anthropology

This dissertation explores one of the most ubiquitous aspects of human daily life: the interaction of the foot with the ground while walking bipedally in our environment. Specifically, this dissertation examines the mechanics of the foot-ground interaction during walking outside of the confines of the laboratory and the link between this foot-ground interaction and the energetic cost of locomotion. The first study examined the magnitude of the peak forces occurring at the foot across different velocities and surfaces and found that treadmill walking results in significantly different force magnitudes than free walking. The second study examined the location of the center of pressure on the foot during these peak forces across various terrains and velocities, as well as the consistency of these locations. The results showed that the location of the center of pressure during peak braking is consistently less consistent than during peak propulsion. Finally, the third study explored the relationship between the energetic cost of

locomotion and various gait parameters, concluding that the energetic cost of walking is closely related to the magnitude of anteroposterior ground reaction forces as well as the time duration of foot-ground contact during the gait cycle. These results highlight the importance of exploring habitual human locomotion outside of the confines of the laboratory to fully understand the mechanics and energetic cost of walking.

TABLE OF CONTENTS

LIST OF FIGURES

LIST OF TABLES

ACKNOWLEDGEMENTS

It is with sincere gratitude that I would like to thank those who have mentored me and collaborated with me on these dissertation chapters. Foremost is my major professor, Dr. Patricia Ann Kramer, who has truly made my time in graduate school the best academic experience of my career. There are few students, I think, who have the privilege to work with a professor of the caliber of Dr. Kramer in her dedication to her students and her craft. Dr. Kramer's interdisciplinary mindset and willingness to take a chance on a rogue engineer were what brought me into the Primate Evolutionary Biomechanics Laboratory, but it was her mentorship that made me want to stay. Dr. Kramer, thank you for allowing me to go down all the research rabbit holes, winding side project paths, and strange university connections during my five years, but also for knowing when to nudge me back on track. Having a major professor who expects and encourages curiosity in their students is rare, therefore it was an absolute privilege to have Dr. Kramer as my mentor. I can only hope to emulate her leadership and attitude towards learning in my future career.

I would also like to acknowledge the PEBL people and Gayoung. For the lab, the ongoing (as of the date of this writing) pandemic meant that our time together in Denny was cut short, but I think this pandemic also built a lab bond that was maybe a bit stronger that it otherwise would have been. Thank you all for being there on the other side of my computer screen every week for these past 60 weeks (and counting), laughing over memes, poking fun at journal articles (and sometimes their authors), commiserating, imbibing (sometimes a bit too much), putting up with my over-excitement over some new material research, and generally keeping me grounded. For Gayoung, from our adventures in TAing together when we weren't always sure what was going

on, to our lengthy coffee chats about our work and our lives, you've been someone I'm so glad to be friends with through it all. I'm looking forward to your visits, wherever in the world I end up.

And, finally, I'd like to thank Brandon. Your willingness to try almost anything, patience (especially in teaching me how to ski), and astounding ability to think the best of everyone and make friends with anyone will always be a marvel to me. Thank you for always picking me up when I'm down, making me laugh, chasing the cat around when I'm trying to work, and being the best pandemic partner a girl could ask for. There's no one else I'd rather be quarantined with.

DEDICATION

This dissertation is dedicated to my parents, JoAnn and Bruce. Thank you for always being there with advice, encouragement, and sometimes a little prodding. You've given me the best lesson parents can give: to go through life with your eyes wide open, with curiosity about everything, and, above all, with kindness, is truly the best way to live. I'll keep opening doors to see where they lead. I love you both.

Chapter 1. INTRODUCTION

The overarching theme of this dissertation is human movement through the environment, and my goal is to explore the importance of examining movement outside of laboratory conditions. Habitual bipedalism is a derived trait of modern humans and a complex structural problem (e.g. Cavagna & Margaria 1966). Although walking has been one of the defining, ubiquitous characteristics for hominins throughout evolutionary history, from quadrupedalism to bipedalism, walking is biomechanically complicated. Walking on four limbs maintains ground contact of two supporting points at all times, whereas walking on two limbs requires periods of time where there is only one limb in ground-contact while the other swings. An intricate and dynamic system of bony scaffolding connected and surrounded by muscle and other soft tissue, balanced on two relatively small ground-contact points, i.e. the feet, the evolution of the human form towards bipedalism has long intrigued researchers.

A critical component of this change in morphology is the response of the structure itself. Bone is arguably the most important component of the bipedal system simply by dint of being the foundation for the rest of the structure it supports, but it is also a fascinating material. Bone responds to applied forces whether they are internal muscular forces, or external ground reaction forces, adding or removing material based on use (Wolff original 1867, reprinted 2010, Frost 2003). It then follows that understanding the locations and magnitudes of applied forces is crucial for understanding the resultant musculoskeletal response.

While one approach to untangling the origins of bipedalism is to look to the fossil record, hominin fossils bridging the gap between habitual quadrupedalism and habitual bipedalism are elusive. It is generally accepted that changes in the environmental landscape, food resources, or

other energetic resource pressures led to this shift—although the specific selective pressure remains unknown—but the system-wide adjustments required for this shift are impressive. A second approach to understanding bipedalism is to examine the biomechanics of modern human movement and use these data to inform our view of bipedal evolution. This may seem straightforward, but, as mentioned above, the system is complex with layers of musculoskeletal redundancy at almost every length scale. Broadly, this shift in locomotor behavior required morphological changes to the musculoskeletal system to accommodate the change in magnitudes and locations of the application of the forces produced during locomotion (e.g. Lovejoy 2005, Ruff 2017). Therefore, understanding the biomechanics of hominin mobility is key to understanding human evolution.

This introductory chapter serves to contextualize this dissertation work. The second chapter of this dissertation provides background for the material in the subsequent chapters and addresses the overall motivation for this research. Chapters three and four focus on ground reaction force (GRF) magnitudes and center of pressure (CoP) locations during peak braking and peak propulsion in contiguous walking steps within and outside of the confines of the laboratory environment and are currently in review for publication. Chapter five attempts to identify a quantifiable and accurate mechanical proxy for the energetic cost of walking to facilitate mobility research outside of the laboratory and is "in work" for publication. The final chapter concludes the dissertation and discusses avenues for future work. Each chapter is followed by its associated list of references.

Chapter 2. BACKGROUND

Understanding the evolutionary history of mobility has been of interest to biological anthropologists since the origin of the field given that mobility plays a critical role in the activity budgets of all animals by influencing, for example, foraging (e.g. Ross & Winterhalder 2015), predation avoidance (e.g. Howland 1974), and reproductive behavior (e.g. Gibson & Mace 2006). The derived bipedalism of humans is of particular interest since humans are the only extant habitual, terrestrial primate bipeds. Despite decades of speculation, though, the selective pressures that stimulated the shift to habitual bipedalism remain obscure (e.g. Sylvester 2008, Bramble 2004, Rosenberg 2017, etc.). Nonetheless, this shift in mobility pattern from that of a nonbipedal last common ancestor with *Pan* to a bipedal one required morphological changes to the musculoskeletal system to accommodate the change in applied forces (e.g. Lovejoy 2005, Ruff 2017). Consequently, because humans are the only habitually bipedal primates, to understand the evolution of bipedalism we must examine the movement of modern humans. Further, bipedalism needs to be evaluated in the environments in which it arose—encompassing movement over differing terrains, gradients, burden regimes, and speeds. Bipedalism is, additionally, a foundational condition of contemporary human biological variation and morbidity of the musculoskeletal system is a prominent human health concern.

Habitual, terrestrial bipedalism, a derived trait of hominins, including modern humans, is a complex structural problem (e.g. Cavagna & Margaria 1966). Walking on four limbs maintains contact between the ground and two supporting elements at all times, whereas walking on two limbs requires periods of time where only one foot is in contact with the ground while the other swings off the ground. The contact between the ground and the foot produces an equal and opposite force (the ground reaction force, GRF) in each: the body through the foot pushes on the

ground and the ground pushes back. The GRF has components in the three cartesian coordinates that are typically used to describe motion: anteroposterior (usually the direction of travel), mediolateral (side), and inferior-superior (vertical). GRFs are discussed in more detail below in section 2.1

The complexity of the structural requirements of bipedalism impacts the energy expenditure of a biped because GRF magnitudes and locations determine joint moments throughout the bipedal body (e.g. Perry 1992), and these joint moments dictate which muscle groups activate and the magnitude of their activation (e.g. Sylvester 2021). The term 'joint moment' will be used throughout this dissertation to describe the mechanical reaction to forces acting across articulating surfaces in the joints of the body, i.e., the knee, ankle, hip. Moments are the action of a force through a distance; in the case of joint moments the force is the GRF and the distance is between the center of the joint and the point of application of the GRF (although this is a simplification; see section 2.2 below). Figure 2.1 is a simplified illustration of a joint moment around the ankle. The joint moments are transferred between skeletal elements (e.g. tibia to femur) by direction contact (compression) of the skeletal elements (e.g. the condyles) and by the action of the soft tissues, particularly the muscles (e.g. gastrocnemius). Muscle activation requires metabolic energy (e.g. Ortega 2015, Enoka 2008, Taylor 1980, etc.).

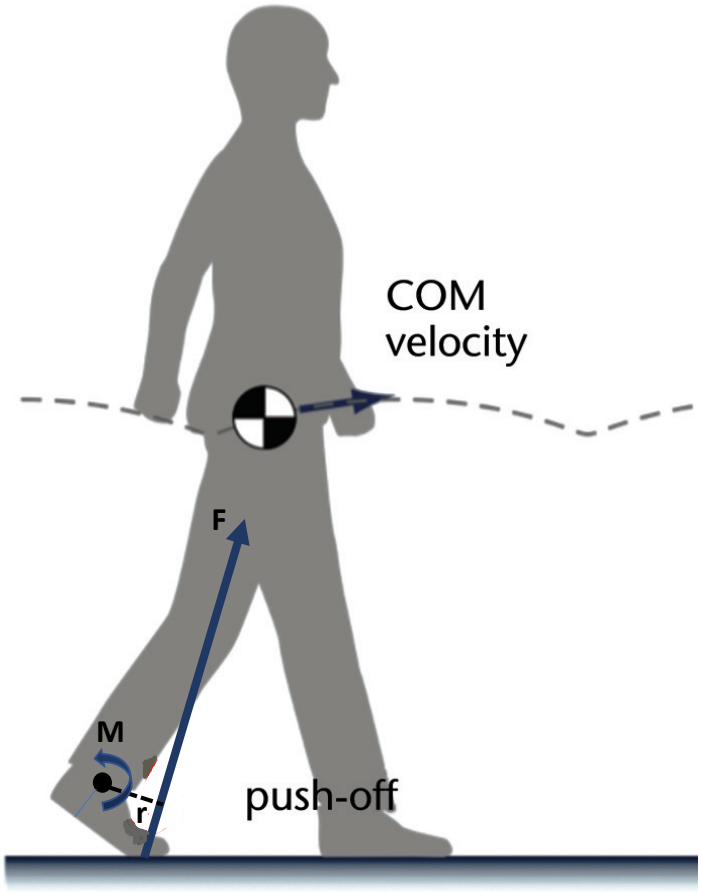

Figure 2.1. A simplified free body diagram illustrating the reaction moment of a force acting through a distance; in the case of joint moments the force is the GRF and the distance is between the center of the joint, in this case the ankle, and the point of application of the GRF, in this case the toe.

The metabolic energy required for locomotion has been extensively investigated through empirical means. Volumetric rate of Oxygen consumption, or VO_2, is a widely-utilized chemical proxy for metabolic energy expenditure due to oxygen's direct relationship to cellular respiration during muscle activation (which is discussed further in section 2.3). From direct measurement of VO_2, two main mechanical contributors to the explanation of metabolic energy expenditure (in all creatures) emerged immediately: the mass being moved and the velocity of movement (Taylor

1980). However, neither of these capture the complexity of the morphology of the body shape. Mechanical analyses indicate that shape, not just size, of the mass influences muscle activation. As humans do not scale linearly as size changes (Kramer 2009, Sylvester 2008), this has posed a challenge for researchers attempting to predict metabolic cost from morphology.

In a further complication to the system, the muscular forces produced by locomotion also influence the morphology of the skeletal system (Frost 2003). This mechanism is discussed in more detail below, but, broadly, bone is strain-sensitive and responds to both internally and externally applied forces (Wolff 1867, reprinted 2010). Evidence of morphological changes in response to changes in applied forces can be observed in the evolutionary history of bipedalism (e.g. pelvic morphology Ruff 2017, Lovejoy 2005, foot morphology Morton 1924, Lovejoy 2009 etc.). GRF magnitudes and locations through their influence on joint moments throughout the body create the counteracting muscular forces which determine the morphology of bones (in evolutionary and developmental time scales).

In summary, the mechanical demands of locomotion require muscle activation and muscle activation requires metabolic energy. It follows, therefore, that locomotor activity costs metabolic energy (e.g. Rubenson 2006). Although logical, the connection between the mechanical and the metabolic realms has remained elusive to characterize (e.g. Kramer & Sylvester 2011). This dissertation seeks to add some insight into the problem. The following sections detail the key components of the mechanical and metabolic systems and provide the foundation for the analyses in the subsequent chapters.

2.1 GROUND REACTION FORCES

Chapter 3 of this dissertation research extends the work of previous walking studies (e.g. McIntosh 2006, DeWit 2000, Divert 2008, Squadrone & Gallozzi 2009, Lieberman 2010, Hatala 2015, Ardigò 1995, Bobbert 1992) to gather ground reaction force (GRF) data from the foot/surface interaction outside of the confines of the laboratory. GRFs reflect the interaction between the foot and the substrate during the stance phase of gait and are generally split into components that align with the anatomical axes: anteroposterior (direction of travel, X), mediolateral (side, Y), and superoinferior (vertical, Z). The vertical component is much higher than the anteroposterior and mediolateral components due to the vertical effect of gravity acting upon the body. In other words, gravity acting on body mass is an intrinsic vertical force.

Two peaks in the vertical component of the GRF are typical in walking (Figure 2.2). The body slows in early stance (the braking period) producing a GRF peak, passes above the stance foot in midstance with a decrease in the GRF, and accelerates in late stance (the propulsive period) producing another GRF peak. The magnitude of these peaks has been shown to be directly related to walking velocity (Winter 1988), when normalized for bodyweight. In conjunction with the vGRFs, anteroposterior GRFs (apGRFs) are also required to move along surfaces, and, although they are smaller than vGRFs (Nilsson & Thorstensson 1989), they are the primary mechanisms for forward movement. Anteroposterior GRFs are sometimes referred to as shear forces or horizontal GRFs, i.e., forces that act parallel to the contact surface. Prior work has shown the importance of anteroposterior forces in walking (e.g. Gottschall 2003, Cavagna & Margaria 1966, Cavagna 1975, etc.), as these are the primary braking and accelerating mechanisms for forward motion across planar surfaces. They potentially account for 50% of the energetic cost of walking (Gottschall

2003). Side forces also act in the horizontal plane as stabilizer muscles maintain upright balance, but these are low in walking in a straight line on flat terrain (Damavandi 2012).

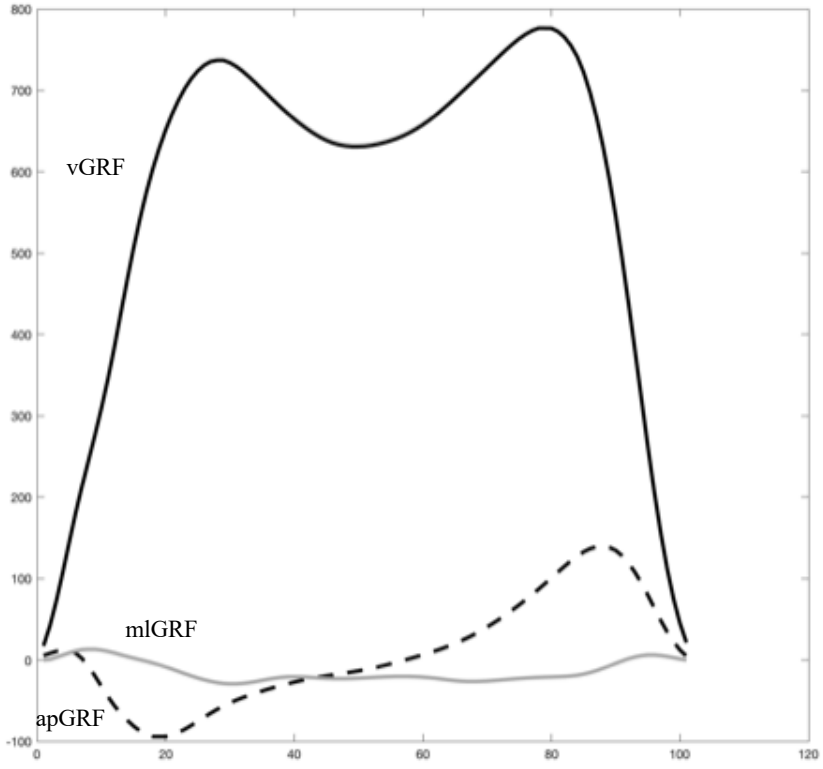

Figure 2.2. Ground reaction force (GRF) curves during foot-ground contact along anteroposterior (direction of travel, X, apGRF), mediolateral (side, Y, mlGRF), and superoinferior (vertical, Z, vGRF) axes.

Modern humans encounter a variety of different surfaces and terrain conditions in their day-to-day lives, not just flat surfaces. These terrains may be variable in gradient, contain obstacles, or be loose surfaces, to name a few out of the many possibilities. It is very difficult to approximate these conditions in a traditional laboratory with space and data capture constraints,

so researchers look to advances in remote sensing technology or mechanical proxies that are measurable in “the wild” - for example acceleration, position, or surface deformation (e.g. Pandolf 1976). Recent vertical GRF sensing technology has advanced enough to allow for remote data capture, freeing participants from the constraints of the laboratory and opening up possibilities for data collection across this multitude of unexplored walking substrates. Unfortunately, while vertical force sensing technology has progressed to the point of allowing data collection outside of the laboratory, shear sensing technology has not yet caught up. Currently the only way to capture anteroposterior GRF magnitudes is through force sensing treadmills or embedded force plates.

2.2 CENTER OF PRESSURE

The fourth chapter of this dissertation examines the spatial locations of these peak braking and peak propulsive GRFs on the foot while walking within and outside of the confines of the laboratory. Specifically, the aim was to quantify the consistency of the spatial occurrence of the center of pressure (CoP) during peak braking vertical GRF and peak propulsive vertical GRF. The CoP at peak GRFs indicates where the resultant of the contact forces between the foot and substrate act on the foot during a gait cycle. This resultant is a weighted average of all the contact forces acting across the sole of the foot at each instant in the gait cycle. (See Figure 2.3.)

Figure 2.3. Pressure (or force per sensor area) scan of a full ground-contact cycle. The black dots indicate the progression of the CoP that is a weighted average of the force in each area of the foot. Red indicates areas of high pressure while blue indicates low pressure.

The CoP at peak GRFs over multiple gait cycles describe the nature of the cyclic loading of the musculoskeletal system. As with any dynamic system, repeated loading patterns play an important part in system design to ensure durability, i.e., these systems are designed for cyclic loading. The derived morphology of the modern human foot is one of the more substantial differences between the anatomy of modern humans and extant nonhuman primates, and this morphology is associated with bipedalism (e.g. Lovejoy 2005, Latimer & Lovejoy 1989). Further

discussion on the interaction between form and function can be found below in section 2.4, but, for a brief example, it has been postulated that habitual bipedalism required the development of the non-divergent hallux and a medial arch of the human foot (e.g. Morton 1924). These work in tandem to create a relatively stiff lever for propulsion of the rest of the body over a substrate. The changes to the foot in response to bipedalism are part of the morphological adjustments of the musculoskeletal system that are a result of changes to the locations of the applied forces (e.g. Currey 2003, Farris 2019, Hatala 2016). It is crucial, therefore, that we understand where the CoPs at peak forces occur on the foot, not just over one loading cycle, but over many loading cycles to fully grasp the system dynamics as a whole and what it implies for human bipedal mobility.

The expectation for the location of the CoP at peak vertical GRF was less established than the expectations for peak GRF magnitudes. While the heel is typically the first anatomical feature to strike the ground and the toes are the last to leave during a step (Grundy 1975), the CoP location when peak vertical (braking and propulsion) force occurs is less explored in the previous literature (e.g. Louey 2017). These CoP locations, in conjunction with the associated GRF magnitudes, are critically important variables from the perspectives of both understanding musculoskeletal growth and development and appreciating the evolution of pedal morphology. In addition to the role that the location of the applied forces plays in skeletal element morphology (as discussed above in the example of foot morphology), the difference in location of a joint center and the CoP of the GRF is the distance over which the GRF acts to produce the joint moment. Given that joint moments require muscular activation, changes in CoP potentially change muscle activations and therefore metabolic energy expenditure.

There are a variety of quantitative methods for assessing the location of the CoP on the foot during locomotion, from pedobarography to principal component analysis (PCA). While these

are the more traditional methodologies, this dissertation identifies a new statistical methodology for analyzing the spatial nature of CoP points on the foot. Spatial statistics is more often found in epidemiology papers or environmental studies that require a geographic robusticity to the analysis of the data (e.g. Diggle 2007, Ben-Hamo 2020, Elliott & Wakefield 2001). By treating the foot as geography at a smaller length scale, this dissertation accommodates the spatial nature of the CoP data and assess clustering of these points over multiple gait cycles, as documented in Chapter 4.

2.3 ENERGETIC COST OF WALKING

As stated above, mobility, or movement through an environment, is a critical component of the activity budgets of all animals, and humans are no exception (e.g. Ross 2015, Howland 1974, Gibson 2006, Kramer 1998). The energetic cost of movement, however, is difficult to quantify due to the vast number of associated variables, the most fundamental of which pertain to the muscles that are required to move a body through space. At the most basic level, muscles activate to apply forces across joints to move the limbs and to counteract joint moments (Taylor 1980). However, muscle activation varies across activity, individual, trial sequence, day, etc. and is still not fully understood (e.g. Enoka 2008, Wang 2019). Broadly, however, both the initial muscle firing and its maintenance over a period of time require metabolic energy (e.g. Ortega 2015, Enoka 2008, Taylor 1980, etc.).

The energetic cost of locomotion is intrinsically tied to physiology, and is, therefore, highly variable across individuals (Kramer & Sylvester 2011). This presents challenges for researchers when quantifying the energetic cost of locomotor activities. Muscular action presents metabolic costs, dependent, for example, on the magnitude of the muscular action and duration of the action (e.g. Ortega 2015, Enoka 2008, Taylor 1980, etc.). Muscle activity can now be quantified with advances in sensing technology such as electromyography (e.g. Gottschall 2003), or estimated

using, for example, muscle belly volume and length (e.g. Rubenson 2006), or modeling software (e.g. Sylvester 2021), but the complexity of the body moving as a dynamic system and, broadly, individual variation, are motivation for identifying methods of quantifying energetic cost through mechanical proxies.

Two primary approaches to estimating energetic cost exist currently: metabolic and mechanical. The metabolic estimation approach utilizes the relationship mentioned above between muscle activation and physiological cost. Energy is a finite resource within the body (Smith 1984) that has to be replenished with nutrient consumption, and these nutrients are then converted into chemical energy-carrying ATP molecules via the Krebs Cycle. Cells then use the chemical energy within the bonds of ATP molecules in cellular respiration, which, in turn, fuels muscle activation, among other processes (Britannica 2020). CO_2 is a waste product of this process and its rate of production is a chemical proxy for the rate of cellular respiration. O_2 is considered a standard chemical proxy for measuring metabolic cost as the exhaled air is high in waste CO_2, and low in O_2 compared to the surrounding air. Volumetric rate of Oxygen consumption (VO_2) is the amount of O2 that is consumed per unit time and is typically measured in in mL/s. Standing Resting Metabolic Rate (stRMR) is the baseline measurement of cellular respiration when a subject is standing quietly, measured as VO_2 and is correlated with the mass of active tissue in a body. Activities increase VO_2 above the stRMR baseline. Mass and stRMR are included *a priori* as participant metrics to predict metabolic cost of locomotion in Chapter 5. Activities increase VO_2 above the stRMR baseline.

Extensive prior work demonstrates the use of VO_2 as a measure of metabolic energy required to perform various activities (e.g. Rue & Kramer 2016, O'Driscoll 2018, Pontzer 2013 etc.), but much of this work is also devoted to attempting to predict metabolic cost based on

physiological or morphological measurements such as stature, leg length, BMI, etc. (e.g. Kramer & Sylvester 2011, Kramer & Sylvester 2012, Heglund 1988, Taylor 1980, Roberts 1998 etc.). The classic "mouse-to-elephant" model (Taylor 1980) broadly indicated that body size (mass) influences energetic expenditure across species of very different sizes, but within-species variation is more complicated to quantify. While generally accepted that body size accounts for most of the energetic difference within species, body shape does not scale linearly, or even consistently in humans (Kramer & Sylvester 2009, Sylvester 2008) and seems to play a more critical role in differences in metabolic energy expenditure within species. To that end, researchers continue to look for morphological determinates of metabolic energy expenditure.

On the mechanical side, prior research that has attempted to quantify the energetic cost of locomotion through the mechanics of locomotion often focuses on quantifying the potential energy (PE) and kinetic energy (KE) of motion and their relationship to external work (eW), i.e. the rise and fall of the center of mass (CoM) of the body during the gait cycle (e.g. Cavagna & Margaria 1966, Cavagna 1975) as well as the internal work (iW) of the musculoskeletal system. The PE of bipedal activity is dependent on the vertical displacement (i.e., with and against gravity) and KE is responsible for the forward velocity of the body (Cavagna & Margaria 1966). The model for this mechanical motion is commonly referred to as the 'inverted pendulum' model (e.g. Cavagna 1977) for walking, which, in its original configuration, is based on the body moving over a stiff leg structure. Geyer's more recent model (Geyer 2006) refined this mechanism to include a compliant leg structure as part of the inverted pendulum, which is more comprehensive of bipedal walking mechanics, but also more parsimonious than more complex spring/damper models for the leg musculoskeletal system. The compliant inverted pendulum model is also a more accurate

representation of the movement of the CoM—and therefore the eW and iW—for bipedal walking than the stiff inverted pendulum model (Geyer 2006).

The goal of quantifying eW and iW has, historically, been to find a mechanical proxy for measuring metabolic cost. While prior research has attempted to disentangle the relationship between locomotion and metabolic cost via eW and iW (e.g. Cavagna 1977, Geyer 2006), mechanical work, overall, is not a fully satisfactory parameter for explaining metabolic cost of locomotion, particularly for the complex movement that is bipedal walking. The black box that separates eW and iW from metabolic cost contains many other variables that are not fully measurable, so, while theoretically sound, the mechanical model of the inverted pendulum does not fully explain the metabolic cost of locomotion (e.g. Kuo & Donelan 2010). To that end, researchers continue to search for a comprehensive mechanical proxy for measuring the metabolic cost of walking.

Cavagna showed in his 1975 work that measuring the GRFs during walking using a force plate was an indirect method for measuring CoM acceleration through space (Cavagna 1975). GRFs generated through walking are implicitly related to muscular forces, as discussed above, and should, therefore, be relatable to the metabolic cost of transport (CoT). Taylor's 1985 work showed strong evidence for the metabolic cost of locomotion being directly tied to the time course of force development in running (Taylor 1985). Later work (Roberts 1998) upheld this finding across species, both bipedal and quadrupedal, but did not distinguish between the locomotor behaviors of walking and running. Running is a different biomechanical mechanism than walking; walking includes a period of double stance where both feet are in contact with the ground, whereas only one foot is in contact with the ground at a time and there is a period of 'flight' (no foot on the ground) during a running gait cycle. Running also consists of more vertical displacement of the

CoM and higher associated vGRFs as the body essentially bounces from one leg to another along the path of locomotion. While muscular recruitment is the primary metabolic cost for both activities, the timing of muscular recruitment during the gait cycle is very different. Cavagna & Margaria note that the muscular activity of running increases the PE and KE in each step simultaneously, whereas in walking muscular activity drives the increase in KE at a distinctly different phase of a step than when the increase in PE occurs (Cavagna & Margaria 1966).

Energetics in the walking literature addresses variations in "baseline" metabolic cost from pathology (e.g. Waters 1999), aging (e.g. Schrack 2012), or foot posture (e.g. Cunningham 2009), but there are fewer examples in the literature that addresses the association between GRF development, time, and metabolic cost in walking. In much of the previous literature, time is a crucial component of metabolic cost that is often obscured within calculations for other mechanical proxies, such as Work, PE, or KE. This neglect is not warranted, as time is one of the few distinctly quantifiable variables unifying the calculated mechanical proxies of locomotion and the black box of energy expenditure. Gottschall et. al. (1998) noted a relationship between contact time of the foot with the ground and "metabolic cost", but did not distinguish between walking and running. Other authors have examined the optimization of the human foot for bipedal locomotion in terms of length (e.g. Adamczyk 2013) and morphology (e.g. Morton 1924).

Generally, muscles require more metabolic energy to produce more force, whether that is maintaining force across time or increasing the force magnitude over the same time duration (e.g. Ortega 2015, Taylor 1980). Therefore, to quantify the metabolic cost of an activity, it is crucial for time to be included as a parameter. The fifth chapter of this dissertation explores whether vertical and anteroposterior GRF development over time during the foot-ground interaction is a predictive mechanical proxy for metabolic cost in walking.

2.4 FORM & FUNCTION

The morphological changes required to adapt to bipedal locomotion from quadrupedal locomotion are, as mentioned above, system-wide, span several length-scales, and involve both soft tissue and bone. Since the adaptation of the human form to this function is a very large topic, this dissertation will only touch upon morphological changes to the bipedal system in passing, but, the author would like to note that it is still important to contextualize the three foci of this dissertation, GRF magnitude, GRF location, and energetic cost, with their relationship to the bipedal form. As the body is a complex, dynamic system, a holistic view of how these four components interact is vital for a full appreciation and understanding of the implications of this work.

GRF magnitude varies with, for example, mass of the body in motion, velocity of travel (e.g. Winter 1988), system pathology (e.g. Perry 1992), burdens carried (e.g. James 2015), and surface type (e.g. Pandolf 1976). The width of this range in magnitude is an engineering challenge; the system must accommodate very high, abrupt loads such as occur in jumping, as well as lower-magnitude but highly cyclic loading in movements such as walking, but bone is not your standard engineering material. The beauty of this system is in its plasticity. Bone is strain sensitive and remodels in response to applied forces, whether they are internal or external (e.g. Wolff original 1867, reprinted 2010). This remodeling occurs at both the system-level and locally, so both magnitude and location of these applied forces matters (Frost 2003). There is a lack of consensus regarding the sensitivity of this response, i.e. whether bone reenforces areas of peak strain to prevent acute failure, or areas of chronic, lower-magnitude cyclic loading (e.g. Kivell 2016, Currey 2003). Precise mechanisms aside, the bony morphology of the skeletal system is dependent on the magnitudes and locations of these applied forces. Therefore, quantifying these forces and their

locations is crucial to furthering our understanding of both the modern human musculoskeletal system and the evolutionary influences that led to our current morphology.

As discussed above, the mechanics of walking dictate the energetics of walking through joint moments and associated muscle activation (e.g. Sousa 2012, Gottschall 2002, Kuo 2007, etc.). The link between energetic cost and form is, perhaps, one of the most foundational relationships in evolution (Darwin 1883). Much, but not all, of evolution is motivated by energetic optimization, because energy is a finite, non-renewable resource directly tied to survival and reproduction (Smith 1984) and, as movement within an environment is required for most higher-order living things in foraging, predation avoidance, and reproduction, it follows that movement is intrinsically linked to this pursuit of energetic efficiency. There is an ongoing literature in modeling human biomechanics with an eye towards optimization of movement and energy expenditure (e.g. Kuo 2007, Kuo 2002, Adamczyk 2013, Kuo 2010, Rebula 2015, etc.), but with a form as complex as the human body, and biomechanics as complicated as they are for walking, it is unsurprising that development of a satisfactory model is still a work in progress. Again, this dissertation will not address the bipedal form in much depth. Instead, the author approaches a more complete understanding of measurable components of walking; GRF magnitudes, GRF locations, and the energetic costs associated with walking.

2.5 MOTIVATION

Humans encounter a wide variety of surfaces and obstacles as they navigate through their daily activities, and yet, most gait and energetics research has been restricted to data collection in laboratories or on tracks using motion-capture (e.g. Cavagna & Margaria 1966, McIntosh 2006). In laboratory-based gait studies, participants must accurately land on a force plate embedded in the floor of a laboratory or locomote on a force-sensing treadmill that records the magnitude and

direction of the GRF (e.g. DeWit 2000, Divert 2008, Squadrone 2009, Lieberman 2010, Hatala 2015, Ardigò 1995, Bobbert 1992). VO_2 monitors are distracting and invasive to the wearer, whether they are strapped to a participant, or, more often, immobile on a lab bench, which constrains participants to a treadmill. It has been repeatedly shown, however, that walking on treadmills, can produce different kinetics than walking over-ground (e.g. Yao 2019, Lim 2018) and many activities of daily living, such as walking along extended gradients, are difficult to accomplish in a laboratory environment.

With recent developments in remote sensing technology, however, it is now possible to gather foot-ground interaction data, specifically vertical GRF and CoP data, outside of the laboratory. Wireless insoles are a mobile alternative to fixed force plates and allow for continual data collection as participants move in less-restricted ways than previously possible, including along gradients (e.g. Braun 2018, He 2019, Björklund 2019, Wei 2019). Consequently, these recent advances in sensing technology open the door to new insights into the mechanics of humans moving freely in their environment. Capturing accurate information on the energetic cost of locomotion outside of the laboratory and anteroposterior GRFs, however, still poses a challenge.

Until VO_2 technology is scaled down and less invasive to the wearer, researchers are constrained to the laboratory or to including the burden of a wearable VO_2 as a limitation in their studies. Identifying a mechanical proxy for VO_2 consumption is an interim solution to this problem. With a measurable mechanical predictor for VO_2 consumption, we gain the ability to form a more complete picture of human mobility in the environment outside of laboratory conditions. The overarching aim of this dissertation is to gain understanding of modern human movement in their environment, ultimately enabling us to more fully understand human mobility.

2.6 REFERENCES

Adamczyk PG, Kuo AD. Mechanical and energetic consequences of rolling foot shape in human walking. J Exp Biol. 2013 Jul 15;216(Pt 14):2722-31. doi: 10.1242/jeb.082347. Epub 2013 Apr 11. PMID: 23580717; PMCID: PMC3694099.

Ardigò LP, Lafortuna C, Minetti AE, Mognoni P, Saibene F. Metabolic and mechanical aspects of foot landing type, forefoot and rearfoot strike, in human running. Acta Physiol Scand. 1995;155(1):17-22. doi:10.1111/j.1748-1716.1995.tb09943.x

Ben-Hamo M, Ezra D, Krasnov H, Blank L. Spatial and Temporal Dynamics of Mal Secco Disease Spread in Lemon Orchards in Israel. Phytopathology. 2020 Apr;110(4):863-872. doi: 10.1094/PHYTO-06-19-0195-R. Epub 2020 Feb 26. PMID: 31821113.

Björklund G, Swarén M, Born DP, Stöggl T. Biomechanical Adaptations and Performance Indicators in Short Trail Running. Front Physiol. 2019;10:506. Published 2019 Apr 30. doi:10.3389/fphys.2019.00506

Bobbert MF, Yeadon MR, Nigg BM. Mechanical analysis of the landing phase in heel-toe running. J Biomech. 1992;25(3):223-234. doi:10.1016/0021-9290(92)90022-s

Bramble DM, Lieberman DE. Endurance running and the evolution of Homo. Nature. 2004 Nov 18;432(7015):345-52. doi: 10.1038/nature03052. PMID: 15549097.

Braun BJ, Veith NT, Hell R, Döbele S, Roland M, Rollmann M, Holstein J, PohlemannT. Validation and reliability testing of a new, fully integrated gait analysis insole. J Foot Ankle Res. 2015;8:54. Published 2015 Sep 22. doi:10.1186/s13047-015-0111-8

Braun BJ, Veith NT, Herath SC, Hell R, Rollmann M, Orth M, Holstein JH, Pohlemann T. Ein neues, kontinuierliches Ganganalysesystem zur Nachbehandlung von Sprunggelenkfrakturen [A new continuous gait analysis system for ankle fracture aftercare]. Unfallchirurg. 2018;121(4):293-299. doi:10.1007/s00113-017-0332-3

Britannica, T. Editors of Encyclopaedia (2020, March 12). Adenosine triphosphate. Encyclopedia Britannica. https://www.britannica.com/science/adenosine-triphosphate

Carrier D, Cunningham C, Schilling N, Anders C. Plantigrade foot posture increases locomotor economy in walking but not in running humans. In AMERICAN JOURNAL OF PHYSICAL ANTHROPOLOGY 2009 Jan 1 (pp. 103-103). DIV JOHN WILEY & SONS INC, 111 RIVER ST, HOBOKEN, NJ 07030 USA: WILEY-LISS.

Cavagna GA. Force platforms as ergometers. J Appl Physiol. 1975 Jul;39(1):174-9. doi: 10.1152/jappl.1975.39.1.174. PMID: 1150585.

Cavagna GA, Heglund NC, Taylor CR. Mechanical work in terrestrial locomotion: two basic mechanisms for minimizing energy expenditure. Am J Physiol. 1977 Nov;233(5):R243-61. doi: 10.1152/ajpregu.1977.233.5.R243. PMID: 411381.

Cavagna GA, Margaria R. Mechanics of walking. J Appl Physiol. 1966;21(1):271-278. doi:10.1152/jappl.1966.21.1.271

Chau T. A review of analytical techniques for gait data. Part 2: neural network and wavelet methods. Gait Posture. 2001;13(2):102-120. doi:10.1016/s0966-6362(00)00095-3

Currey JD. The many adaptations of bone. J Biomech. 2003 Oct;36(10):1487-95. doi: 10.1016/s0021-9290(03)00124-6. PMID: 14499297.

Damavandi M, Dixon PC, Pearsall DJ. Ground reaction force adaptations during cross-slope walking and running. Hum Mov Sci. 2012 Feb;31(1):182-9. doi: 10.1016/j.humov.2011.06.004. Epub 2011 Aug 12. PMID: 21840076.

Darwin, C. (1883). On the Origin of Species: By Means of Natural Selection, Or, the Preservation of Favored Races in the Struggle for Life. United States: Appleton.

De Wit B, De Clercq D, Aerts P. Biomechanical analysis of the stance phase during barefoot and shod running. J Biomech. 2000;33(3):269-278. doi:10.1016/s0021-9290(99)00192-x

Diggle PJ, Gómez-Rubio V, Brown PE, Chetwynd AG, Gooding S. Second-order analysis of inhomogeneous spatial point processes using case-control data. Biometrics. 2007;63(2):550-557. doi:10.1111/j.1541-0420.2006.00683.x

Divert C, Mornieux G, Freychat P, Baly L, Mayer F, Belli A. Barefoot-shod running differences: shoe or mass effect?. Int J Sports Med. 2008;29(6):512-518. doi:10.1055/s-2007-989233

Donelan JM, Kram R, Kuo AD. Mechanical work for step-to-step transitions is a major determinant of the metabolic cost of human walking. J Exp Biol. 2002 Dec;205(Pt 23):3717-27. PMID: 12409498.

Elliott P, Wakefield J. Disease clusters: should they be investigated, and, if so, when and how?. Journal of the Royal Statistical Society: Series A (Statistics in Society), 2001;164: 3-12. doi:10.1111/1467-985X.00180

Enoka RM, Duchateau J. Muscle fatigue: what, why and how it influences muscle function. J Physiol. 2008 Jan 1;586(1):11-23. doi: 10.1113/jphysiol.2007.139477. Epub 2007 Aug 16. PMID: 17702815; PMCID: PMC2375565.

Farris DJ, Kelly LA, Cresswell AG, Lichtwark GA. The functional importance of human foot muscles for bipedal locomotion. Proc Natl Acad Sci U S A. 2019 Jan 29;116(5):1645-1650. doi: 10.1073/pnas.1812820116. Epub 2019 Jan 17. PMID: 30655349; PMCID: PMC6358692.

Frost HM. A 2003 update of bone physiology and Wolff's Law for clinicians. Angle Orthod. 2004 Feb;74(1):3-15. doi: 10.1043/0003-3219(2004)074<0003:AUOBPA>2.0.CO;2. PMID: 15038485.

Geyer H, Seyfarth A, Blickhan R. Compliant leg behaviour explains basic dynamics of walking and running. Proc Biol Sci. 2006 Nov 22;273(1603):2861-7. doi: 10.1098/rspb.2006.3637. PMID: 17015312; PMCID: PMC1664632.

Gibson MA, Mace R. An energy-saving development initiative increases birth rate and childhood malnutrition in rural Ethiopia. PLoS Med. 2006;3(4):e87. doi:10.1371/journal.pmed.0030087

Gottschall JS, Kram R. Energy cost and muscular activity required for propulsion during walking. J Appl Physiol (1985). 2003 May;94(5):1766-72. doi: 10.1152/japplphysiol.00670.2002. Epub 2002 Dec 27. PMID: 12506042.

Grundy M, Tosh PA, McLeish RD, Smidt L. An investigation of the centres of pressure under the foot while walking. J Bone Joint Surg Br. 1975 Feb;57(1):98-103. PMID: 1117028.

Hatala KG, Wunderlich RE, Dingwall HL, Richmond BG. Interpreting locomotor biomechanics from the morphology of human footprints. J Hum Evol. 2016;90:38-48. doi:10.1016/j.jhevol.2015.08.009

He J, Lippmann K, Shakoor N, Ferrigno C, Wimmer MA. Unsupervised gait retraining using a wireless pressure-detecting shoe insole. Gait Posture. 2019;70:408-413. doi:10.1016/j.gaitpost.2019.03.021

Heglund NC, Taylor CR. Speed, stride frequency and energy cost per stride: how do they change with body size and gait? J Exp Biol. 1988 Sep;138:301-18. PMID: 3193059.

Howland HC. Optimal strategies for predator avoidance: the relative importance of speed and manoeuvrability. J Theor Biol. 1974;47(2):333-350. doi:10.1016/0022-5193(74)90202-1

James CR, Atkins LT, Yang HS, Dufek JS, Bates BT. Kinematic and ground reaction force accommodation during weighted walking. Hum Mov Sci. 2015 Dec;44:327-37. doi: 10.1016/j.humov.2015.10.004. Epub 2015 Nov 2. PMID: 26540454.

Jung Y, Jung M, Lee K, Koo S. Ground reaction force estimation using an insole-type pressure mat and joint kinematics during walking. J Biomech. 2014;47(11):2693-2699. doi:10.1016/j.jbiomech.2014.05.007

Kivell TL. A review of trabecular bone functional adaptation: what have we learned from trabecular analyses in extant hominoids and what can we apply to fossils? J Anat. 2016 Apr;228(4):569-94. doi: 10.1111/joa.12446. Epub 2016 Feb 16. PMID: 26879841; PMCID: PMC4804137.

Kram R, Taylor CR. Energetics of running: a new perspective. Nature. 1990;346(6281):265-267. doi:10.1038/346265a0

Kramer PA. The costs of human locomotion: maternal investment in child transport. Am J Phys Anthropol. 1998;107(1):71-85. doi:10.1002/(SICI)1096-8644(199809)107:1<71::AID-AJPA6>3.0.CO;2-G

Kramer PA. The effect on energy expenditure of walking on gradients or carrying burdens. Am J Hum Biol. 2010;22(4):497-507. doi:10.1002/ajhb.21027

Kramer PA and Sylvester AD (2009) *Bipedal form and locomotor function: Understanding the affects of size and shape on velocity and energetics*. PaleoAnthropology, 238-251.

Kramer PA, Sylvester AD. (2011) *The energetic cost of walking: a comparison of predictive methods.* PLoS One. 6:e21290.

Kramer PA, Sylvester AD. Humans, geometric similarity and the Froude number: is "reasonably close" really close enough? Biol Open. 2013 Feb 15;2(2):111-20. doi: 10.1242/bio.20122691. Epub 2012 Nov 20. PMID: 23431123; PMCID: PMC3575646.

Kuo AD. The six determinants of gait and the inverted pendulum analogy: A dynamic walking perspective. Hum Mov Sci. 2007 Aug;26(4):617-56. doi: 10.1016/j.humov.2007.04.003. Epub 2007 Jul 6. PMID: 17617481.

Kuo AD, Donelan JM. Dynamic principles of gait and their clinical implications. Phys Ther. 2010 Feb;90(2):157-74. doi: 10.2522/ptj.20090125. Epub 2009 Dec 18. PMID: 20023002; PMCID: PMC2816028.

Latimer B, Lovejoy CO. The calcaneus of Australopithecus afarensis and its implications for the evolution of bipedality. *Am J Phys Anthropol*. 1989;78(3):369-386. doi:10.1002/ajpa.1330780306

Lieberman DE, Venkadesan M, Werbel WA, Daoud AI, D'Andrea S, Davis IS, Mang'eni RO, Pitsiladis Y. Foot strike patterns and collision forces in habitually barefoot versus shod runners. Nature. 2010;463(7280):531-535. doi:10.1038/nature08723

Lim SY, Lee WH. Effects of pelvic range of motion and lower limb muscle activation pattern on over-ground and treadmill walking at the identical speed in healthy adults. J Phys Ther Sci. 2018;30(4):619-624. doi:10.1589/jpts.30.619

Louey MGY, Mudge A, Wojciechowski E, Sangeux M. A model to calculate the progression of the centre of pressure under the foot during gait analysis. Gait Posture. 2017;57:147-153. doi:10.1016/j.gaitpost.2017.06.004

Lovejoy CO. The natural history of human gait and posture. Parts 1-3. Gait Posture. 2005;21(1):113-124. doi:10.1016/j.gaitpost.2004.06.010

Lovejoy CO, Latimer B, Suwa G, Asfaw B, White TD. Combining prehension and propulsion: the foot of Ardipithecus ramidus. Science. 2009 Oct 2;326(5949):72e1-8. PMID: 19810198.

McIntosh AS, Beatty KT, Dwan LN, Vickers DR. Gait dynamics on an inclined walkway. J Biomech. 2006;39(13):2491-2502. doi:10.1016/j.jbiomech.2005.07.025

Minetti AE. Optimum gradient of mountain paths. J Appl Physiol (1985). 1995;79(5):1698-1703. doi:10.1152/jappl.1995.79.5.1698

Minetti AE, Formenti F, Ardigò LP. Himalayan porter's specialization: metabolic power, economy, efficiency and skill. Proc Biol Sci. 2006;273(1602):2791-2797. doi:10.1098/rspb.2006.3653

Morton DJ. Evolution of the human foot II. Am. J. Phys. Anthropol. 1924; 7:1-52. doi:10.1002/ajpa.1330070114

Muniz AM, Nadal J. Application of principal component analysis in vertical ground reaction force to discriminate normal and abnormal gait. Gait Posture. 2009;29(1):31-35. doi:10.1016/j.gaitpost.2008.05.015

Nilsson J, Thorstensson A. Ground reaction forces at different speeds of human walking and running. Acta Physiol Scand. 1989;136(2):217-227. doi:10.1111/j.1748-1716.1989.tb08655.x

O'Driscoll R, Turicchi J, Beaulieu K, Scott S, Matu J, Deighton K, Finlayson G, Stubbs J. How well do activity monitors estimate energy expenditure? A systematic review and meta-analysis of the validity of current technologies. Br J Sports Med. 2020 Mar;54(6):332-340. doi: 10.1136/bjsports-2018-099643. Epub 2018 Sep 7. PMID: 30194221.

Ortega JO, Lindstedt SL, Nelson FE, Jubrias SA, Kushmerick MJ, Conley KE. Muscle force, work and cost: a novel technique to revisit the Fenn effect. J Exp Biol. 2015 Jul;218(Pt 13):2075-82. doi: 10.1242/jeb.114512. Epub 2015 May 11. PMID: 25964423; PMCID: PMC6514452.

Pandolf KB, Haisman MF, Goldman RF. Metabolic energy expenditure and terrain coefficients for walking on snow. Ergonomics. 1976;19(6):683-690. doi:10.1080/00140137608931583

Perry J. Gait Analysis: Normal and Pathological Function. 1992. https://doi.org/9781556421921

Pontzer H, Raichlen DA, Rodman PS. Bipedal and quadrupedal locomotion in chimpanzees. J Hum Evol. 2014 Jan;66:64-82. doi: 10.1016/j.jhevol.2013.10.002. Epub 2013 Dec 5. PMID: 24315239.

Rebula JR, Kuo AD. The cost of leg forces in bipedal locomotion: a simple optimization study. PLoS One. 2015 Feb 23;10(2):e0117384. doi: 10.1371/journal.pone.0117384. PMID: 25707000; PMCID: PMC4338056.

Ripley BD. Statistical Inferences for Spatial Processes. Cambridge: Cambridge University Press. 1987.

Roberts TJ, Chen MS, Taylor CR. Energetics of bipedal running. II. Limb design and running mechanics. J Exp Biol. 1998 Oct;201(Pt 19):2753-62. PMID: 9732330.

Rosenberg KR, DeSilva JM. Evolution of the Human Pelvis. Anat Rec (Hoboken). 2017 May;300(5):789-797. doi: 10.1002/ar.23580. PMID: 28406563.

Ross CT, Winterhalder B. Sit-and-wait versus active-search hunting: A behavioral ecological model of optimal search mode. J Theor Biol. 2015;387:76-87. doi:10.1016/j.jtbi.2015.09.022

Rue MJ, Kramer PA. Minimal energetic expenditure of women walking burdened on gradients in urban environments. Am J Hum Biol. 2017;29(1):10.1002/ajhb.22907. doi:10.1002/ajhb.22907

Rubenson J, Henry HT, Dimoulas PM, Marsh RL. The cost of running uphill: linking organismal and muscle energy use in guinea fowl (Numida meleagris). J Exp Biol. 2006 Jul;209(Pt 13):2395-408. doi: 10.1242/jeb.02310. PMID: 16788023.

Ruff C. Mechanical Constraints on the Hominin Pelvis and the "Obstetrical Dilemma". Anat Rec (Hoboken). 2017;300(5):946-955. doi:10.1002/ar.23539

Schrack JA, Simonsick EM, Chaves PH, Ferrucci L. The role of energetic cost in the age-related slowing of gait speed. J Am Geriatr Soc. 2012 Oct;60(10):1811-6. doi: 10.1111/j.1532-5415.2012.04153.x. Epub 2012 Oct 4. PMID: 23035640; PMCID: PMC3470763.

Smith E, Winterhalder B (1984) Natural Selection and Decision Making: Some Fundamental Principles. In: Smith E, Winterhalder B, eds. EvolutionaryEcology and Human Behavior. New York: Aldine de Gruyter. pp 25–60.

Sousa AS, Santos R, Oliveira FP, Carvalho P, Tavares JM. Analysis of ground reaction force and electromyographic activity of the gastrocnemius muscle during double support. Proc Inst Mech Eng H. 2012 May;226(5):397-405. doi: 10.1177/0954411912439671. PMID: 22720393.

Squadrone R, Gallozzi C. Biomechanical and physiological comparison of barefoot and two shod conditions in experienced barefoot runners. J Sports Med Phys Fitness. 2009;49(1):6-13.

Sylvester AD, Kramer PA. Brief Communication: Stand and shuffle: when does it make energetic sense? Am J Phys Anthropol. 2008 Apr;135(4):484-8. doi: 10.1002/ajpa.20752. PMID: 18000893.

Sylvester AD, Kramer PA, Jungers WL. Modern humans are not (quite) isometric. Am J Phys Anthropol. 2008 Dec;137(4):371-83. doi: 10.1002/ajpa.20880. PMID: 18613073.
McIntosh AS, Beatty KT, Dwan LN, Vickers DR. Gait dynamics on an inclined walkway, J. Biomech. 39 (2006) 2491–2502. https://doi.org/10.1016/j.jbiomech.2005.07.025.

Sylvester AD, Lautzenheiser SG, Kramer PA. Muslce forces and the cost of human walking. BiologyOpen. (In review 2021).

Taylor CR. Force development during sustained locomotion: a determinant of gait, speed and metabolic power. J Exp Biol. 1985;115:253-262.

Taylor CR, Heglund NC, McMahon TA, Looney TR. Energetic Cost of Generating Muscular Force During Running: A Comparison of Large and Small Animals. J Exp Biol.1980;86: 9-18.

Wang AB, Perreault EJ, Royston TJ, Lee SSM. Changes in shear wave propagation within skeletal muscle during active and passive force generation. J Biomech. 2019 Sep 20;94:115-122. doi: 10.1016/j.jbiomech.2019.07.019. Epub 2019 Jul 25. PMID: 31376979; PMCID: PMC6736689.

Warabi T, Kato M, Kiriyama K, Yoshida T, Kobayashi N. Treadmill walking and overground walking of human subjects compared by recording sole-floor reaction force, Neurosci. Res. 53 (2005) 343–348. https://doi.org/10.1016/j.neures.2005.08.005.

Waters RL, Mulroy S. The energy expenditure of normal and pathologic gait. Gait & posture. 1999 Jul 1;9(3):207-31.

Wei F, Crechiolo A, Haut RC. Prediction of ground reaction forces in level and incline/decline walking from a multistage analysis of plantar pressure data. J Biomech. 2019;84:46-51. doi:10.1016/j.jbiomech.2018.12.015

Winter DA. The Biomechanics and Motor Control of Human Gait. 1988. https://doi.org/10.1016/s0031-9406(10)63713-3

Wolff J. The classic: on the inner architecture of bones and its importance for bone growth. 1870. Clin Orthop Relat Res. 2010 Apr;468(4):1056-65. doi: 10.1007/s11999-010-1239-2. PMID: 20162387; PMCID: PMC2835576.

Yao J, Guo N, Xiao Y, Li Z, Li Y, Pu F, Fan Y. Lower limb joint motion and muscle force in treadmill and over-ground exercise. Biomed Eng Online. 2019;18(1):89. Published 2019 Aug 22. doi:10.1186/s12938-019-0708-4

Chapter 3. PEAK BRAKING AND PROPULSIVE FORCES

Preface

This manuscript has been submitted for publication under the title "Peak Braking and Propulsive Forces Over Contiguous Steps in Gradient and Level Walking" and authored by Alexandra G. Hammerberg and Patricia Ann Kramer.

3.1 ABSTRACT

Background: Naturally occurring variation in terrain influences the peak braking and propulsive ground reaction forces (GRFs) and pressure distribution across the planter surface of the foot in walking, but most biomechanical studies have been constrained to laboratory protocols that cannot fully capture adaptations to terrain over multiple connected gait cycles.

Research Question: We investigated the effect of over-ground gradient walking on peak vertical GRFs during braking and propulsion over multiple, contiguous steps.

Methods: The data were collected from eleven participants aged 20 to 42 years without gait pathology or injury. Each participant was fitted to a pair of wireless insoles with an array of force sensors distributed across each insole surface. Participants completed seven trials: walk on a level treadmill at 0.89m/s, 1.34m/s, and 1.79m/s; on a 10% inclined treadmill at 0.89m/s; along a straight, level, 78.4m indoor walkway; and in a straight line on an outdoor sidewalk downhill and uphill 70.5 meters over an 9% slope. We analyzed 6711 steps total.

Results: We found that peak braking and propulsive GRFs differ significantly between trials when we control for participant mass and velocity. Overground downhill walking results in significantly

higher peak braking forces than any other tested walking condition ($p<0.001$), including fast (1.79m/s) walking, after controlling for velocity.

Significance: Conditions experienced in daily activities, such as walking on inclined surfaces, produce higher GRFs.

3.2 INTRODUCTION

Ground reaction forces (GRFs) reflect the interaction of the foot and the surface during the stance phase of gait and two peaks in the vertical component of the GRF are typical in walking (Figure 1 panel iii). The body slows in early stance (the braking period) producing a GRF peak, passes above the stance foot in midstance with a decrease in the GRF, and accelerates in late stance (the propulsive period) producing another GRF peak. Although anteroposterior forces brake and accelerate the body, vertical forces are almost five times larger in walking [1].

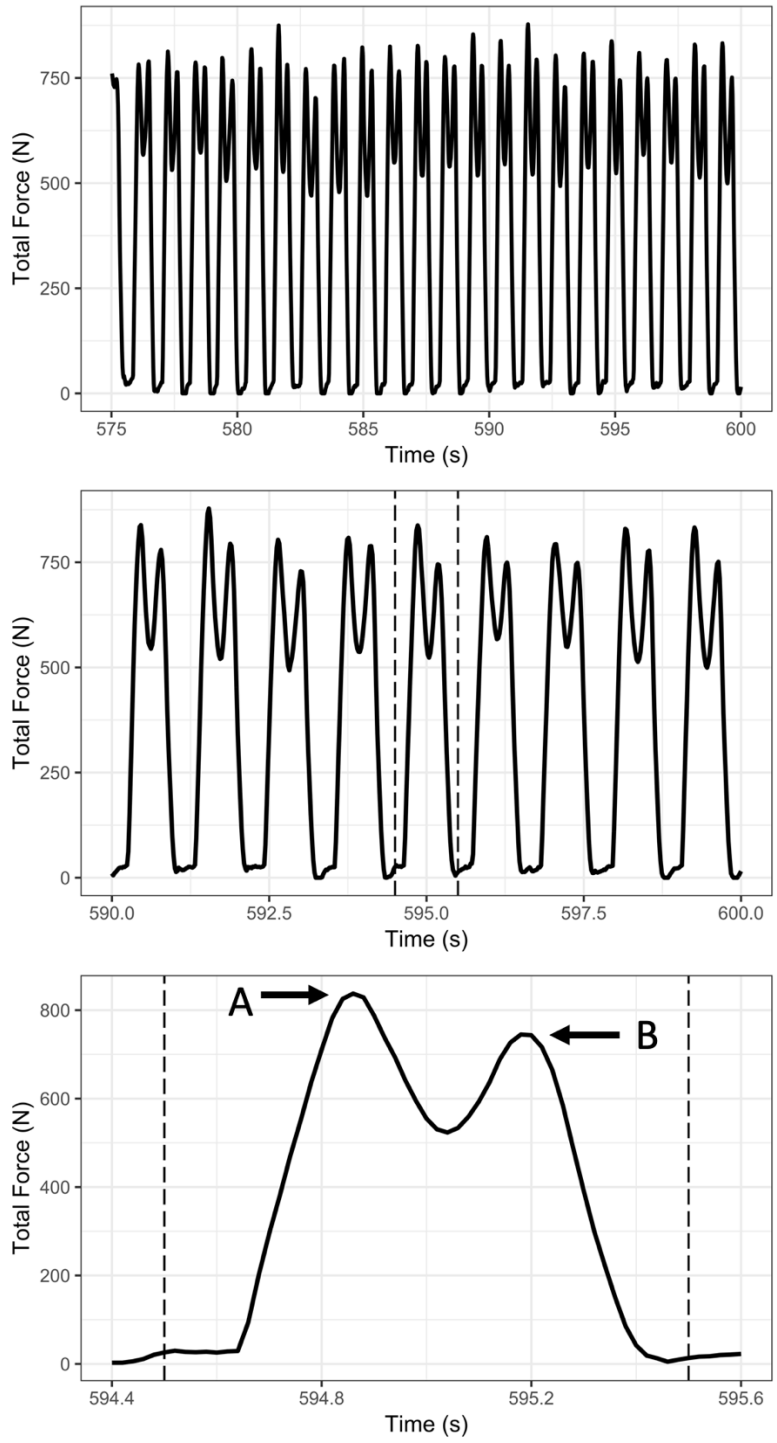

Figure 3.1. Isolated individual left foot steps for one participant (body weight at stance = 812 N) during hallway walking at self-selected velocity. The vertical force curve for a single foot over

the course of the gait cycle. “A” denotes peak vertical force at braking and “B” denotes peak vertical force at propulsion. Panel i.) twenty-two steps ii.) nine steps iii.) single step.

The GRF magnitude varies with factors that include, but are not limited to, mass of the body in motion, velocity of travel (e.g. [2]), system pathology (e.g. [3]), burdens carried (e.g. [4]), and surface type (e.g. [5]). While the heel is typically the first anatomical feature to strike the ground and the toes are the last to leave during a step, the center of pressure (CoP) location when peak vertical (braking and propulsion) force occurs is less explored (e.g. [6]). These CoP locations, in conjunction with the associated GRF magnitudes, are critically important variables from the perspectives of both understanding musculoskeletal growth and development and appreciating clinical requirements for patient recovery. While the anteroposterior shear forces are also required to move along surfaces, because vertical GRFs are larger, they are the focus of this work.

Humans encounter a wide variety of surfaces and obstacles as they navigate through their daily activities, and yet, most gait research has been restricted to data collection in laboratories using embedded force plates or on tracks using motion-capture (e.g. [7], [8]). A standard protocol involves study participants walking or running across a force plate embedded in the floor of a laboratory or on a force-sensing treadmill that records the magnitude and direction of the GRF (e.g. [9], [10], [11], [12], [13], [14], [15]). But, many activities of daily living, such as walking along extended gradients or stair walking, are difficult to accomplish in a laboratory environment.

With recent developments in remote sensing technology, however, we are now able to gather vertical GRF and CoP data outside of the laboratory. Wireless insoles are a mobile alternative to fixed force plates and allow for continual data collection as participants move in less-restricted ways than previously possible, including along gradients (e.g. [16], [17], [18], [19]).

Consequently, these recent advances in sensing technology open the door to new insights. For instance, predictive models for estimating the horizontal plane components of the GRF in level walking using inverse dynamics solutions of virtual musculoskeletal models have been developed [20].

Utilizing wireless force-sensing insoles (ReGo, Moticon AG, Munich, Germany), our work builds on previous gradient kinetic research [8]. We focus on extending our understanding of the vertical GRF magnitudes and CoP during peak braking and peak propulsion in contiguous walking steps both within and outside of the confines of the laboratory environment. While the previous work is a key point of comparison for our results, by utilizing the wireless insoles we were able to measure vertical GRFs for repeated gait cycles and along longer gradients.

We hypothesized that peak vertical GRFs during braking and propulsion for multiple, contiguous steps would not differ significantly between treadmill and over-ground walking when controlling for velocity. We also hypothesized that the CoP at peak braking and peak propulsive vertical force would be clustered in the hindfoot and forefoot, respectively, in all walking activities.

3.3 METHODS

3.3.1 *EXPERIMENTAL SETUP*

Each participant was fitted with a pair of ReGo (Moticon, Munich, Germany) wireless pressure-sensing insoles worn in a pair of Fitkicks™ water socks. We used the socks to limit the effect of variability in shoe sole stiffness. Thirteen sensors are distributed across the insole surface (Supplementary Figure 1) and were set to collect data at 50Hz (i.e., every 0.02 seconds). Each sensor recorded a force value at each timepoint. The total force summed across the sensors and the center of pressure (CoP) x and y coordinates were also determined at each timepoint.

We investigated seven walking conditions. Participants walked on a treadmill at 0.89m/s ("slow"), 1.34m/s ("moderate"), and 1.79m/s ("fast") for 60 seconds at each velocity. The order of these treadmill tests was randomized. Participants then walked on the treadmill set to a 10% (5.7°) slope at 0.89m/s. Participants also walked at their comfortable pace along a straight, flat, 78.4m indoor hallway. Lastly, participants walked in a straight line on an outdoor sidewalk downhill and uphill 70.5m over an 8.8% (5.0°) slope in dry conditions. Research personnel ensured that the hallway and outside paths were unobstructed. This project was approved by the University of Washington Institutional Review Board.

3.3.2 *PARTICIPANTS*

The data were collected from a convenience sample of eleven participants (six females and five males) ages 20 to 42 years (Supplementary Table 1), who were without gait pathology or injury to their lower limbs within the last 2 years. Participants' arch index (AI) was calculated [21] from footprints obtained from a pressure mat (RSscan International, Olen, Belgium). We measured their mass (kg) with a standard scale and calculated a neutral stance force, which was equal to the sum of the force exerted on both insoles while the participant stood quietly [20].

3.3.3 *DATA ACQUISITION & PROCESS*

We isolated individual steps for each trial for the left and right foot of each participant (Figure 1) and determined the local force maxima for the braking and propulsive phases of stance from each step using a custom written MATLAB (MathWorks) program. We removed steps with fewer or more than two peaks as indicative of non-normal (e.g. "a stumble") steps. 6711 steps were analyzed across all participants and all trials (Supplementary Table 2).

The peak forces were normalized for each subject by dividing the total force output from the insole at each peak during the walking trials by the total force output when the subject was standing quietly (neutral stance force). We standardized the x and y coordinates of the CoP to account for insole size differences between participants by multiplying by the insole scaling factor provided by manufacturer. We compared the peak vertical forces and the position of the CoP during the braking and propulsive phases between conditions and between individuals in each condition. We calculated the individual velocities for each participant's hallway, downhill, and uphill trials from time and distance travelled (Supplementary Table 3).

3.3.4 *STATISTICAL ANALYSIS*

Regression analyses were performed using RStudio statistical software. To account for the hierarchical nature of the data, we used the lmer4 [31] and lmerTest [32] packages for our multilevel linear models. We performed pairwise comparisons between trials, clustering by participant. We also performed within-individual analyses, grouped by trial. Significance was set at an alpha of $p=0.005$ after Bonferroni correction for multiple comparisons.

3.4 RESULTS

Participant weight (N) and neutral standing force ($r=0.88$), peak braking force ($r=0.65$), and peak propulsive force ($r=0.69$) are correlated. Velocity and peak braking force ($r=0.26$) are correlated. Participant AI and peak braking force ($r=0.35$), peak propulsive force ($r=0.41$), and participant weight ($r=0.61$) are also correlated (Supplementary Table 4).

All participants walked significantly faster ($p<0.0001$) during the downhill and uphill walking trials than the hallway walking trial. Participants also, on average, walked faster going

uphill than downhill (Figure 2), but the difference between the average velocities was non-significant (p=0.029). All three self-selected velocities averaged closest to the moderate treadmill velocity (1.34m/s): hallway = 1.21m/s (+/-0.08); downhill = 1.42m/s (+/-0.08); uphill = 1.43m/s (+/-0.10), shown by lines on Figure 2, but the self-selected velocities were still significantly different from any of the treadmill velocities (all p<0.0001).

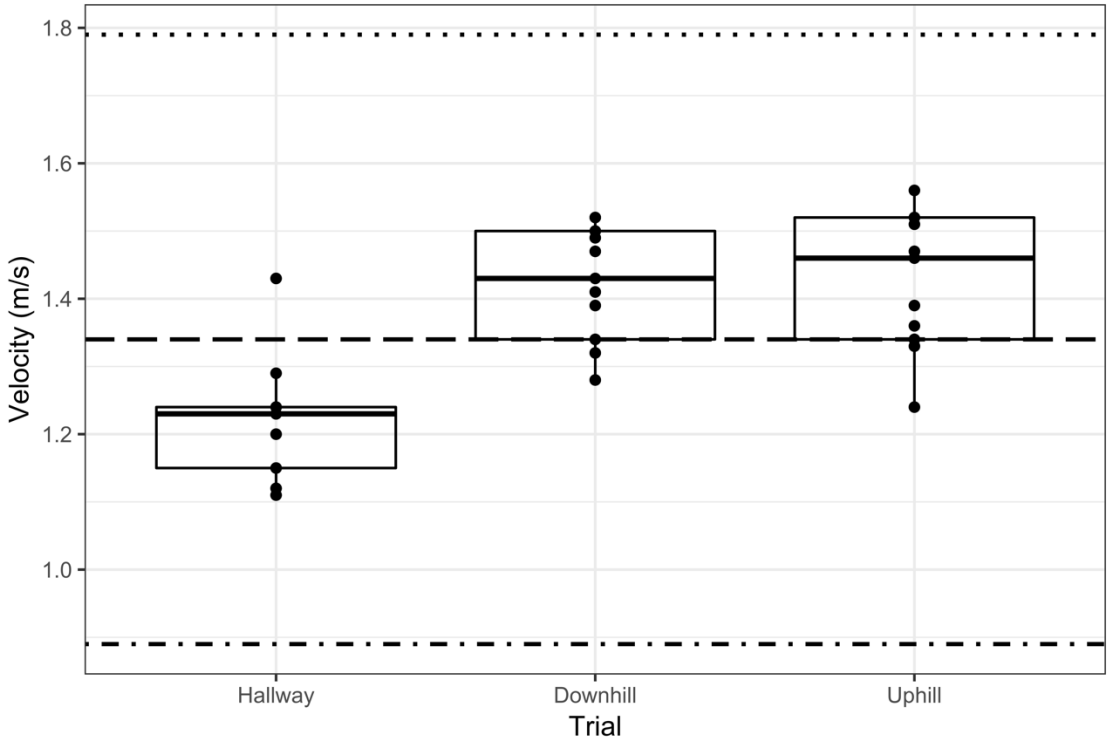

Figure 3.2. Self-selected velocities for hallway and outdoor walking with treadmill velocities indicated by horizonal lines (slow (dash dot), moderate (dash), and fast (dot)). Participants' self-selected velocities are best approximated by the moderate (1.34m/s) treadmill condition.

When we control for velocity, the normalized peak braking forces from the hallway condition are not significantly different from those obtained from the flat treadmill conditions (p > 0.005), except that peak braking force for slow (0.89m/s) treadmill is significantly less than

hallway walking ($p<0.0001$, Table 1). The normalized propulsive hallway forces are higher than those of the slow (0.89m/s), moderate (1.34m/s) and fast (1.79m/s) velocity treadmill walking conditions, but the difference is significant only for the moderate and fast conditions (Table 1, $p<0.0001$ for both).

Braking	Slow Treadmill	Moderate Treadmill	Fast Treadmill	Incline Treadmill	Hallway	Downhill	Uphill
Slow Treadmill	-	-	-	-	-	-	-
Moderate Treadmill	p<0.0001	-	-	-	-	-	-
Fast Treadmill	p<0.0001	p<0.0001	-	-	-	-	-
Incline Treadmill	NS (p=0.624)	p<0.0001	p<0.0001	-	-	-	-
Hallway	p<0.0001	NS (p=0.0347)	NS (p=0.0637)	p<0.0001	-	-	-
Downhill	p=0.000673	p<0.0001	p<0.0001	p=0.000151	p<0.0001	-	-
Uphill	NS (p=0.426))	p<0.0001	NS (p=0.130)	p=0.00262	p<0.0001	p<0.0001	-
Propulsion	Slow Treadmill	Moderate Treadmill	Fast Treadmill	Incline Treadmill	Hallway	Downhill	Uphill
Slow Treadmill	-	-	-	-	-	-	-
Moderate Treadmill	NS (p=0.00505)	-	-	-	-	-	-
Fast Treadmill	p<0.0001	p<0.0001	-	-	-	-	-
Incline Treadmill	p<0.0001	p<0.0001	p<0.0001	-	-	-	-
Hallway	NS (p=0.0174)	p<0.0001	p<0.0001	p=0.00455	-	-	-
Downhill	p<0.0001	p<0.0001	p<0.0001	p<0.0001	p<0.0001	-	-
Uphill	NS (p=0.0202)	p<0.0001	NS (p=0.774)	p=0.000191	NS (p=0.882)	p<0.0001	-

Table 3.1. Significance of differences in peak braking and peak propulsive forces between each trial. Velocity parameters for ‘slow’, ‘moderate’, ‘fast’, and ‘incline’ treadmill trials were held constant by the researcher between participants. All other trials were performed at participant-selected speeds.

When we control for velocity, the normalized vertical peak braking and propulsive forces for incline treadmill walking were significantly different from the peak braking and propulsive forces for outdoor uphill walking (braking p=0.0026, propulsive p=0.00019, Table 1). The peak braking force for uphill walking was significantly higher than incline treadmill walking and the peak propulsive force for uphill walking was also significantly higher than peak propulsive force for incline treadmill walking (Table 2). When we control for velocity, normalized peak braking force is significantly higher for downhill walking than all other trials (Table 1 and Figure 3).

Trial	Mean Peak Braking Force (N)	Mean Peak Propulsive Force (N)
1: Slow Treadmill	663.4 +/- 115.8	724.5 +/- 118.4
2: Moderate Treadmill	710.6 +/- 129.1	727.7 +/- 104.1
3: Fast Treadmill	741.6 +/- 124.8	694.2 +/- 96.1
4: Incline Treadmill	655.9 +/- 110.4	733.5 +/- 86.8
5: Hallway	725.1 +/- 116.8	758.7 +/- 97.7
8: Downhill	854.0 +/- 170.2	696.2 +/- 115.0
9: Uphill	732.7 +/- 112.0	765.2 +/- 100.7

Table 3.2. Peak braking and peak propulsive forces (Newtons) for each trial, averaged across participants with their standard deviations.

The locations of the CoP at the peak braking force are consistently in the hindfoot or midfoot for all trials. The CoPs at the propulsive peaks for all conditions are located in the forefoot region (Figure 5).

3.5 DISCUSSION

Most kinetic analyses of gait depend on data collected using force plates embedded in the floor or force-sensing treadmills, which potentially creates a compromise between statistical power and representativeness of the data. On the one hand, many steps can be obtained from force-sensing treadmills but treadmill walking can be kinetically different from over-ground movement [22], [23]. On the other, data from, at most, only several consecutive steps can be collected using floor-based force plates. Our work bridges this compromise in that it includes many contiguous, over-ground steps and it builds on studies that have emphasized collecting data over the course of several contiguous steps as a necessity for fully understanding gait GRFs (e.g. [9], [10], [16], [17], [18]). Capturing several steps per trial is not necessarily representative of normal movement. The fewest number of steps per trial we examined was 572 during slow treadmill walking (Supplementary Table 2). In the over-ground walking trials outside of the laboratory, which are more representative of everyday walking, we analyzed a minimum of 955 steps. The number of over-ground contiguous steps we examined as well as the variety of terrains and the velocities represented are, to our knowledge, novel to this work.

Force plates are also rarely embedded in ramps to assess incline/decline walking, except in customized laboratory setups (e.g. [4], [8], [24]). Although other researchers have attempted to examine the change in ground reaction forces when participants transverse slopes [25], [26] or along substrates with differing compliances or frictional coefficients (e.g. [27], [28]), we sought to understand the forces exerted between the foot and the substrate in conditions that are not those found in typical laboratories by asking participants to walk freely using vertical force sensing insoles. To provide a comparison, we also had participants walk on a level treadmill at three velocities and on an inclined treadmill at slow velocity. Given that the typical vertical GRF curve

for walking has two peaks, we evaluated the peak force in the first half of stance (the braking period) and that of the second half (the propulsive period) independently. We also determined the location of the CoP when these two peaks occur. The water socks we used in our protocol limited the effect of variability in shoe stiffness or cushioning. These allowed us to keep the insole secured to the sole of the foot during the walking trials and was closer to unshod walking than shod walking in modern shoes.

As walking velocity increases, the vertical GRF increases (e.g. [2]). We expected, therefore, that, when we controlled for participant mass and trial velocity, no differences would emerge in peak braking or propulsive forces in walking trials across level surfaces or treadmills. Instead, hallway braking forces are higher than slow and moderate treadmill walking and hallway propulsive forces are higher than all those from treadmill walking (Table 2) despite controls for mass and velocity.

Gait dynamics on inclines have been shown to differ considerably from flat-surface walking (e.g. [8], [27]). McIntosh et.al. [8] investigated a range of gradient values for both inclines and declines using an instrumented ramp. Our testing gradient was 5.0°, where their range was 5°, 8°, and 10° of incline/decline. They noted an increase in peak braking vertical GRFs for the higher incline gradients and a significant increase in vertical GRFs during peak propulsion from 0° to 10°, but most of the observed difference occurs for the steeper gradients (Figure 5, [8]). We found significant differences in vertical GRFs during peak braking between hallway (0°) and uphill walking, but the differences in vertical GRFs during peak propulsion between hallway and uphill walking were non-significant (Table 2). The difference between our results and those of McIntosh and colleagues is potentially due to the difference in walkway length (which allowed us to collect

at least 55 contiguous steps for each individual) and the gradient of the slope. More research on steeper inclines and declines is warranted.

We also investigated the peak vertical forces for walking on an inclined treadmill compared to walking uphill on slopes that were less than a degree apart in gradient (5.7° along the treadmill compared to 5.0° along the uphill), and we expected to see little difference in the peak forces generated for incline treadmill and free uphill walking. Unexpectedly, both peak braking forces and peak propulsive forces were higher for walking freely uphill than on an inclined treadmill when controlling for velocity, which is similar to the pattern seen for flat-surface walking. This calls into question the assumption that treadmill walking is directly comparable to walking freely on level or inclined surfaces and agrees with prior work demonstrating that significant differences exist between the kinetics of walking freely and walking on treadmills (e.g. [22], [23]).

We expected to find higher peak braking and lower propulsive forces for downhill than for level walking and lower braking and higher propulsion for incline than level walking due to the effect of gravity. We confirmed this with our data, apart from incline braking, which was significantly higher than hallway and moderate treadmill walking (Table 2 and Figure 3). McIntosh et.al. [8] previously observed a significant increase in peak braking GRFs as the angle of decline increased, but little change in the peak propulsive GRFs with increasing declines and an increase in peak propulsion with little change in braking with increasing incline. We saw significant differences in both peak braking (higher) and peak propulsive (lower) GRFs for downhill compared to flat walking and inclines (Tables 1 and 2). Prior work (e.g. [4], [24], [29]) has demonstrated that downhill walking effects gait kinetics and energy expenditure, but how downhill walking influences GRFs has been less well understood. Renner et.al. [30] found changes in peak forces of approximately 10% for downhill compared to level walking at 1.3m/s. We found that

downhill forces are more than 10% higher than the next highest peak braking force, which occurred in fast treadmill walking (Table 2) and more than 15% higher compared to hallway walking. This reinforces the need for gait studies to be conducted outside of the laboratory.

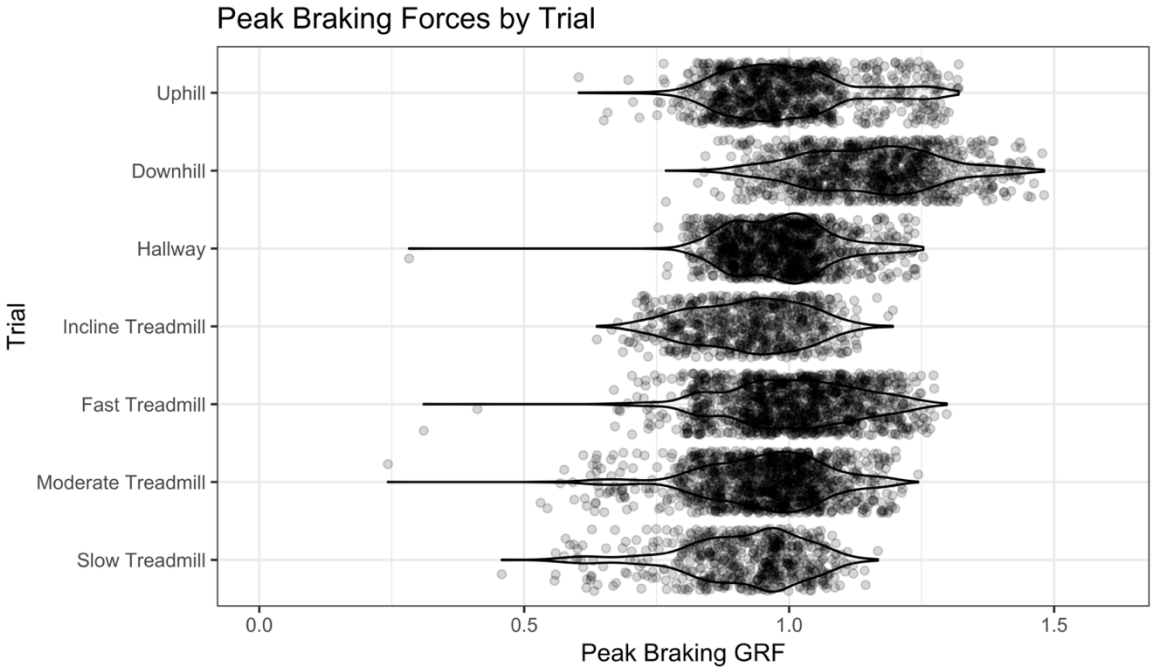

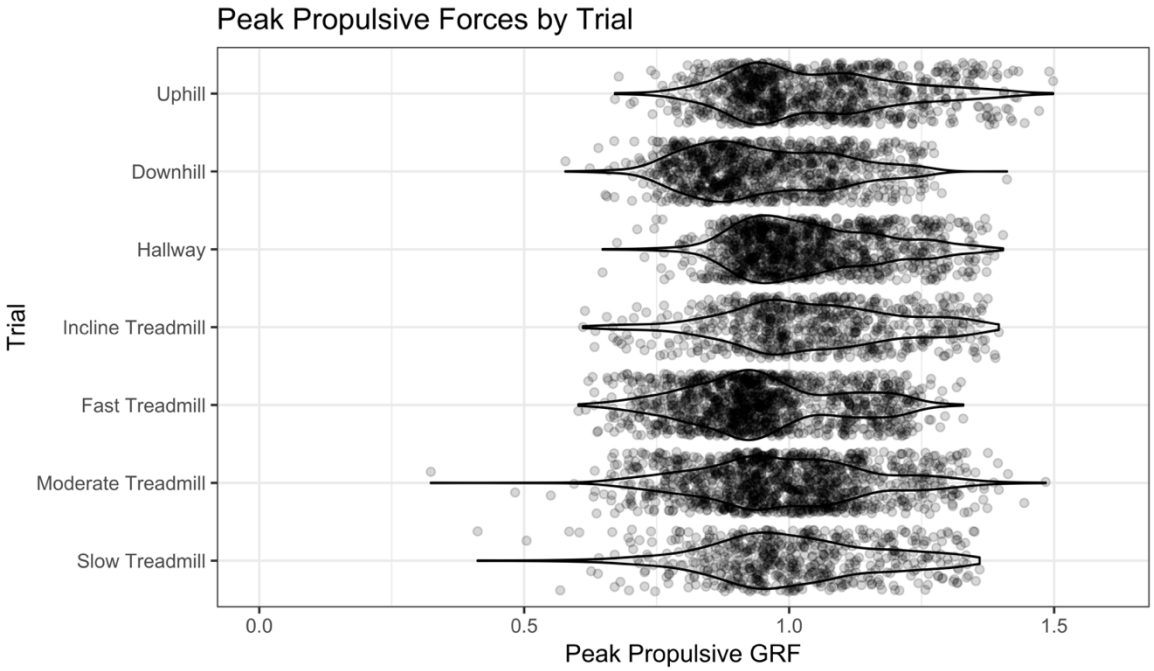

Figure 3.3. Peak braking and propulsive forces by trial, normalized by participant mass with overlaid violin density plots. Data points were jittered vertically to better display visually the density of points for each trial.

Given that ramps are usually suggested as the preferred alternative to stairs for patients recovering from traumatic injury or surgery, our results may provide important information to inform rehabilitation protocols. Patients struggle to maintain consistency and adherence to recovery protocols on level surfaces [16]; the challenges of walking on gradients should not be discounted. The forces generated on these non-level surfaces could impact recovery in ways not fully understood at present. We have shown here as have others (e.g. [4], [8], [18], [19], [24], [29]) that incline and decline walking generates high forces in the foot during braking and propulsion. We suggest that gradient walking is a more complicated biomechanical process than, and cannot be treated as the same process as, walking along level surfaces, especially when considering patient recovery from an injury to the foot.

We also noted that participants' self-selected velocities for uphill walking outdoors were significantly higher than the incline treadmill velocity, and all participants walked significantly faster outdoors going up and downhill than along the level indoor hallway (Figure 2). We do not have an explanation for why participants elected to walk faster, and this goes against some previous work (e.g. [29]), which further emphasizes the need for more biomechanical research in conditions more closely resembling what participants encounter in daily activities.

We also captured information regarding the location of the center of pressure (CoP) at peak braking and propulsive forces for each gait cycle. We expected the CoP at peak braking force to be consistently located towards the rear of the foot, because the initial contact is with the heel and the CoP travels from the heel along the lateral margin of the foot and then medially toward the

first and second metatarsal heads. Consistent with our expectations, all trials demonstrate a greater intensity of CoP locations posterior to the forefoot at peak braking and within the forefoot at peak propulsion (Figure 4). CoP at peak propulsion appears more consistent in location than CoP at peak braking force within trials. Further assessment of the spatial relationship of the CoP with the foot for differing walking conditions and velocities is required and will be the subject of future analyses.

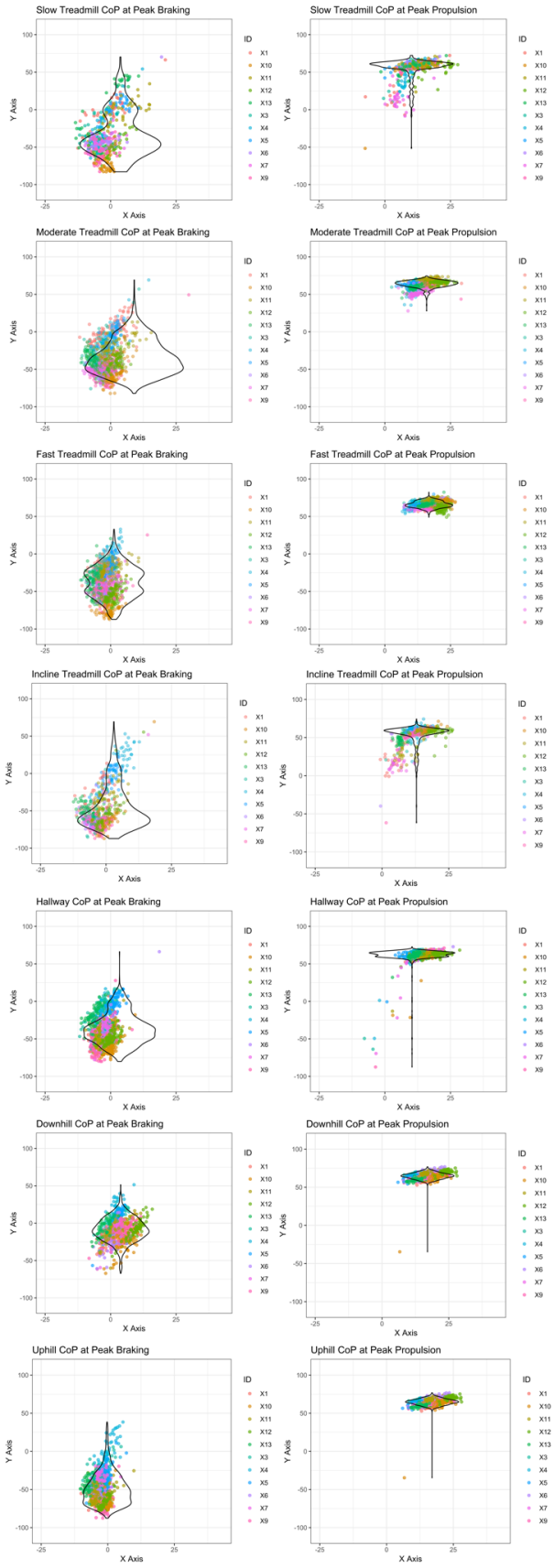
Slow Treadmill CoP at Peak Braking
Slow Treadmill CoP at Peak Propulsion
Moderate Treadmill CoP at Peak Braking
Moderate Treadmill CoP at Peak Propulsion
Fast Treadmill CoP at Peak Braking
Fast Treadmill CoP at Peak Propulsion
Incline Treadmill CoP at Peak Braking
Incline Treadmill CoP at Peak Propulsion
Hallway CoP at Peak Braking
Hallway CoP at Peak Propulsion
Downhill CoP at Peak Braking
Downhill CoP at Peak Propulsion
Uphill CoP at Peak Braking
Uphill CoP at Peak Propulsion
X Axis
Y Axis
ID
X1
X10
X11
X12
X13
X3
X4
X5
X6
X7
X9

Figure 3.4. Center of pressure (CoP) points at peak braking and peak propulsive forces for each trial for each participant with overlaid violin density plots for point clustering, with CoP points normalized for insole size. All trials show a higher density of CoP points posterior to the forefoot during peak braking. CoP at peak propulsive force was most distinctly forefoot centered; all trials showed a higher density of CoP points at the forefoot at peak propulsive force.

3.6 CONCLUSION

Performing biomechanics studies outside of the laboratory and over multiple, contiguous steps is crucial to our understanding of how humans interact with their environment in more natural and less restricted movement patterns. This study extends previous work but only begins to explicate the effect that terrains and environments that modern humans encounter and navigate on a daily basis have on forces developed between the foot and substrate. The forces of both braking and propulsion are significantly different depending on gradient and speed of travel. Velocity does not, however, completely account for the differences in peak braking and peak propulsive forces between level surfaces that previously have been considered comparable. Further, the peak braking forces appear to produce CoPs that are less consistent in location within a trial than CoPs at peak propulsive forces. These results have important implications for evolutionary biomechanics as well as patient rehabilitation protocols.

3.7 REFERENCES

[1] Nilsson, J., & Thorstensson, A. (1989). Ground reaction forces at different speeds of human walking and running. *Acta Physiologica Scandinavica*, *136*(2), 217–227. https://doi.org/10.1111/j.1748-1716.1989.tb08655.x

[2] D.A. Winter, The Biomechanics and Motor Control of Human Gait, 1988. https://doi.org/10.1016/s0031-9406(10)63713-3.

[3] J. Perry, Gait Analysis: Normal and Pathological Function, 1992. https://doi.org/9781556421921.

[4] P.A. Kramer, The effect on energy expenditure of walking on gradients or carrying burdens, Am. J. Hum. Biol. 22 (2010) 497–507. https://doi.org/10.1002/ajhb.21027.

[5] K.B. Pandolf, M.F. Haisman, R.F. Goldman, Metabolic Energy Expenditure and Terrain Coefficients for Walking on Snow, Ergonomics. 19 (1976) 683–690.

[6] M.G.Y. Louey, A. Mudge, E. Wojciechowski, M. Sangeux, A model to calculate the progression of the centre of pressure under the foot during gait analysis, Gait Posture. 57 (2017) 147-153. https://doi.org/10.1053/j.jfas.2018.06.015

[7] G.A. Cavagna, R. Margaria, Mechanics of walking., J. Appl. Physiol. 21 (1966) 271–278. https://doi.org/10.1152/jappl.1966.21.1.271.

[8] A.S. McIntosh, K.T. Beatty, L.N. Dwan, D.R. Vickers, Gait dynamics on an inclined walkway, J. Biomech. 39 (2006) 2491–2502. https://doi.org/10.1016/j.jbiomech.2005.07.025.

[9] B. De Wit, D. De Clercq, P. Aerts, Biomechanical analysis of the stance phase during barefoot and shod running, J. Biomech. 33 (2000) 269–278. https://doi.org/10.1016/S0021-9290(99)00192-X.

[10] C. Divert, G. Mornieux, P. Freychat, L. Baly, F. Mayer, A. Belli, Barefoot-shod running differences: Shoe or mass effect?, Int. J. Sports Med. 29 (2008) 512–518. https://doi.org/10.1055/s-2007-989233.

[11] R. Squadrone, C. Gallozzi, Biomechanical and physiological comparison of barefoot and two shod conditions in experienced barefoot runners, J Sport. Med Phys Fit. 49 (2009) 6–13.

[12] D.E. Lieberman, M. Venkadesan, W.A. Werbel, A.I. Daoud, S. Dandrea, I.S. Davis, R.O. Mangeni, Y. Pitsiladis, Foot strike patterns and collision forces in habitually barefoot versus shod runners, Nature. 463 (2010) 531–535. https://doi.org/10.1038/nature08723.

[13] K.G. Hatala, R.E. Wunderlich, H.L. Dingwall, B.G. Richmond, Interpreting locomotor

biomechanics from the morphology of human footprints, J. Hum. Evol. 90 (2016) 38–48. https://doi.org/10.1016/j.jhevol.2015.08.009.

[14] L. Ardigò, C. Lafortuna, A. Minetti, P. Mognoni, F. Saibene, Metabolic and mechanical aspects of foot landing type, forefoot and rearfoot strike, in human running, Acta Physiol. Scand. 155 (1995) 17–22. https://doi.org/10.1111/j.1748-1716.1995.tb09943.x.

[15] M.F. Bobbert, M.R. Yeadon, B.M. Nigg, Mechanical analysis of the landing phase in heel-toe running, J. Biomech. 25 (1992) 223–234. https://doi.org/10.1016/0021-9290(92)90022-S.

[16] B.J. Braun, N.T. Veith, S.C. Herath, R. Hell, M. Rollmann, M. Orth, J.H. Holstein, T. Pohlemann, Ein neues, kontinuierliches Ganganalysesystem zur Nachbehandlung von Sprunggelenkfrakturen, Unfallchirurg. 121 (2018) 293–299. https://doi.org/10.1007/s00113-017-0332-3.

[17] J. He, K. Lippmann, N. Shakoor, C. Ferrigno, M.A. Wimmer, Unsupervised gait retraining using a wireless pressure-detecting shoe insole, Gait Posture. 70 (2019) 408–413. https://doi.org/10.1016/j.gaitpost.2019.03.021.

[18] G. Björklund, M. Swarén, D.P. Born, T. Stöggl, Biomechanical adaptations and performance indicators in short trail running, Front. Physiol. 10 (2019) 1–10. https://doi.org/10.3389/fphys.2019.00506.

[19] F. Wei, A. Crechiolo, R.C. Haut, Prediction of ground reaction forces in level and incline/decline walking from a multistage analysis of plantar pressure data, J. Biomech. 84 (2019) 46-51. https://doi.org/10.1016/j.jbiomech.2018.12.015.

[20] Y. Jung, M. Jung, K. Lee, S. Koo, Ground reaction force estimation using an insole-type pressure mat and joint kinematics during walking, J. Biomech. 47 (2014) 2693-2699. http://dx.doi.org/10.1016/j.jbiomech.2014.05.007.

[21] P.R. Cavanagh, M.M. Rodgers, The Arch Index: A Useful Measure From Footprints, J. Biomech. 20 (1987) 547–551.

[22] T. Warabi, M. Kato, K. Kiriyama, T. Yoshida, N. Kobayashi, Treadmill walking and overground walking of human subjects compared by recording sole-floor reaction force, Neurosci. Res. 53 (2005) 343–348. https://doi.org/10.1016/j.neures.2005.08.005.

[23] F. Alton, L. Baldey, S. Caplan, M.C. Morrissey, A kinematic comparison of overground and treadmill walking, Clin. Biomech. 13 (1998) 434–440.

[24] M. Kuster, S. Sakurai, G.A. Wood, Kinematic and kinetic comparison of downhill and level walking, Clin. Biomech. 10 (1995) 79–84. https://doi.org/10.1016/0268-0033(95)92043-L.

[25] M. Damavandi, P.C. Dixon, D.J. Pearsall, Kinematic adaptations of the hindfoot, forefoot, and hallux during cross-slope walking, Gait Posture. 32 (2010) 411–415. https://doi.org/10.1016/j.gaitpost.2010.07.004.

[26] S.P. Breloff, C. Wade, D.E. Waddell, Lower extremity kinematics of cross-slope roof walking, Appl. Ergon. 75 (2019) 134–142. https://doi.org/10.1016/j.apergo.2018.09.013.

[27] H. Wang, L. An, X. Feng, J. Zhao, A. Merryweather, H. Xu, Ground reaction force adaptation during cross-slope walking on railroad ballast, Gait Posture. 75 (2020) 66–71. https://doi.org/10.1016/j.gaitpost.2019.10.001.

[28] K.B. Pandolf, B. Givoni, R.F. Goldman, Predicting energy expenditure with loads while standing or walking very slowly, J. Appl. Physiol. 43 (1977) 577–581. https://doi.org/10.1152/jappl.1977.43.4.577.

[29] J.C. Wall, J.W. Nottrodt, J. Charteris, The effects of uphill and downhill walking on pelvic oscillations in the transverse plane, Ergonomics. 24 (1981) 807–816. https://doi.org/10.1080/00140138108924901.

[30] K.E. Renner, D.B. Williams, R.M. Queen, The reliability and validity of the Loadsol under various walking and running conditions, Sensors. 19 (2019) 1-14. doi:10.3390/s19020265.

[31] B. Douglas, M. Maechler, B. Bolker, S. Walker (2015). Fitting Linear Mixed-Effects Models Using lme4. Journal of Statistical Software, 67(1), 1-48. doi:10.18637/jss.v067.i01.

[32] A. Kuznetsova, PB Brockhoff, RHB Christensen (2017). “lmerTest Package: Tests in Linear Mixed Effects Models.” _Journal of Statistical Software_, *82*(13), 1-26. doi: 10.18637/jss.v082.i13 (URL: http://doi.org/10.18637/jss.v082.i13).

Chapter 4. FORCE LOCATIONS AT BRAKING AND PROPULSION

Preface

This manuscript is in revision for publication to The Royal Society's Interface Focus under the title "Consistent Inconsistencies in Braking: A Spatial Analysis" and authored by Alexandra G. Hammerberg and Patricia Ann Kramer.

4.1 ABSTRACT

The dynamic system that is the bipedal body in motion has been, and continues to be, of interest to engineers, clinical practitioners, and biological anthropologists alike. Spatial statistics is a tool familiar to most public health researchers as a way of analysing geographical data of disease clustering and spread, but is less often applied to biomechanical data. Nonetheless, spatial statistics is a practical approach when working with the two-dimensional topography of the foot in contact with the ground, i.e., geography on a smaller distance scale. In this work we quantified the degree of clustering of the centre of pressure (CoPs) on the foot for peak braking and propulsive vertical ground reaction force (GRF) over multiple, contiguous steps to assess the consistency in the location of peak forces on the foot during walking. The vertical GRFs of eleven participants were collected continuously via a wireless insole system (Moticon ReGo AG) across various speeds and in different experimental conditions (i.e., dedicated treadmill and over-ground walking trials). We hypothesized that CoPs would cluster in the hindfoot for braking and forefoot for propulsion and that braking would demonstrate more consistent clusters than propulsion. Contrary to our hypotheses, we found that CoPs during braking are inconsistent in their location on the foot and CoPs during propulsion are significantly more consistent and clustered than those during braking

across all participants and all trials. These results add to our understanding of the applied forces on the foot so that we can better predict and prevent fatigue failures and better understand the mechanism that shaped the modern bipedal form.

4.2 INTRODCUTION

The portion of the human foot that is in contact with the ground (the sole of the foot) during bipedal walking is the primary point of balance for the body above it, allowing for movement through a variable environment. Yet, the sole of the foot is not a large surface area compared to the rest of the body. During walking, two maxima in ground reaction force (GRF) occur in each step, one associated with braking and one with propulsion (e.g. [1], [2])). While the magnitude of these forces has received considerable attention (e.g. [3], [4]), the location of the centre of pressure (CoP)-- the resultant location of all force applied to the sole-- has been less investigated [5], [6]. GRFs are a fundamental variable in most biomechanical analyses (e.g. [7], [8], [9], [10]), often used to determine joint moments (e.g. 10), but the location where a force is applied is as critical as its magnitude in determining moments which are defined as the application of a force through a distance [11]. Consequently, knowing the location of the CoP of the GRF, because it determines the distance, is important. Further, gait (e.g. velocity) and substrate (e.g. gradient; treadmill vs. overground) characteristics are known to affect force magnitude (e.g. [7], [10], [12], [13], [14]), but their effect, or lack thereof, on CoP location is unknown.

In this study, we determine the CoP location of the peak braking and propulsion vertical GRF for several walking conditions and consider the degree to which the CoP locations are clustered across multiple contiguous steps. Highly clustered CoP locations indicate that biomechanical analyses might draw on data derived from a few steps as most steps are consistent

with others. Less clustered CoP locations point to the need for more steps to be evaluated as the CoP of any particular step could vary substantially from another. We hypothesize that the CoP location of the peak braking GRF is consistently located in the hindfoot while that of peak propulsion is in the medial forefoot (about which we provide more detail below).

4.2.1 *FORCES MATTER FOR MANY REASONS*

The biomechanics of the human foot is relevant to researchers in many fields, including human evolutionary anthropology, biomechanical engineering, and medicine. The derived bipedalism of hominins is of particular interest to evolutionary anthropology because bipedalism is unique among primates and this shift in locomotor behaviour required morphological changes to the musculoskeletal system to accommodate the change in magnitudes and locations of the application of the forces produced during locomotion (e.g. [15], [16]). Understanding the biomechanics of hominin mobility is key to understanding human evolution and the derived morphology of the modern human foot is one of the more substantial differences between the anatomy of modern humans and extant and extinct nonhuman primates. This morphological difference is associated with bipedalism (e.g. [17], [15]). For example, it has been postulated that habitual bipedalism required the development of the non-divergent hallux and a medial arch of the human foot (e.g. [18]). These human features work in tandem to create a relatively stiff lever, a morphological adjustment to the musculoskeletal system directly connected to the locations of the applied forces (e.g. [19], [20], [21]). The locations and magnitudes of applied forces on bony systems have, therefore, evolutionary and ontogenetic impacts on the musculoskeletal system at level of both short (developmental change in the lifetime of an individual) and long-time scales (evolutionary change over millions of years) (e.g. [19], [20], [21], [17]). Through better understanding the locations of peak ground reaction forces during bipedal walking, we gain insight into not only the

function of the foot, but also the form as it has developed over these multiple time scales (e.g. [18], [22]).

The biomechanics of human movement and its consequences for the musculoskeletal system has also been of long-term interest to engineers. For instance, Wolff's Law was inspired by the observations of structural engineer Karl Culmann of human femoral sections produced by his anatomist colleague Hermann von Meyer [23]. Today the biomechanics of human movement is a key component of engineering from ergonomics (e.g. [24]) to medical device development (e.g. [25]) to product design (e.g. [26]). All musculoskeletal elements are impacted by the magnitude and CoP locations of the GRFs that travel through the foot during the gait cycle (e.g. [2], [27], [3]). For instance, the locations and magnitudes of GRFs determine joint moments throughout the weight-bearing system and joint moments influence muscle forces (e.g. [28], [27], [3], [29]). Slight adjustments to the action of the foot during the gait cycle result in broad changes to the rest of the body in motion (e.g. [28], [3]). For instance, bone is not a standard engineered material like steel or reinforced concrete. Bone is strain sensitive—it grows or resorbs due to loads imposed on it—and strains derive from both force magnitude and application location (e.g. Wolff original 1867, reprinted 2010 [33], [34]). Bone remodels based on the magnitudes and locations of applied forces, whether they are internal muscular forces or external applied forces. Conflicting evidence for the level of this sensitivity, however, and whether bone remodels to prevent fatigue failure (chronic, lower-magnitude loading) or more acute failure (higher-magnitude, but more infrequent loading) muddles our current understanding of skeletal morphology ([35], [36]). Highly precise loads, as mentioned above, may change skeletal morphology in ways that differ from changes that result from more diffuse loading patterns. Disentangling these threads requires

information about loading location because a load with an application area that is concentrated is locally higher than that with similar magnitude spread over a greater application area.

The foot is also clinically relevant. In any system, high forces that repeatedly occur in the same location lead to localized fatigue failures that can be catastrophic to the function of the system (e.g. [31]). In the human body, walking constitutes cyclic loading of the dynamic bipedal system (e.g. [32]). Precision in the location of forces on the foot during the gait cycle, in conjunction with extreme force magnitudes, may lead to localized failures of the system, i.e., acute damage to the soft tissue or bone from a traumatic event. Cyclic loading at non-peak magnitudes, or in more diffuse locations on the foot, can also result in a loss of mobility due to pain or injury over longer periods of time (e.g. [32]), even though the musculoskeletal system has, presumably, developed in response to these chronic loads. Nonetheless, foot structure is variable (e.g. arch height ([37]); midtarsal break ([38]); compliance ([39])) with potential impacts on the location of the CoP (e.g. [6]; [5]). Consequently, in order to understand the evolutionary pressures associated with bipedalism, the biomechanical consequences of human mobility, and the effectiveness of medical treatments, understanding the GRFs and associated CoPs of movement over variable terrains, gradients, burden regimes, and speeds is necessary.

4.2.2 *GROUND REACTION FORCES*

The work described herein extends the work of previous walking studies (e.g. [13], [40], [41], [42], [43], [44], [45]) to gather ground reaction force (GRF) data from the foot/surface interaction outside of the confines of the laboratory across multiple, contiguous steps. GRFs reflect the interaction between the foot and the substrate during the stance phase of gait and two peaks in the vertical component of the GRF are typical in walking (Figure 1). The body slows in early stance (the braking period) producing, on occasion, an early transient force spike, then a GRF peak, passes

above the stance foot in midstance with a decrease in the GRF, and accelerates in late stance (the propulsive period) producing another GRF peak. In healthy adults, the vertical force peaks coincide with peaks in the anteroposterior direction that reflect braking and propulsion, but this congruence does not always manifest in children or people with pathologic gait (e.g. [46]; [47]; [48]). GRF magnitude varies with factors that include, but are not limited to, mass of the body in motion, velocity of travel (e.g. [27]), system pathology (e.g. [1]), burdens carried (e.g. [49]), and surface type (e.g. [12]).

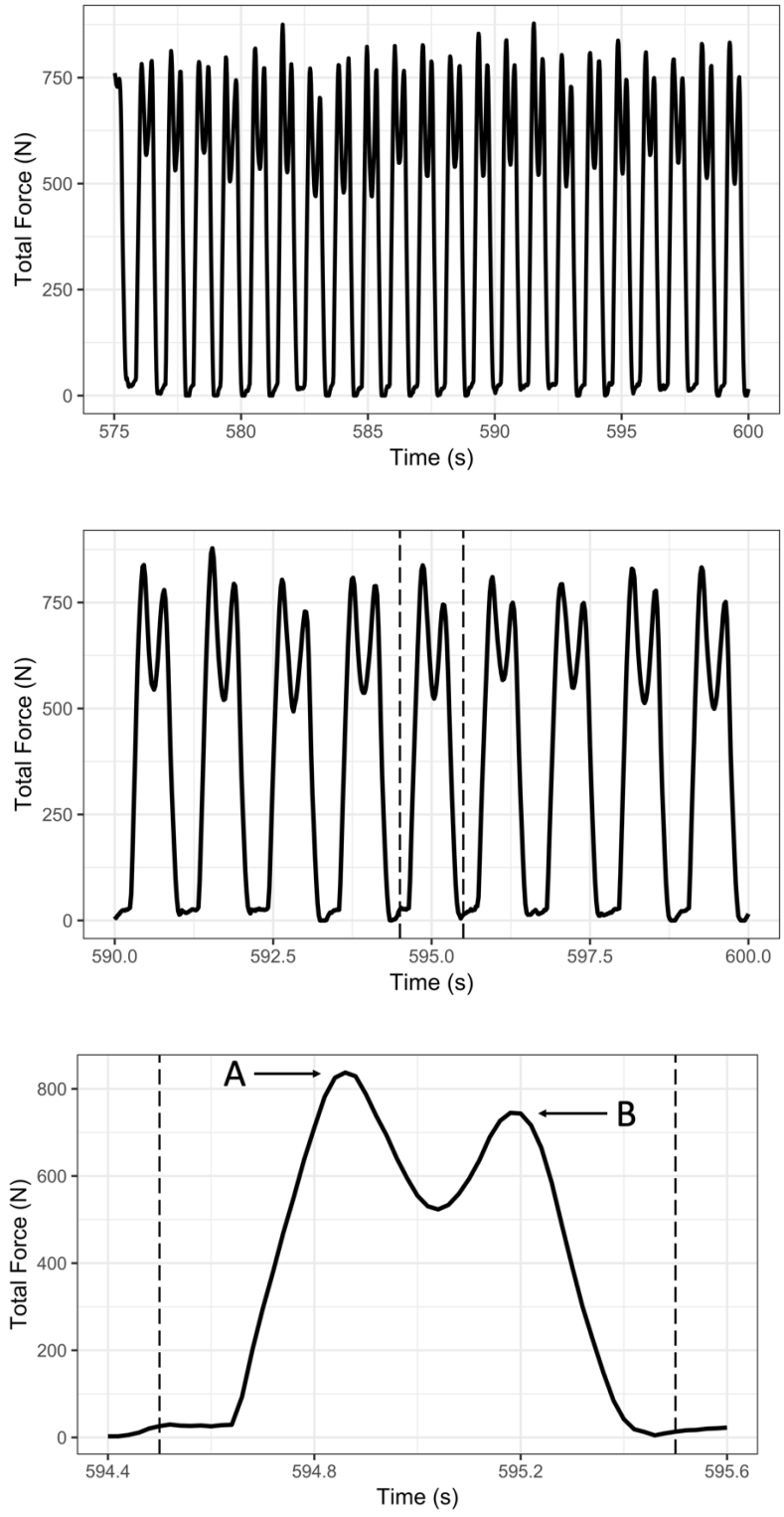

Figure 4.1. Vertical Ground Reaction Forces for Left Foot. Isolated individual left foot steps for one participant (body weight at stance = 812 N) during hallway walking at self-selected velocity.

The vertical force curve for a single foot over the course of the gait cycle. “A” denotes peak vertical force at braking and “B” denotes peak vertical force at propulsion. Dashed lines isolate a single interaction between the foot and the ground, with panels progressively displaying a shorter time frame.

While the variation in GRF magnitude is well-known, the location of the CoP at these peak vertical GRFs, however, is less well established. The heel is typically the first anatomical feature to strike the ground and the toes are the last to leave during a step, but the CoP location when peak vertical (braking and propulsion) force occurs and its consistency of placement is less explored (e.g. [50]). Grundy and colleagues (1975)[5] found that the peak braking vertical GRF occurs when most of the foot is already in contact with the ground, but they were limited by the force plate technology of the time and did not examine in detail the consistency of this placement or whether it varies based on velocity, substrate, or gradient. Croft and Bertram (2020)[6] recently examined the foot-ground interaction during bipedal walking through the lens of bipedal optimization, noting that the CoP, as it travels along the foot, plays an integral role in predicting the overall dynamics of the system. The CoP at peak GRFs indicates where the resultant of the contact forces between the foot and substrate act on the foot during a gait cycle. The CoP at peak GRFs over multiple gait cycles describe the nature of the cyclic loading of the musculoskeletal system. As with any dynamic system, repeated loading patterns play an important part in system design to ensure durability, i.e., these systems are designed for fatigue loading, as discussed above. It is crucial, therefore, that we understand where the CoPs at peak forces occur on the foot, not just over one loading cycle, but over many loading cycles, to fully grasp the system dynamics as a whole and what it implies for human bipedal mobility.

4.2.3 *SPATIAL STATISTICS*

The spatial nature of CoP measurements requires a different methodology than one would use for GRF magnitude data. Spatial statistics is an analytical method for quantifying the distribution of data over a physical region. Most often used in epidemiology or geographical analyses to examine disease events (e.g. [51], [52], [53]), spatial statistics has diverse applications (e.g. tree clusters [54], mineral contents [55], neuron distribution in the brain [56]). Spatial statistics methods are also found in a variety of engineering disciplines (e.g. mechanical engineering [57], geological engineering [58], electrical engineering [59], environmental engineering [60], [61], and petroleum engineering [62]). Applying this methodology to examine point positions of CoP on the sole of the foot is an extension of these problems where we treat the sole of the foot as geography at a smaller length scale.

Pedobarography is the study of the pressure pattern of the sole of the foot during stance or movement (e.g. [63], [64], [65], [66] etc.). Pressure distribution of the GRF drives the biomechanics of the entire body and so has been used to assess the biomechanics of gait (e.g. [21]). Pedobarographic data is also used by clinicians to determine which section of the foot is in contact with the ground in order to assess pathology of movement or investigate the impact of those pathologies on foot mechanics (e.g. [63], [65]). A variety of statistical analysis methodologies have been applied to address the spatiotemporal nature of pedobarographic data, ranging from image analysis techniques (e.g. [64]) to statistical parametric mapping (e.g. [67]) in addition to more simplified analyses of the magnitude of pressures (e.g. [68]).

This project developed from our interest in the consistency of the location of CoPs across many loading cycles and conditions (e.g. speeds, terrains, and gradients). Modern humans do not move only at a single speed along flat surfaces, and we wanted to capture any potential for

variability along different terrains and at different speeds. Most pedobarographic work relies on pressure pads or force plates set into the floor to capture participant data (e.g. [65], [66], etc.). This approach restricts researchers to collecting a few steps over the course of several trials, which increases the potential for variability across trials. By utilizing wireless, pressure-sensing insoles (Moticon ReGo, Munich, Germany), we were able to collect CoP data over multiple, contiguous steps for all participants and all trials both within and outside of the confines of the laboratory. We used Ripley's clustering K-Function [69], [70] to quantify the consistency of CoP location during the peak braking and peak propulsive vertical GRFs. To our knowledge, this work is the first to apply spatial clustering analyses to look at the consistency of CoP on the foot during multiple, contiguous gait cycles across different terrains and at different speeds.

4.2.4 *HYPOTHESES*

Feet are the primary point of contact with the environment and subject to the cyclic forces of locomotion from heel strike to toe off. The applied loads to the hindfoot react directly into the tibia through joint (tibiotalar) contact, forming a stable, compressive column, while loads applied to the forefoot (e.g. loads applied under the metatarsal heads) rely on the mid- and forefoot (which form the longitudinal arch) to act as a rigid, cantilevered beam. Given that this beam is composed of numerous bones linked by ligaments and the action of muscles, some flexibility in the arch is possible. Based on these mechanical considerations, we predict that the location of the CoP will be consistently clustered in the hindfoot for the braking peak and consistently in the forefoot for the propulsion peak across all conditions and all participants. We also predict that there will be no difference in degree of clustering, as assessed by Ripley's K-Function, of CoP points between braking and propulsion within trials.

4.3 METHODS

4.3.1 *PARTICIPANTS*

The data were collected from a convenience sample of eleven participants (six females and five males) ages 20 to 42 years (Table 1), who were without gait pathology or injury to their lower limbs within the last 2 years. We measured their mass (kg) with a standard scale and calculated a neutral stance force, which was equal to the sum of the force exerted on both insoles while the participant stood quietly. Arch index (AI) was calculated as the ratio of midfoot area to total foot area during quiet standing ([72]) from footprints for each participant obtained from a pressure mat (RSscan International, Olen, Belgium).

Participant	Age	Mass (kg)	Neutral Standing Force (N)	Insole Size	Arch Index	Hallway (m/s)	Downhill (m/s)	Uphill (m/s)
X1	26	70.2	868	8/9	0.244	1.43	1.52	1.51
X3	29	86.4	819	9.5/10.5	0.182	1.24	1.5	1.56
X4	20	120	1176	11/12	0.424	1.29	1.49	1.36
X5	21	70.7	692.9	8/9	0.235	1.2	1.43	1.52
X6	28	52	509.6	6.5/7.5	0.252	1.15	1.32	1.46
X7	42	86	842.8	9.5/10.5	0.249	1.24	1.41	1.39
X9	29	55	539	6.5/7.5	0.128	1.12	1.28	1.34
X10	20	48.9	479.2	6.5/7.5	0.089	1.11	1.5	1.33
X11	32	72.9	714.4	8/9	0.162	1.15	1.34	1.24
X12	21	54.6	535.1	6.5/7.5	0.159	1.24	1.39	1.47
X13	32	66.5	651.7	8/9	0.349	1.23	1.47	1.52

Table 4.1. Participant data, including average self-selected velocities for the over-ground walking trials.

4.3.2 *EXPERIMENTAL SETUP*

Each participant was fitted with a pair of Moticon ReGo AG, Munich, Germany wireless pressure-sensing insoles worn in a pair of Fitkicks™ water socks. We used the water socks to limit the effect of variability in shoe sole stiffness and obtain a condition as close to unshod as possible. Thirteen force sensors are distributed across the insole surface and were set to collect data at 50Hz (i.e., every 0.02 seconds). Each sensor recorded a force value at each timepoint. The total force summed across the sensors and the centre of pressure (CoP) X (medial-lateral) and Y (posterior-anterior) coordinates were also determined at each timepoint. The insoles were calibrated through the Moticon ReGo AG software and checked by the researchers to ensure tare had been reached before being donned by the participants. Each participant's mass was recorded using a tared laboratory scale and the insole force reading was compared to the scale reading. The insole's CoP sensitivity falls within +/- 20mm, according to the company's specifications, and has been validated against a force plate system in prior work [73].

We investigated seven walking conditions. Participants walked on a treadmill at 0.89m/s ("slow"), 1.34m/s ("moderate"), and 1.79m/s ("fast") for 60 seconds at each velocity. The order of these treadmill tests was randomized. Participants then walked on the treadmill set to a 10% slope at 0.89m/s. Participants also walked at their comfortable pace along a straight, flat, 78.4m indoor hallway. Lastly, participants walked at a self-selected pace in a straight line on an outdoor sidewalk, downhill and uphill over 70.5m on an 8.8% slope in dry conditions. Research personnel ensured that the hallway and outside paths were unobstructed during the trials. This project was approved by the University of Washington Institutional Review Board.

4.3.3 *DATA ACQUISITION AND INITIAL PROCESSING*

We isolated individual steps for each trial from the total force for the left and right foot of each participant (Figure 1) and determined the local force maxima for the braking and propulsive phases of stance from each step using a custom written MATLAB (MathWorks) program. We removed steps with fewer or more than two peaks as indicative of non-normal (e.g. “stumble”) steps. 6711 steps were analysed across all participants and all trials.

We standardized the X and Y coordinates of the Centre of Pressure (CoP) to account for insole size differences between participants by multiplying by the insole scaling factor provided by manufacturer Moticon ReGo AG. This normalized all participants to the size 8/9 insole coordinate system. In our initial exploration of the data, we found no indication of left-right asymmetries for any of our participants; therefore, the signs on the X coordinates were flipped for the right foot to match the left foot coordinate world. We compared the position of the CoP during the braking and propulsive phases between conditions and between individuals in each condition. We calculated the individual velocities for each participant’s hallway, downhill, and uphill trials from time and distance travelled.

To ensure that the disparity in the number of datapoints between trials did not impact our analysis, we normalized the number of steps in each trial. Slow treadmill walking had 572 steps total, the fewest across our trials, so we took a random sample without replacement of 572 steps from each of our trials.

4.3.4 *STATISTICAL ANALYSIS*

Ripley’s second-order intensity function, $K(d)$, is a method of quantifying clustering [69], [70], [51], [71] and is derived from Ripley 1987 [70] as:

$$K(d) = \frac{\Sigma[number\ of\ further\ events\ within\ distance\ d\ of\ an\ arbitrary\ event]}{\lambda}$$

Where λ is the intensity, or average number of points (n) within a unit area. The formal estimation of the K-Function is described mathematically as:

$$\widehat{K}(d) = \frac{1}{\hat{\lambda}} \sum_{i=1}^{n} \frac{1}{n} \sum_{j \neq i} binary\ indicator\ 1\ if\ (d_{ij} \leq d)$$

Where d_{ij} is the distance between points i and j.

Ripley's K-Function (*K(d)*) is dependent on the number of events within a distance (*d*, in metres), or in this case, the number of CoP point occurrences within a certain distance. If the peaks exhibit complete spatial randomness (CSR), i.e., no discernible clustering, *K(d)* will be approximately equal to ($\pi \cdot d^2$), but if the data are clustered, then we expect *K(d)* > ($\pi \cdot d^2$) for small *d*. From this estimator we can quantitatively compare clustering at a given d between trials as well as between braking and propulsion peaks within a trial to determine consistency of location of CoP points.

4.3.5 *DEFINING SIGNIFICANCE IN SPATIAL CLUSTERING*

We utilized Monte Carlo sampling to establish a baseline variability for our *K(d)* estimation by generating 100 simulations of CSR sets of 572 points. CSR points were generated within the insole polygon boundary using the R packages 'lattice' [74] and 'spatstat' [71]. These generated points form the 95% pointwise simulation envelopes, or "acceptance envelope". We used these CSR

points as our Null *K(d)* to assess clustering for braking and propulsion in each trial. A high degree of clustering, i.e., a *K(d)* value falling above our 95% pointwise acceptance envelopes for a given *d*, indicates consistent CoP placement recurring over multiple gait cycles. Values that fall within the acceptance envelope for a given d are considered non-significant; values that fall outside of the acceptance envelope are considered significant [71].

In order to compare the CoP point patterns between trials, we adapted the methodology typically used to compare the spatial location of case versus control points in public health and epidemiology studies (e.g. [51]), which applies binary marks (e.g. 1=case, 0=control) to each set of points. This enables direct assessment of the clustering in one group of points compared to the other. In our adaptation, we performed pairwise comparisons for all trials; essentially labelling one trial as "cases" and the other as "controls" in each analysis. We analysed between all trials for CoP at peak braking and between all trials for CoP at peak propulsion. We also compared the clustering of peak braking and propulsion CoP points within each trial.

We used the Monte Carlo method for generating our acceptance envelope in each pairwise comparison by randomly re-labelling the points in the two trials over the course of 100 simulations per pairwise comparison [71]. For example, in the pairwise comparison of Slow versus Moderate Treadmill walking, each CoP point during braking was randomly relabelled as either Slow or Moderate to establish the Monte Carlo envelope boundaries. If the difference in *K(d)* between the two trials was outside of that envelope, we determine that the level of clustering between the two trials is significantly different.

Since all participants performed all trials, our covariates were limited to the differences in each trial's velocity, surface type, and gradient. As described above, we define statistical significance for this analysis as values outside of the simulated Monte Carlo acceptance envelopes,

as this is the relevant statistical test for this methodology [71]. For all analyses, values that fall within the acceptance envelope are considered non-significant, values that fall outside of the acceptance envelope are considered significant. For further discussion of Ripley's K-Function as well as Monte Carlo acceptance envelopes for determining significance, please refer to Baddeley et. al. 2015 [71].

Note that the *K(d)* values of trials with CoP points that are similarly distributed will be approximately equal across all values of d, and the difference in *K(d)* will fall within the acceptance envelope (i.e. there is no significant difference (as defined above) in *K(d)* values [71]). For trials where the CoP point distribution is significantly dissimilar (i.e., one trial is very clustered with a high *K(d)* and the other trial has a more diffuse point distribution), the difference in *K(d)* will fall outside of the acceptance envelope. In the case of a large difference in *K(d)* between compared trials, when the d increases beyond the point range of the more clustered trial, *K(d)* falls to zero (because there are no CoP points remaining outside d for that trial), and the difference in *K(d)* between trials is the value of *K* at distance d of the less clustered trial. The difference in *K(d)* between trials, then, is significantly different if it is outside the acceptance envelope in either the positive or negative direction [71].

Using the foot segmentation described above (forefoot, midfoot, hindfoot), we calculated the percentage of CoP points in each region during peak braking GRF and peak propulsive GRF for each trial by dividing the number of CoP points in each region by the total steps in each trial. To assess whether or not a relationship exists between the number of points in a foot region and participant characteristic (e.g. AI), we fit generalized linear models and we accounted for the hierarchical groupings of trial and participant in all analyses.

We used an assortment of RStudio packages in our analyses. These included: lattice, ‘sp’ [75], ‘splancs’ [76], ‘spatstat’ [71], ‘lme4’ [77], and ‘uwIntroStats’ [78].

4.3.6 *SAMPLE AREA*

The boundaries (edges) of the sample area were provided as coordinate points for a size 8/9 US (42/43 UK) insole by Moticon ReGo AG. These points were then converted into a spatial polygon and the insole data points were generated within this boundary using the R packages ‘lattice’ [74] and ‘spatstat’ [71]. We determined that, based on the distribution of points across all trials and the lack of points outside of the sample area, it was not necessary to account for edge effects. None of the CoP points for braking or propulsion for any of the trials were close enough to the edge of the insole to warrant concern regarding edge effects in the analyses and each insole was fit to entirely contain the participant’s foot.

We partitioned the insole into hindfoot, midfoot, and forefoot based on anatomical landmarks. The hindfoot consists of the calcaneus and talus from the posterior heel to the anterior calcaneocuboid joint, which is approximately 38% of the total length of the foot. The midfoot consists of the other tarsals, assessed medially from the navicular tuberosity to the base of the first metatarsal and laterally from the calcaneocuboid junction to the fifth metatarsal tubercle, which is approximately 10% of the total length of the foot. The forefoot consists of the metatarsal and phalangeal systems, medially from the base of the first metatarsal, laterally from the tuberosity of the fifth metatarsal, to the distal phalanges, which is approximately 52% of the total length of the foot. We obtained the proportions of total foot length in each part of the foot by measuring the distances between palpable landmarks. We then applied these proportions for all subjects.

4.4 RESULTS

Based on the *K(d)* estimation, CoP points during peak braking and peak propulsion for each trial display clustering relative to the simulated CSR. The difference between the estimated *K(d)* value for braking and propulsion lies outside of the Monte Carlo acceptance envelope for all trials for $d \leq 0.2$ m. The estimated *K* value for propulsion is greater than the estimated *K* value for braking for all trials, meaning that propulsion peaks are more tightly clustered than braking peaks. The *K(d)* clustering comparison between *K(d)* of braking and *K(d)* of propulsion for the hallway walking trial is shown in Figure 2 as an example of these results. The full graphical results of our clustering analysis for each trial are included in the SI. A difference in *K(d)* (indicated with blue circles) outside the acceptance envelope (indicated by the grey lines in Figure 2) indicates significant clustering. Overall, there are also more pairwise differences in clustering during braking than there are for propulsion.

Panel A

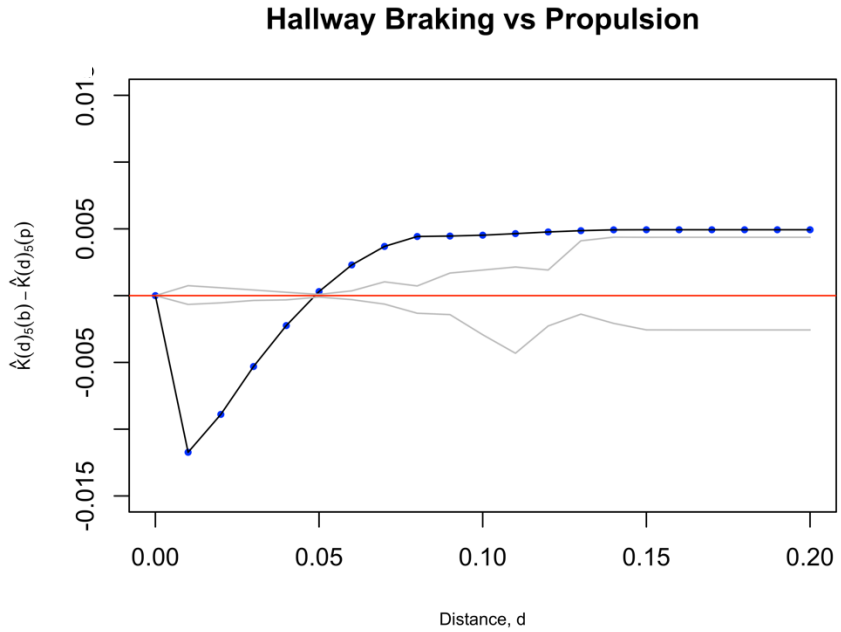

Panel B

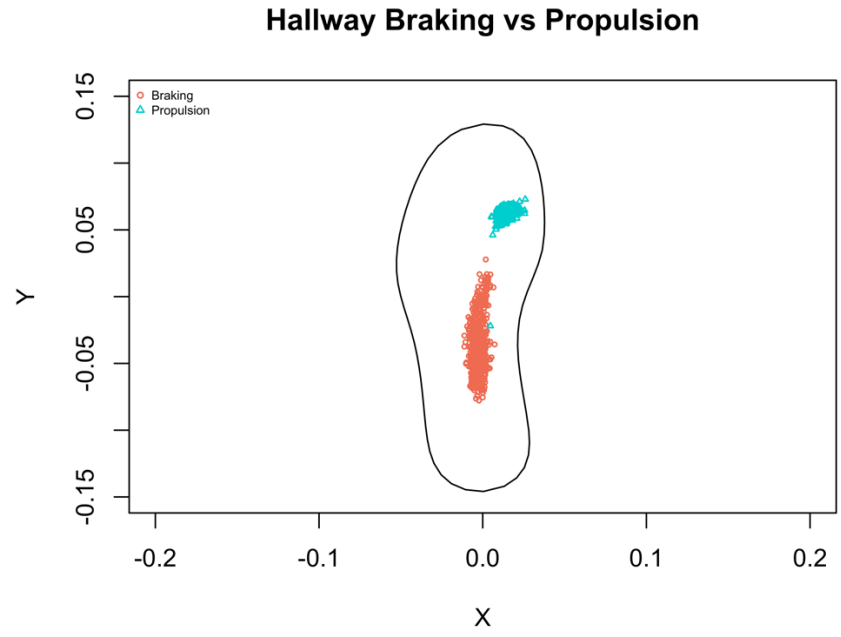

Figure 4.2. K-Function Estimation for Hallway Braking Compared to Propulsion. The solid black line with blue points in panel A shows the difference in *K(d)* clustering values between braking centre of pressure (CoP) points and propulsion CoP points at each tested distance (*d*,

metres). The red line represents no calculable difference in *K(d)* values, and the grey lines denote the Monte Carlo acceptance envelope if there was no significant difference. There is significantly more clustering in CoP points during propulsion than braking (*K(d)* propulsion > *K(d)* braking), so the black line falls outside of the acceptance envelope for distances within the insole area. Panel B shows the CoP points for braking (red) and propulsion (teal) for all participants during the Hallway walking trial.

Table 2 shows the percent of CoP points in each region of the foot at peak braking GRF and peak propulsive GRF across all participants and all steps. The CoP at peak braking GRF was located in the hindfoot for all trials except downhill walking. Uphill walking, in contrast, demonstrated the most consistent CoP location during braking. The CoP points at peak propulsive GRF were consistently located in the forefoot for all trials.

	% of CoP Points at Braking	% of CoP Points at Propulsion
Slow Treadmill		
Forefoot	23.2	**99.8**
Midfoot	24.4	0
Hindfoot	**52.4**	0.2
Moderate Treadmill		
Forefoot	15.1	**100**
Midfoot	39.5	0
Hindfoot	**45.5**	0
Fast Treadmill		
Forefoot	8.4	**100**
Midfoot	44.7	0
Hindfoot	**46.9**	0
Incline Treadmill		
Forefoot	13.9	**99.9**
Midfoot	18.3	0
Hindfoot	**67.8**	0.1
Hallway Walking		
Forefoot	11.9	**99.8**
Midfoot	42.6	0.2
Hindfoot	**45.5**	0
Downhill Walking		
Forefoot	46.8	**99.9**
Midfoot	**49.7**	0.1
Hindfoot	3.5	0
Uphill Walking		
Forefoot	4.5	**99.9**
Midfoot	25.3	0.1
Hindfoot	**70.2**	0

Table 4.2. Percent of CoP points located in each region (fore, mid, or hind) of the foot during peak braking GRF and peak propulsive GRF for each trial across all participants.

Across all steps for all trials and all participants, less than 0.2% of CoP points at peak propulsive GRF were located elsewhere on the foot. Our results indicate that braking is a less consistent

mechanism than propulsion. On the one hand, CoP points at peak braking, while clustered for all trials, are in the hindfoot only 47.4% of the time (Figure 3).

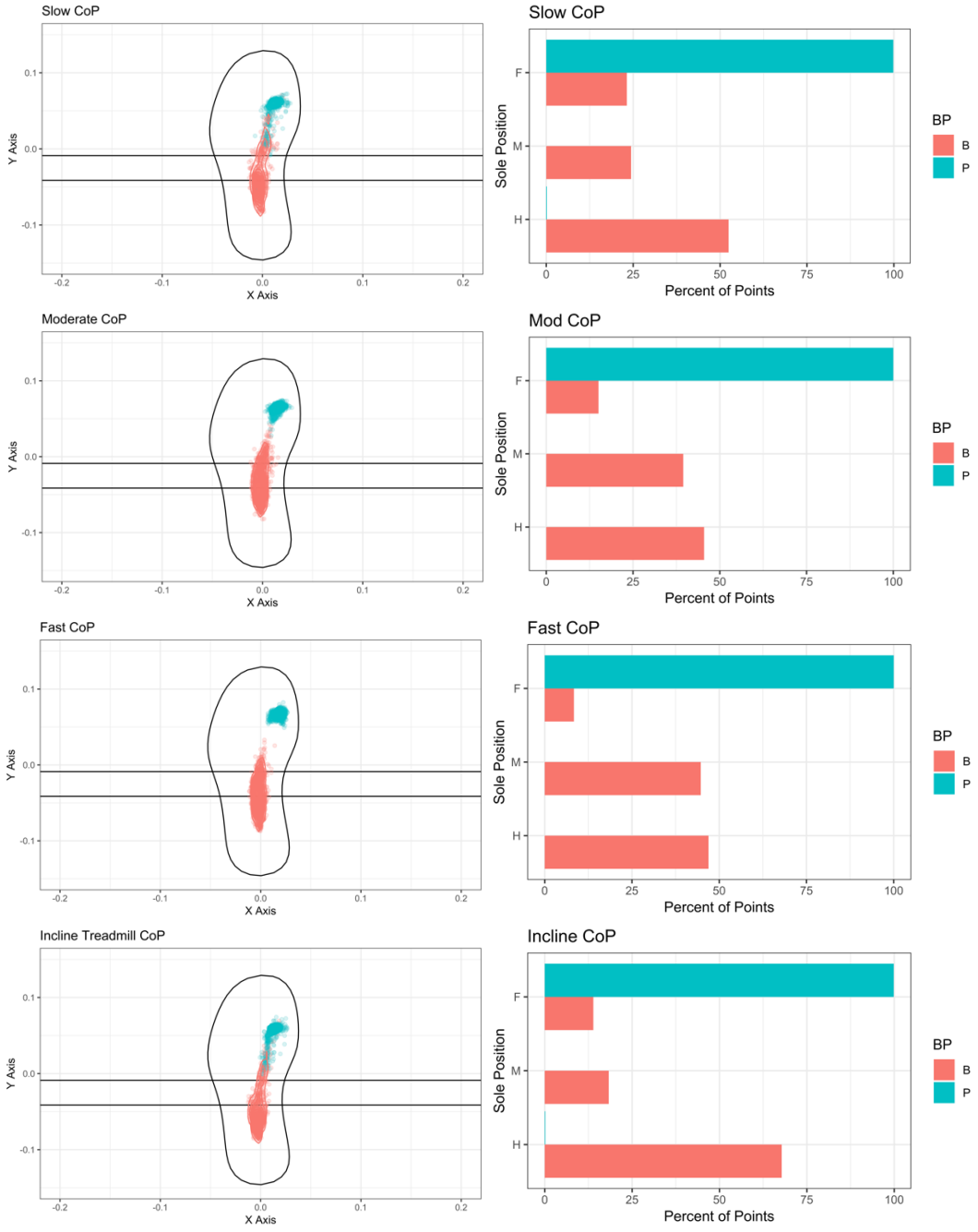

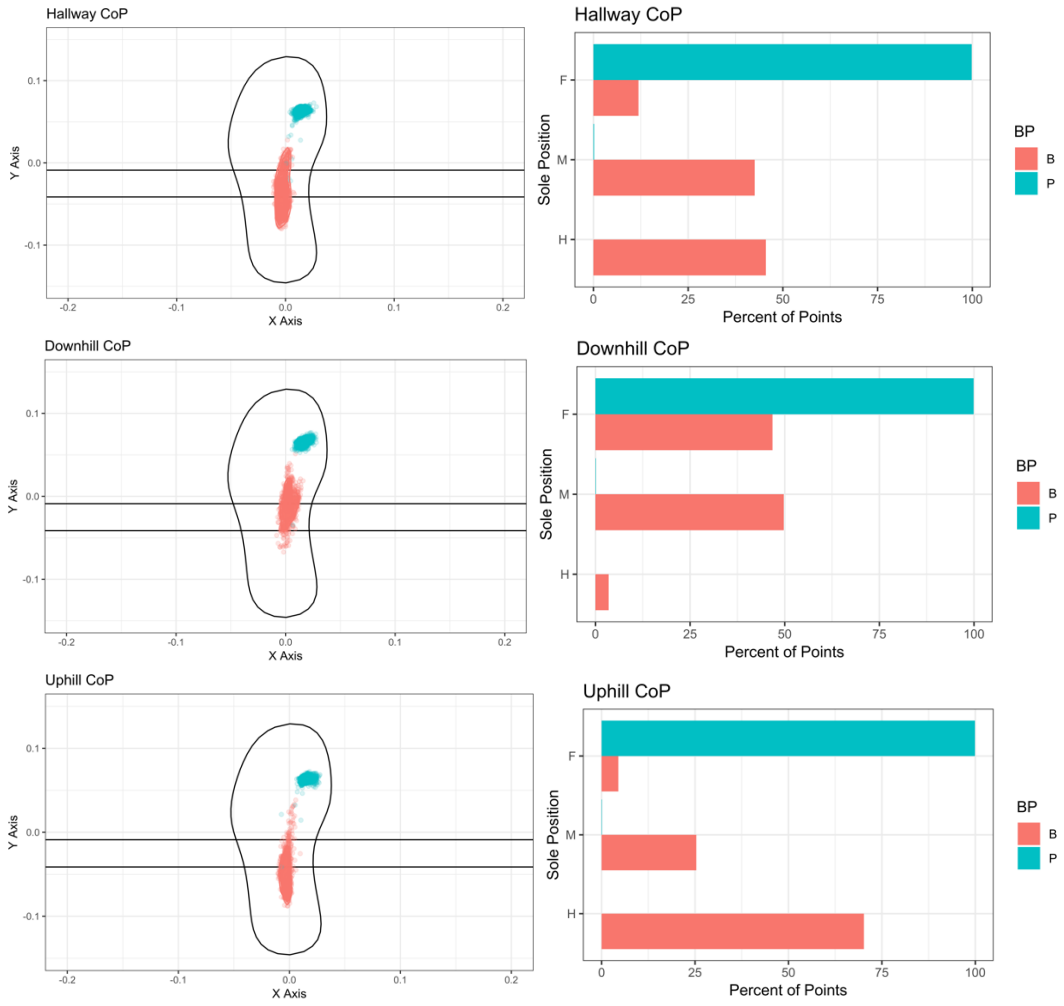

Figure 4.3. Centre of Pressure Points and Corresponding Percentage Graphs for Each Walking Trial. Left column: CoP points at peak braking GRF (red) and propulsion GRF (blue) plotted with lines demarcating fore- (F), mid- (M), and hindfoot (H). Right column: the corresponding breakdown of the percent of points in each region.

CoP at peak propulsion, on the other hand, occurs in the forefoot 99.9% of the time across all trials (Figure 3). Analysing these results by individual reveals the same pattern (Figure 4). Although participants do vary somewhat in the location of their CoP, we found no significant effect of AI or other individual-specific characteristic, so those analyses are not shown.

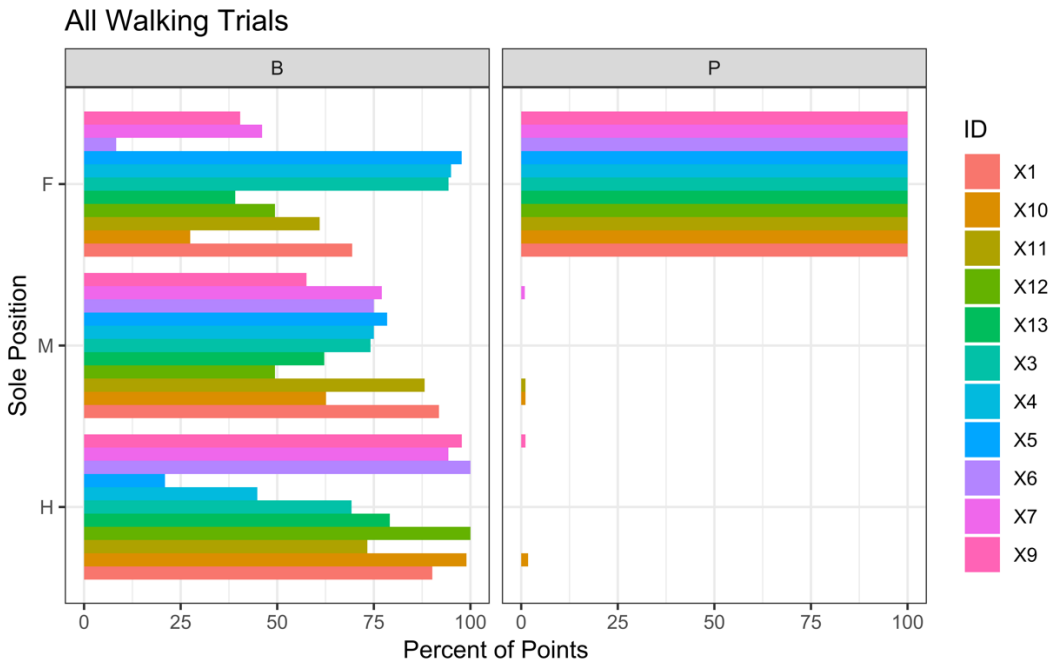

Figure 4.4. Percent of Centre of Pressure Points by Individual – All Walking Trials. The percent of CoP points in each region of the foot (F = forefoot, M = midfoot, H = hindfoot) for all trials, broken down by participant (ID) for braking (column B) and propulsion (column P).

4.5 DISCUSSION

Our goal in conducting this research was to quantify the spatial location and consistency of centre of pressure (CoP) on the foot during peak force application while walking, specifically, during the braking and propulsion components of the gait cycle. To accomplish this, we examined the location of the CoP during peak braking and peak propulsive vertical GRF to determine the clustering pattern of CoP over repeated gait cycles using Ripley's K-Function. We also quantified the effect of different terrains and walking speeds on CoP location and consistency of placement. Although we could draw initial qualitative conclusions based on our visual assessments of the CoP locations on the foot and consistency both within and across gait cycles, we confirmed

quantitatively with Ripley's K-function that our qualitative observations were statistically significant. No researchers, to our knowledge, have utilized clustering analyses from spatial statistical methodologies to assess the consistency of the spatial component of centre of pressure points across multiple, contiguous steps during human walking.

The magnitude and locations of the forces that occur on the foot during habitual movements, e.g. walking, influence the joint moments throughout the musculoskeletal system (e.g. [27]), the potential for fatigue failures at locations of precise, cyclic forces (e.g. [32]), and evolution of human morphology (e.g. [18]). As non-pathological walking along an unobstructed pathway is a consistent, cyclic movement our participants perform daily, we expected the locations of the CoP at peak vertical forces (braking and propulsion) to be relatively consistent across gait cycles. The applied loads to the hindfoot (calcaneus and talus) can react directly into the shank (tibia) through joint (tibiotalar) contact, essentially creating a stable, compressive column. Loads applied to the distal foot rely on the mid- and forefoot to act as a cantilevered beam. Given that the hindfoot load path is much stiffer than that of the forefoot, we expected that the CoP during peak braking would be clustered consistently in the hindfoot, with the potential for shifting proximally towards the midfoot along gradients. We expected CoP at peak propulsion to occur primarily in the forefoot, but, due to the flexibility of the foot, we expected to see CoP spread across the first and second metatarsal heads across gait cycles and participants.

Previous work has examined the locations and magnitudes of peak pressures on the foot during walking (e.g. [79], [63], [65], [80], [66], [81], [82], [5], etc.), but the consistency of these locations over multiple gait cycles has been less documented. In our initial exploration of the CoP data we noted that, visually, CoP points at peak propulsion were consistently concentrated in the forefoot, with few outliers (Figure 3). In contrast, the CoP points at peak braking were diffuse

across the foot (Figure 3). As this was contrary to our initial expectations, we sought to quantify these qualitative observations. Evaluating the spatial clustering of CoP points over multiple gait cycles using spatial clustering affirmed our qualitative observations regarding the precision or diffusion of CoP at peak forces on the foot. This, in turn, adds to our understanding of where peak cyclic loads occur on the foot and, therefore, throughout the musculoskeletal system. For example, the role of the lateral midfoot in transferring the braking peak from the substrate to the body may be underappreciated (although variability in pressures exerted by the lateral foot is documented (e.g. [39]; [38])), which suggests that additional investigation of the lateral foot is warranted. In addition, the lack of consistency in the location of the braking peak has potentially important implications for biomechanical analyses: a small number of steps may be insufficient to capture the full range of lower limb joint moments at the braking peak of the GRF. Although we did not evaluate the shape of the vertical GRF curve, it seems reasonable to extrapolate that the entire first half of stance may not have a consistent pattern of location of the CoP. The location of the CoP of the propulsive vertical GRF peak was remarkably consistent (Figure 4). This consistency was apparent even in the participant with the lowest arch (participant X4), potentially indicating that a low AI does not impact the foot's ability to act as a lever during propulsion. Future work should explore the relationship of foot stiffness and its impact on GRF magnitude and location.

The advantage of using Ripley's K-Function [69], [70], [51], [71] to quantify spatial clustering is that it allowed us the flexibility to assess the clustering of point data from single trials as well as pairwise point dataset comparisons of clustering. If there was no significant difference in clustering in a pairwise comparison, the difference in $K(d)$ values between the pairs ($K_1(d) - K_0(d)$) would lie within the acceptance envelope. Our primary analysis compared the clustering of CoP points at peak braking GRF to the clustering of CoP points at peak propulsive GRF. We found

that the difference in the estimated *K(d)* value between baking and propulsion lay outside of the acceptance envelope for all trials. The estimated *K* value for propulsion is greater than the estimated *K* value for braking for all trials, which indicates that propulsion is significantly more clustered than braking for all trials.

We also calculated the percentage of CoP points in each region of the foot (fore, mid, hind) and confirmed that braking is a more variable mechanism. CoP points at peak braking, while clustered for all trials, were in the hindfoot only 47.4% of the time across all trials and in the midfoot 34.9% of the time across all trials (Table 2). CoP during peak propulsion occurred in the forefoot 99.9% of the time across all trials. Across all steps for all trials and all participants, less than 0.2% of CoP points during peak propulsive GRF were located elsewhere on the foot. CoP during peak propulsion was tightly clustered around the medial forefoot (e.g. the heads of the first and second metatarsals). This consistency is striking and offers insight into the forces as they are applied to the foot and, subsequently, the body as a dynamic system. Peak braking forces that load the foot and, therefore, the rest of the body, were more diffuse over the course of many gait cycles, suggesting less potential for fatigue failures to localized areas of the hind and midfoot over cyclic loading cycles compared to the forefoot and potentially suggesting more variability in load transfer through the leg. With peak vertical GRFs during propulsion falling consistently under the heads of the medial metatarsals, it is unsurprising that pathologies are frequent in this region (e.g. [32]).

We found less variability in CoP location during peak braking when we examined the trial data by participant (Figure 4), but there was still more variability in an individual's braking CoP than in an individual's propulsive CoP. The consistency in CoP location during propulsion within individuals was equally pronounced within individuals as across individuals. While the data reveal some structuring by participant (Figure 4), we found no predictive metric for this structure. Arch

index was assessed as a covariate in the statistical models, but was not found to be a statistically significant predictor of clustering or location of CoP on the foot during braking or propulsion. While one participant had a low arch (AI = 0.4), no one exhibited a high arch (AI =0), so this sample is not an ideal one with which to evaluate the potential of AI to influence the location of the CoP. This limitation warrants future exploration of foot morphology (e.g. AI, midtarsal break, medial column divergence) that may influence the location of CoP during peak braking GRF. Future work should also increase the power of these metrics by recruiting participants based on aspects of foot shape. Another limitation was our use of water socks to hold the insole in place against the foot. While we used the socks as a best approximation of barefoot walking in order to gather data across multiple, contiguous steps outside of the laboratory, future work should include comparative, fully barefoot trials along a force plate or pressure pad walkway. Future work also should investigate consistency in peak force location at other times in the gait cycle, such as the point immediately after heelstrike where lower-magnitude, but high impact, transient forces that can occur at initial heel contact [83], [84].

Although we did not extend our hypotheses and statistical analyses to specific circumstances, many debates in various fields might potentially be informed by our results, so we note several here. The following examples are not meant to be exhaustive, but rather demonstrative. First, discussions of the evolution of the hominin foot have assumed that a pronounced longitudinal arch (e.g. rigid foot) is a requirement for effective propulsion ([18]; [85]; [86]) , even if the arch is achieved through facultative muscular contraction ([87]). Our results, as mentioned above, indicate that it is possible that a foot with a low arch, which is, presumably, less rigid ([18]), exhibits the same consistency in CoP location at peak propulsion vertical GRF as a

higher arched foot. This suggests that future work should examine the relationship among foot stiffness, GRFs, and CoP locations to understand the role of the longitudinal arch in walking.

Another, more clinically-applied, area which might be informed by our results is prosthetic design. Insights from considerable effort to understand such gait-based topics as the importance of weight acceptance (e.g. [88]) and of prosthetic foot stiffness (e.g. [89]) for performance has been used to guide prosthetic design. Nonetheless, lower limb prosthetic design has still failed to reach parity in performance across multiple mobility tasks with that of the natural limb (e.g. [90]; [91]; [92]). Braking and propulsive efforts are known to differ (e.g. [93]) and gait deviations in amputees are common (e.g. [90]). Timmermans and colleagues (2018)[94] has demonstrated the usefulness of insoles for determining gait temporal parameters in amputees, but less work has been directed at understanding the role of the variability in CoP location on lower limb biomechanics in amputees. Our work establishes a baseline of expected variability in CoP location in natural limbs that can be used comparatively with prosthesis-ground interactions and that may assist in identifying prosthetic design choices to minimize gait asymmetries between a prosthetic and natural limb.

Finally, while musculoskeletal modelling has become widespread, the inputs frequently include less than a dozen steps even in work designed to understand the impact of variability on the gait metric of interest (e.g. [95]; [96]). Our results suggest that while appropriate for the propulsion portion of stance, evaluation of a limited number of steps is not sufficient for the braking portion of stance because the location of the CoP varies even though the magnitude of the GRF may not. We found these inconsistencies in braking by measuring CoP location over a minimum of 574 steps per individual.

4.6 CONCLUSION

The dynamic, bipedal system that is the human body is complex. Movement through the environment is a foundational part of this dynamic system, and humans devote a large proportion of their energetic resources to this function (e.g. [29], [30]). Understanding the dispersion of peak forces on the foot is crucial to understanding bipedal movement in modern humans and informs our understanding of human morphology within the lifetime of an individual and across evolutionary history (e.g. [18], [22]). The feet of bipeds are the primary point of contact with the environment and subject to the forces that constitute self-propelled locomotion. The forces associated with the interaction of the human body with the environment through the foot dictate how this movement occurs. While a stable braking mechanism may be helpful, our work indicates that it is not, and therefore does not have to be, a precise mechanism in healthy adults. The consistency of CoP at the peak propulsion suggests that this is the mechanism that is precise, whether due to a requirement for efficiency of forward movement, by necessity for stability, or for other reasons. The consistency also implies that the joint moments during peak propulsion are more consistent throughout the weight-bearing system.

Our results regarding the inconsistency of the CoP at peak braking, combined with consistency at peak propulsion, have implications for understanding the evolution of the foot, for its treatment after trauma, and for prosthetic design. Engineered systems see localized fatigue failures when subjected to high magnitude, precise cyclic loading (e.g. [31]), and the human body is no different (e.g. [32]). The engineering of the foot, both in material composition and form, reflects the need of the system to endure high, contained forces over a small area throughout a human lifespan. By understanding the locations and magnitudes of the forces on the system, we can not only better predict and prevent fatigue failures of the system before they become

catastrophic, but we can also better understand the mechanism that has shaped the bipedal form with which we are familiar today.

4.7 REFERENCES

1. Perry J. Gait Analysis: Normal and Pathological Function. 1992. https://doi.org/9781556421921
2. Inman VT. Human locomotion. 1966. Clin Orthop Relat Res. 1993 Mar;(288):3-9. PMID: 8458148.
3. Cavagna GA, Margaria R, Mechanics of walking., J. Appl. Physiol. 1966; 21:271–278. https://doi.org/10.1152/jappl.1966.21.1.271.
4. Wei F, Crechiolo A, Haut RC, Prediction of ground reaction forces in level and incline/decline walking from a multistage analysis of plantar pressure data, J. Biomech. 84 (2019) 46-51. https://doi.org/10.1016/j.jbiomech.2018.12.015.
5. Grundy M, Tosh PA, McLeish RD, Smidt L. An investigation of the centres of pressure under the foot while walking. J Bone Joint Surg Br. 1975 Feb;57(1):98-103. PMID: 1117028.
6. Croft JL, Bertram JEA. Form in the context of function: Fundamentals of an energy effective striding walk, the role of the plantigrade foot and its expected size. Am J Phys Anthropol. 2020 Sep 15:e24122. doi: 10.1002/ajpa.24122. Epub ahead of print. PMID: 32932555.
7. Nilsson J, & Thorstensson A. Ground reaction forces at different speeds of human walking and running. Acta Physiologica Scandinavica, (1989) 136(2), 217–227. https://doi.org/10.1111/j.1748-1716.1989.tb08655.x
8. Jung Y, Jung M, Lee K, Koo S. Ground reaction force estimation using an insole-type pressure mat and joint kinematics during walking, J. Biomech. 47 (2014) 2693-2699. http://dx.doi.org/10.1016/j.jbiomech.2014.05.007.
9. Warabi T, Kato M, Kiriyama K, Yoshida T, Kobayashi N. Treadmill walking and overground walking of human subjects compared by recording sole-floor reaction force, Neurosci. Res. 53 (2005) 343–348. https://doi.org/10.1016/j.neures.2005.08.005
10. Wang X, Ma Y, Hou BY, Lam WK. Influence of Gait Speeds on Contact Forces of Lower Limbs. J Healthc Eng. 2017;2017:6375976. doi: 10.1155/2017/6375976. Epub 2017 Jul 9. Erratum in: J Healthc Eng. 2018 Jul 18;2018:9291423. PMID: 29065630; PMCID: PMC5523200.
11. Johnston ER, Mazurek DF, Beer FP, Eisenberg ER. (2010). Vector Mechanics for Engineers: Statics. Singapore: McGraw-Hill.
12. Pandolf KB, Haisman MF, Goldman RF. Metabolic Energy Expenditure and Terrain Coefficients for Walking on Snow, Ergonomics. 19 (1976) 683–690
13. McIntosh AS, Beatty KT, Dwan LN, Vickers DR. Gait dynamics on an inclined walkway, J. Biomech. 39 (2006) 2491–2502. https://doi.org/10.1016/j.jbiomech.2005.07.025.
14. Björklund G, Swarén M, Born DP, Stöggl T. Biomechanical adaptations and performance indicators in short trail running, Front. Physiol. 10 (2019) 1–10. https://doi.org/10.3389/fphys.2019.00506.
15. Lovejoy CO. The natural history of human gait and posture. Part 1. Spine and pelvis. Gait Posture. 2005 Jan;21(1):95-112. doi: 10.1016/j.gaitpost.2004.01.001. PMID: 15536039.
16. Ruff C. Mechanical Constraints on the Hominin Pelvis and the "Obstetrical Dilemma". Anat Rec (Hoboken). 2017 May;300(5):946-955. doi: 10.1002/ar.23539. PMID: 28406558.

17. Latimer B, Lovejoy CO. The calcaneus of Australopithecus afarensis and its implications for the evolution of bipedality. *Am J Phys Anthropol*. 1989;78(3):369-386. doi:10.1002/ajpa.1330780306
18. Morton DJ. Evolution of the human foot II. Am. J. Phys. Anthropol. 1924; 7:1-52. doi:10.1002/ajpa.1330070114
19. McNutt EJ, Zipfel B, DeSilva JM. The evolution of the human foot. Evol Anthropol. 2018 Sep;27(5):197-217. doi: 10.1002/evan.21713. Epub 2018 Sep 22. PMID: 30242943.
20. Farris DJ, Kelly LA, Cresswell AG, Lichtwark GA. The functional importance of human foot muscles for bipedal locomotion. Proc Natl Acad Sci U S A. 2019 Jan 29;116(5):1645-1650. doi: 10.1073/pnas.1812820116. Epub 2019 Jan 17. PMID: 30655349; PMCID: PMC6358692.
21. Hatala KG, Wunderlich RE, Dingwall HL, Richmond BG. Interpreting locomotor biomechanics from the morphology of human footprints. J Hum Evol. 2016;90:38-48. doi:10.1016/j.jhevol.2015.08.009
22. Ruff C, Holt B, Trinkaus E. Who's afraid of the big bad Wolff?: "Wolff's law" and bone functional adaptation. Am J Phys Anthropol. 2006 Apr;129(4):484-98. doi: 10.1002/ajpa.20371. PMID: 16425178.
23. Skedros JG, Brand RA. Biographical sketch: Georg Hermann von Meyer (1815-1892). Clin Orthop Relat Res. 2011 Nov;469(11):3072-6. doi: 10.1007/s11999-011-2040-6. PMID: 21901583; PMCID: PMC3183195.
24. Suri C, Shojaei I, Bazrgar B. Effects of School Backpacks on Spine Biomechanics During Daily Activities: A Narrative Review of Literature. Human Factors. 2020 62(6):909-918.
25. Russell F, Kormushev P, Vaidyanathan R, Ellison P. The Impact of ACL Laxity on a Bicondylar Robotic Knee and Implications in Human Joint Biomechanics. IEEE Trans Biomed Eng. 2020 Oct;67(10):2817-2827. doi: 10.1109/TBME.2020.2971855. Epub 2020 Feb 5. PMID: 32031928; PMCID: PMC7116099.
26. Schmalz T, Schändlinger J, Schuler M, Bornmann J, Schirrmeister B, Kannenberg A, Ernst M. Biomechanical and Metabolic Effectiveness of an Industrial Exoskeleton for Overhead Work. Int J Environ Res Public Health. 2019 Nov 29;16(23):4792. doi: 10.3390/ijerph16234792. PMID: 31795365; PMCID: PMC6926884.
27. Winter DA, The Biomechanics and Motor Control of Human Gait, 1988. https://doi.org/10.1016/s0031-9406(10)63713-3.
28. Fischer AG, Wolf A. Body weight unloading modifications on frontal plane joint moments, impulses and Center of Pressure during overground gait. Clin Biomech (Bristol, Avon). 2016 Nov;39:77-83. doi: 10.1016/j.clinbiomech.2016.09.005. Epub 2016 Sep 13. PMID: 27697627.
29. Taylor CR. Force development during sustained locomotion: a determinant of gait, speed and metabolic power. J Exp Biol. 1985 Mar;115:253-62. PMID: 4031768.
30. Kram R, Taylor CR. Energetics of running: a new perspective. Nature. 1990 Jul 19;346(6281):265-7. doi: 10.1038/346265a0. PMID: 2374590.
31. Schijve, J. Fatigue of Structures and Materials. 2009. Ed 2. Springer Science & Business Media. ISBN: 0306483963, 9780306483967
32. Folman Y, Wosk J, Voloshin A, Liberty S. Cyclic impacts on heel strike: a possible biomechanical factor in the etiology of degenerative disease of the human locomotor

system. Arch Orthop Trauma Surg. 1986;104(6):363-5. doi: 10.1007/BF00454431. PMID: 3964043.
33. Wolff J. The classic: on the inner architecture of bones and its importance for bone growth. 1870. Clin Orthop Relat Res. 2010 Apr;468(4):1056-65. doi: 10.1007/s11999-010-1239-2. PMID: 20162387; PMCID: PMC2835576.
34. Frost HM. A 2003 update of bone physiology and Wolff's Law for clinicians. Angle Orthod. 2004 Feb;74(1):3-15. doi: 10.1043/0003-3219(2004)074<0003:AUOBPA>2.0.CO;2. PMID: 15038485.
35. Kivell TL. A review of trabecular bone functional adaptation: what have we learned from trabecular analyses in extant hominoids and what can we apply to fossils? J Anat. 2016 Apr;228(4):569-94. doi: 10.1111/joa.12446. Epub 2016 Feb 16. PMID: 26879841; PMCID: PMC4804137.
36. Currey JD. The many adaptations of bone. J Biomech. 2003 Oct;36(10):1487-95. doi: 10.1016/s0021-9290(03)00124-6. PMID: 14499297.
37. Lautzenheiser SG, Kramer PA. Linear and angular measurements of the foot of modern humans: a test of Morton's foot types. Anat Rec (Hoboken). 2013 Oct;296(10):1526-33. doi: 10.1002/ar.22764. Epub 2013 Aug 20. PMID: 23963833.
38. DeSilva JM, Bonne-Annee R, Swanson Z, Gill CM, Sobel M, Uy J, Gill SV. Midtarsal break variation in modern humans: Functional causes, skeletal correlates, and paleontological implications. Am J Phys Anthropol. 2015 Apr;156(4):543-52. doi: 10.1002/ajpa.22699. Epub 2015 Jan 16. PMID: 25594359.
39. Bates KT, Collins D, Savage R, McClymont J, Webster E, Pataky TC, D'Aout K, Sellers WI, Bennett MR, Crompton RH. The evolution of compliance in the human lateral mid-foot. Proc Biol Sci. 2013 Aug 21;280(1769):20131818. doi: 10.1098/rspb.2013.1818. PMID: 23966646; PMCID: PMC3768320.
40. De Wit B, De Clercq D, Aerts P. Biomechanical analysis of the stance phase during barefoot and shod running. J Biomech. 2000;33(3):269-278. doi:10.1016/s0021-9290(99)00192-x
41. Divert C, Mornieux G, Freychat P, Baly L, Mayer F, Belli A. Barefoot-shod running differences: shoe or mass effect?. Int J Sports Med. 2008;29(6):512-518. doi:10.1055/s-2007-989233
42. Squadrone R, Gallozzi C. Biomechanical and physiological comparison of barefoot and two shod conditions in experienced barefoot runners. J Sports Med Phys Fitness. 2009;49(1):6-13.
43. Lieberman DE, Venkadesan M, Werbel WA, Daoud AI, D'Andrea S, Davis IS, Mang'eni RO, Pitsiladis Y. Foot strike patterns and collision forces in habitually barefoot versus shod runners. Nature. 2010;463(7280):531-535. doi:10.1038/nature08723
44. Ardigò LP, Lafortuna C, Minetti AE, Mognoni P, Saibene F. Metabolic and mechanical aspects of foot landing type, forefoot and rearfoot strike, in human running. Acta Physiol Scand. 1995;155(1):17-22. doi:10.1111/j.1748-1716.1995.tb09943.x
45. Bobbert MF, Yeadon MR, Nigg BM. Mechanical analysis of the landing phase in heel-toe running. J Biomech. 1992;25(3):223-234. doi:10.1016/0021-9290(92)90022-s
46. Heidner GS, Nascimento RB, Aires AG, Baptista RR. Barefoot walking changed relative timing during the support phase but not ground reaction forces in children when compared to different footwear conditions. Gait Posture. 2020 Nov 2;83:287-293. doi: 10.1016/j.gaitpost.2020.10.034. Epub ahead of print. PMID: 33232866.

47. Kim HY, Shin HS, Ko JH, Cha YH, Ahn JH, Hwang JY. Gait Analysis of Symptomatic Flatfoot in Children: An Observational Study. Clin Orthop Surg. 2017 Sep;9(3):363-373. doi: 10.4055/cios.2017.9.3.363. Epub 2017 Aug 4. PMID: 28861205; PMCID: PMC5567033.
48. Badhyal S, Dhole SR, Gopinathan NR, Dhillon MS, Dhiman V, Jayal AD, Prasad J. Kinetic and Kinematic Analysis of Gait in Type IV Osteogenesis Imperfecta Patients: A Comparative Study. Indian J Orthop. 2019 Jul-Aug;53(4):560-566. doi: 10.4103/ortho.IJOrtho_291_18. PMID: 31303673; PMCID: PMC6590020.
49. Kramer PA. The effect on energy expenditure of walking on gradients or carrying burdens. Am J Hum Biol. 2010;22(4):497-507. doi:10.1002/ajhb.21027
50. Louey MGY, Mudge A, Wojciechowski E, Sangeux M. A model to calculate the progression of the centre of pressure under the foot during gait analysis. Gait Posture. 2017 Sep;57:147-153. doi: 10.1016/j.gaitpost.2017.06.004. Epub 2017 Jun 10. PMID: 28641159.
51. Diggle PJ, Gómez-Rubio V, Brown PE, Chetwynd AG, Gooding S. Second-order analysis of inhomogeneous spatial point processes using case-control data. Biometrics. 2007;63(2):550-557. doi:10.1111/j.1541-0420.2006.00683.x
52. Ben-Hamo M, Ezra D, Krasnov H, Blank L. Spatial and Temporal Dynamics of Mal Secco Disease Spread in Lemon Orchards in Israel. Phytopathology. 2020 Apr;110(4):863-872. doi: 10.1094/PHYTO-06-19-0195-R. Epub 2020 Feb 26. PMID: 31821113.
53. Elliott P, Wakefield J. Disease clusters: should they be investigated, and, if so, when and how?. Journal of the Royal Statistical Society: Series A (Statistics in Society), 2001;164: 3-12. doi:10.1111/1467-985X.00180
54. Maciel-Nájera JF, Hernández-Velasco J, González-Elizondo MS, Hernández-Díaz, JC, López-Sánchez CA, Antúnez P, Bailón-Soto CE, Wehenkel C. Unexpected spatial patterns of natural regeneration in typical uneven-aged mixed pine-oak forests in the Sierra Madre Occidental, Mexico. Global Ecology and Conservation. 2020;23. doi:10.1016/j.gecco.2020.e01074.
55. Lisitsin V. Spatial data analysis of mineral deposit point patterns: Applications to exploration targeting. Ore geology reviews. 2015;71:861–881. doi:10.1016/j.oregeorev.2015.05.019.
56. Jafari-Mamaghani M, Andersson M, Krieger P. Spatial Point Pattern Analysis of Neurons Using Ripley's K-Function in 3D. Front Neuroinform. 2010 May 21;4:9. doi: 10.3389/fninf.2010.00009. PMID: 20577588; PMCID: PMC2889688.
57. Ge W, Wang L, Sun, Y, Liu, X. An efficient method to generate random distribution of fibers in continuous fiber reinforced composites. *Polymer Composites*. 2019; 40: 4763– 4770. https://doi-org.offcampus.lib.washington.edu/10.1002/pc.25344
58. Tianbo C, Sun Y, Maadooliat M. Collective spectral density estimation and clustering for spatially-correlated data. Spatial Statistics. 2020; 38: 100451. https://doi.org/10.1016/j.spasta.2020.100451
59. Zhou Y, Lau BPL, Koh Z, Yuen C, Ng BKK. Understanding Crowd Behaviors in a Social Event by Passive WiFi Sensing and Data Mining. *IEEE Internet of Things Journal*. 2020; 7(5):4442-4454, doi: 10.1109/JIOT.2020.2972062

60. Cao R, Li B, Wang Z, Peng ZR, Tao S, Lou S. Using a distributed air sensor network to investigate the spatiotemporal patterns of PM2.5 concentrations. Environmental Pollution. 2020; 264: 114549. https://doi.org/10.1016/j.envpol.2020.114549.
61. Zia A, Ding S, Messer KD, Miao H, Suter JF, Fooks JR, Guilfoos T, Trandafir S, Uchida E, Tsai Y, Merrill S, Turnbull S, Koliba C. Characterizing heterogeneous behavior of non-point-source polluters in a spatial game under alternate sensing and incentive designs. Journal of Water Resources Planning and Management. 2020 Aug; 146(8).
62. Ahmadi R, Shahrabi J, Aminshahidy B. Forcasting multiple-well flow rates using a novel space-time modeling approach. Journal of Petroleum Science and Engineering. 2020 Aug; 191: 107027. https://doi.org/10.1016/j.petrol.2020.107027
63. Hofmann UK, Götze M, Wiesenreiter K, Müller O, Wünschel M, Mittag F. Transfer of plantar pressure from the medial to the central forefoot in patients with hallux valgus. BMC Musculoskelet Disord. 2019 Apr 9;20(1):149. doi: 10.1186/s12891-019-2531-2. PMID: 30961591; PMCID: PMC6454622.
64. Pataky TC. Spatial resolution in plantar pressure measurement revisited. J Biomech. 2012 Aug 9;45(12):2116-24. doi: 10.1016/j.jbiomech.2012.05.038. Epub 2012 Jun 22. PMID: 22727521.
65. Maurer JD, Ward V, Mayson TA, Davies KR, Alvarez CM, Beauchamp RD, Black AH. Classification of midfoot break using multi-segment foot kinematics and pedobarography. Gait Posture. 2014 Jan;39(1):1-6. doi: 10.1016/j.gaitpost.2013.08.015. Epub 2013 Aug 19. Erratum in: Gait Posture. 2014 Apr;39(4):1162. PMID: 24001869.
66. Bosch K, Nagel A, Weigend L, Rosenbaum D. From "first" to "last" steps in life--pressure patterns of three generations. Clin Biomech (Bristol, Avon). 2009 Oct;24(8):676-81. doi: 10.1016/j.clinbiomech.2009.06.001. Epub 2009 Jun 26. PMID: 19560242.
67. Booth BG, Keijsers NLW, Sijbers J, Huysmans T. STAPP: Spatiotemporal analysis of plantar pressure measurements using statistical parametric mapping. Gait Posture. 2018 Jun;63:268-275. doi: 10.1016/j.gaitpost.2018.04.029. Epub 2018 May 3. PMID: 29793187.
68. Hughes J, Clark P, Jagoe RR, Gerber C, Klenerman L. The pattern of pressure distribution under the weightbearing forefoot. The Foot. Nov 1991; 1(3):117-124. Doi: https://doi.org/10.1016/0958-2592(91)90020-C
69. Ripley B. The second-order analysis of stationary point processes. Journal of Applied Probability. 1976; 13: 255–266.
70. Ripley BD. Statistical inference for spatial processes. Cambridge university press; 1991 Jul 18.
71. Baddeley, A., Turner, R., Rubak, E. (2015). Spatial Point Patterns: Methodology and Applications with R. United Kingdom: CRC Press.
72. Cavanagh PR, Rodgers MM. The Arch Index: A Useful Measure From Footprints, J. Biomech. 20 (1987) 547–551.
73. Stöggl T, Martiner A. Validation of Moticon's OpenGo sensor insoles during gait, jumps, balance and cross-country skiing specific imitation movements. J Sports Sci. 2017 Jan;35(2):196-206. doi: 10.1080/02640414.2016.1161205. Epub 2016 Mar 24. PMID: 27010531; PMCID: PMC5214925.
74. Sarkar D. (2008) Lattice: Multivariate Data Visualization with R. Springer, New York. ISBN 978-0-387-75968-5

75. Pebesma EJ, Bivand RS. (2005) Classes and methods for spatial data in R. R News 5 (2), https://cran.r-project.org/doc/Rnews/.
76. Rowlingson B, Diggle P. (2017). splancs: Spatial and Space-Time Point Pattern Analysis. R package version 2.01-40. https://CRAN.R-project.org/package=splancs
77. Bates D, Maechler M, Bolker B, Walker S. (2015). Fitting Linear Mixed-Effects Models Using lme4. Journal of Statistical Software, 67(1), 1-48. doi:10.18637/jss.v067.i01.
78. Emerson SS, Spieker AJ, Williamson BD, Hee Wai TY, Lim S. (2018). uwIntroStats: Descriptive Statistics, Inference, Regression, and Plotting in an Introductory Statistics Course. R package version 0.0.7. https://CRAN.R-project.org/package=uwIntroStats
79. Hennig EM, Staats A, Rosenbaum D. Plantar pressure distribution patterns of young school children in comparison to adults. Foot Ankle Int. 1994 Jan;15(1):35-40. doi: 10.1177/107110079401500107. PMID: 7981794.
80. Rosenbaum D. Foot loading patterns can be changed by deliberately walking with in-toeing or out-toeing gait modifications. Gait Posture. 2013 Sep;38(4):1067-9. doi: 10.1016/j.gaitpost.2013.04.001. Epub 2013 Apr 25. PMID: 23623607.
81. McKay MJ, Baldwin JN, Ferreira P, Simic M, Vanicek N, Wojciechowski E, Mudge A, Burns J; 1000 Norms Project Consortium. Spatiotemporal and plantar pressure patterns of 1000 healthy individuals aged 3-101 years. Gait Posture. 2017 Oct;58:78-87. doi: 10.1016/j.gaitpost.2017.07.004. Epub 2017 Jul 18. PMID: 28763713.
82. Jameson EG, Davids JR, Anderson JP, Davis RB 3rd, Blackhurst DW, Christopher LM. Dynamic pedobarography for children: use of the center of pressure progression. J Pediatr Orthop. 2008 Mar;28(2):254-8. doi: 10.1097/BPO.0b013e318164ee6e. PMID: 18388725.
83. Blackburn JT, Pietrosimone BG, Harkey MS, Luc BA, Pamukoff DN. Comparison of three methods for identifying the heelstrike transient during walking gait. Med Eng Phys. 2016 Jun;38(6):581-5. doi: 10.1016/j.medengphy.2016.04.008. Epub 2016 Apr 21. PMID: 27118622.
84. Whittle MW. Generation and attenuation of transient impulsive forces beneath the foot: a review. Gait Posture. 1999 Dec;10(3):264-75. doi: 10.1016/s0966-6362(99)00041-7. PMID: 10567759.
85. Takahashi KZ, Gross MT, van Werkhoven H, Piazza SJ, Sawicki GS. Adding Stiffness to the Foot Modulates Soleus Force-Velocity Behaviour during Human Walking. Sci Rep. 2016 Jul 15;6:29870. doi: 10.1038/srep29870. PMID: 27417976; PMCID: PMC4945910.
86. Holowka NB, Lieberman DE. Rethinking the evolution of the human foot: insights from experimental research. J Exp Biol. 2018 Sep 6;221(Pt 17):jeb174425. doi: 10.1242/jeb.174425. PMID: 30190415.
87. Lovejoy CO, Latimer B, Suwa G, Asfaw B, White TD. Combining prehension and propulsion: the foot of Ardipithecus ramidus. Science. 2009 Oct 2;326(5949):72e1-8. PMID: 19810198.
88. Perry J, Boyd LA, Rao SS, Mulroy SJ. Prosthetic weight acceptance mechanics in transtibial amputees wearing the Single Axis, Seattle Lite, and Flex Foot. IEEE Trans Rehabil Eng. 1997 Dec;5(4):283-9. doi: 10.1109/86.650279. PMID: 9422453.
89. Halsne EG, Czerniecki JM, Shofer JB, Morgenroth DC. The effect of prosthetic foot stiffness on foot-ankle biomechanics and relative foot stiffness perception in people with transtibial amputation. Clin Biomech (Bristol, Avon). 2020 Jul 31;80:105141. doi: 10.1016/j.clinbiomech.2020.105141. Epub ahead of print. PMID: 32763624.

90. Rábago CA, Wilken JM. The Prevalence of Gait Deviations in Individuals With Transtibial Amputation. Mil Med. 2016 Nov;181(S4):30-37. doi: 10.7205/MILMED-D-15-00505. PMID: 27849459.
91. Pew CA, Roelker SA, Klute GK, Neptune RR. Analysis of the Relative Motion Between the Socket and Residual Limb in Transtibial Amputees While Wearing a Transverse Rotation Adapter. J Appl Biomech. 2020 Nov 3:1-9. doi: 10.1123/jab.2019-0362. Epub ahead of print. PMID: 33152690.
92. Kim M, Lyness H, Chen T, Collins S. Prosthesis Inversion/Eversion Stiffness Reduces Balance-Related Variability During Level Walking. J Biomech Eng. 2020 Apr 13. doi: 10.1115/1.4046881. Epub ahead of print. PMID: 32280955.
93. Fey NP, Klute GK, Neptune RR. The influence of energy storage and return foot stiffness on walking mechanics and muscle activity in below-knee amputees. Clin Biomech (Bristol, Avon). 2011 Dec;26(10):1025-32. doi: 10.1016/j.clinbiomech.2011.06.007. Epub 2011 Jul 20. PMID: 21777999.
94. Timmermans C, Cutti AG, van Donkersgoed H, Roerdink M. Gaitography on lower-limb amputees: Repeatability and between-methods agreement. Prosthet Orthot Int. 2019 Feb;43(1):71-79. doi: 10.1177/0309364618791618. Epub 2018 Aug 13. PMID: 30101682.
95. Serrancolí G, Kinney AL, Fregly BJ. Influence of musculoskeletal model parameter values on prediction of accurate knee contact forces during walking. Med Eng Phys. 2020 Nov;85:35-47. doi: 10.1016/j.medengphy.2020.09.004. Epub 2020 Sep 18. PMID: 33081962.
96. Charles JP, Fu FH, Anderst W. Predictions of Anterior Cruciate Ligament Dynamics From Subject-Specific Musculoskeletal Models and Dynamic Biplane Radiography. J Biomech Eng. 2020 Oct 8. doi: 10.1115/1.4048710. Epub ahead of print. PMID: 33030199.

Chapter 5. A MECHANICAL PROXY FOR ENERGETIC COST

5.1 ABSTRACT

Ground reaction force (GRF) development over time has been shown to be predictive of metabolic cost in running, but this relationship has not been established for walking. In this chapter, we look for mechanical proxies that are predictive of metabolic cost during human walking, by exploring the influence of foot-ground contact duration and GRF development at different velocities. Participants walked on a treadmill at self-selected Slow, Medium Slow, Normal, Medium Fast, and Fast velocities while VO_2 measurements were recorded and over-ground across an in-ground force plate at self-selected Slow, Normal, and Fast velocities. We found that foot-ground contact time and anteroposterior GRF were significant predictors of VO_2 when included in a regression model with velocity, participant mass, and participant standing resting metabolic rate (stRMR).

5.1 INTRODUCTION

Mobility, or movement through an environment, is a critical component of the activity budgets of all animals, and humans are no exception (e.g. Ross 2015, Howland 1974, Gibson 2006, Kramer 1998). The energetic cost of movement, however, is difficult to quantify due to the complexity of the physiological processes that create movement, resulting in vast number of potential associated variables. Most fundamentally, muscles are required to move a body through space. They activate to apply forces across joints to move the limbs and to counteract joint moments (Taylor 1980), but muscle activation varies across activity, individual, trial sequence, day, etc. and is still not fully understood (e.g. Enoka 2008, Wang 2019). Broadly, however, both the initial muscle firing and its maintenance over a period of time require metabolic energy (e.g. Ortega 2015, Enoka 2008,

Taylor 1980, etc.). Muscles require more metabolic energy to produce more force, whether that is maintaining force across time or increasing the force magnitude over the same time duration (e.g. Ortega 2015, Taylor 1980). To quantify the metabolic cost of an activity, then, time and force magnitude are important parameters.

As discussed in Chapter 2, habitual bipedalism is a derived trait of modern humans and a complex structural problem (e.g. Cavagna & Margaria 1966). Walking on four limbs maintains ground contact of two supporting points at all times, whereas walking on two limbs requires periods of time where there is only one limb in ground-contact while the other swings. The vertical (superoinferior, Z direction) ground reaction force (vGRF) curve for bipedal walking has two peaks: at peak braking and peak propulsion. The magnitude of these peaks has been shown to be directly related to walking velocity (Winter 1988). In conjunction with the vGRFs, anteroposterior GRFs (apGRFs, direction of travel, X direction) are required to move along surfaces and, although they are almost five times smaller (Figure 2.1 and Figure 5.2) than vGRFs (Nilsson & Thorstensson 1989), apGRFs cause forward movement. Despite the existence of a rich literature on GRFs and walking (e.g. Jung 2014, Nilsson & Thorstensson 1989, Warabi 2005, etc.), we found little work investigating the relationship between the crucial time component of GRFs and the metabolic cost of walking.

5.2 BACKGROUND

As discussed in Chapter 2, the energy required to move a mass through its environment is one of the primary expenditures of an activity budget and therefore of considerable interest to biological anthropologists (e.g. Kramer 2010). Metabolic energy expenditure is inherently tied to mechanical energy as the body consumes metabolic energy to mechanically propel itself through space, although the exact relationship is not well understood. Muscles require metabolic energy to

generate and maintain forces, but the details of this relationship and how it translates to locomotion are complex and not well understood (e.g. Ortega 2015). Prior work has attempted to simplify the human bipedal system using a variety of pendulum models (e.g. Cavagna 1977, Geyer 2006, Rebula & Kuo 2015, etc.), but these often focus on the mechanical optimization of the bipedal system (e.g. a bipedal robot designed to walk), and, therefore, have had little success in predicting metabolic energy expenditure in situations where optimization may not be feasible (e.g. in a living system with many demands on its energy and morphology). While less common, some of these mechanical models have examined the foot and its role in the energetic cost of bipedal locomotion, sometimes utilizing interesting methods of experimental validation (e.g. Gottschall & Kram 2002, Adamczyk & Kuo 2013), but these models have not been successful in fully predicting the energetic cost of walking.

Seminal work (Kram & Taylor 1990) on the relationship of metabolic energy, which is consumed by muscular contraction, and mechanical output during running demonstrated that force development over time determines the metabolic energy requirements and not the mechanical work of the system (Taylor 1980, Taylor 1985, Kram & Taylor 1990). Mechanical work (W) is formally described as the integral of the vector of force (F) through the derivative of the path vector (s) or:

$$Work = \int F ds \tag{5.1}$$

This distinction between the relationship of GRFs with time rather than with path has not been fully evaluated in walking. Since foot contact time and force are metabolic determinants for running, we hypothesize that this may also be the case for walking. It is, however, inappropriate to assume that the relationship for running can be extended to walking without quantitative support because walking and running are different movements. Bipedal walking includes a period of

double stance where both feet are in contact with the ground, whereas only one foot is contact with the ground at a time and there is a period of flight during a running gait cycle. While walking is characterized as an inverted pendulum, running is more like a bouncing ball (Cavagna 2006). The spring-dominated mechanics of running is only marginally comparable to the pendular mechanics of walking.

To our knowledge, the potential relationship between ground contact time, GRF magnitude, and metabolic cost has not been established for walking; therefore, in this work, we investigate the relationship between GRF development over time (both apGRF and vGRF) and metabolic cost during walking at various speeds. Based on Taylor's results for running (Taylor 1985), we expect that GRF development over the time will be predictive of metabolic cost.

5.3 HYPOTHESES & SPECIFIC AIMS

Our hypotheses were as follows:

H1: Metabolic cost is predicted by the magnitude of the anteroposterior and vertical GRFs.

H2: Metabolic cost is predicted by the contact time between the foot and the ground.

5.4 METHODS

5.4.1 *DATA COLLECTION*

In this project, we performed a secondary analysis of participant data collected in 2010-2013. The data were collected from a convenience sample of sixteen female participants who were without gait pathology or injury to their lower limbs within the last two years. Data from two participants were excluded. Participant E02 had an undisclosed skeletal condition (scoliosis with leg length discrepancy) that was disclosed post-data-collection and, therefore, she did not meet inclusion criteria. The force plate malfunctioned during the participant E12's trials and the data could not be

salvaged, leading to exclusion from the analyses. This dataset contains data from two experiments, one in which oxygen consumption was monitored while participants walked on a treadmill and another in which participants walked overground in the Human Motion Analysis Lab (HMAL, Department of Rehabilitative Medicine, UW) across a force plate while the position of their bodies was tracked by infrared markers. These experiments occurred within a week of each other and all participants completed both experiments. Oxygen consumption was measured for participants walking at five, self-selected velocities and apGRF and vGRF data obtained for participants walking at three, self-selected velocities (Table 5.1).

Participant	Mass (kg)	stRMR	Stature (cm)	Leg Length (cm)	Foot Length (cm)	Bitrochanteric Breadth (cm)	Condition	VO2 Velocities (m/s)	HMAL Velocities (m/s)
E01	63.9	3.63	169.5	85.8	22.4	37.2	Slow	0.224	0.526
							Medium Slow	0.805	
							Normal	1.207	1.42
							Medium Fast	1.475	
							Fast	1.788	1.934
E03	59	3.23	171.5	81.8	21.6	37.5	Slow	0.402	0.795
							Medium Slow	0.805	
							Normal	1.252	1.412
							Medium Fast	1.475	
							Fast	1.788	1.755
E04	56.8	2.9	162	74.8	19.1	37.4	Slow	0.447	0.504
							Medium Slow	0.805	
							Normal	1.207	1.299
							Medium Fast	1.565	
							Fast	1.922	1.723
E05	52.9	2.65	166	91.9	21.8	36.8	Slow	0.447	1.189
							Medium Slow	0.76	
							Normal	1.118	1.644
							Medium Fast	1.475	
							Fast	1.788	1.841
E06	64.5	2.94	162	79.5	22	37.5	Slow	0.536	0.821
							Medium Slow	0.805	
							Normal	1.073	1.454
							Medium Fast	1.386	
							Fast	1.699	1.675
E07	91.7	2.96	174	86.8	23.9	42	Slow	0.447	0.664
							Medium Slow	0.76	
							Normal	1.073	1.009
							Medium Fast	1.207	
							Fast	1.296	1.523
E08	66.8	3.85	166	75.9	22.4	38	Slow	0.447	1.068
							Medium Slow	0.849	
							Normal	1.252	1.481
							Medium Fast	1.52	
							Fast	1.833	1.747
E09	85.4	5.45	172	81.4	23.2	43.9	Slow	0.536	0.991
							Medium Slow	0.805	
							Normal	1.118	1.288
							Medium Fast	1.386	
							Fast	1.788	1.574
E10	68.7	3.89	161	74.4	21	41.2	Slow	0.447	0.719
							Medium Slow	0.76	
							Normal	1.118	1.212
							Medium Fast	1.475	
							Fast	1.788	1.498
E11	52.7	1.59	164	78.7	19.8	32.7	Slow	0.447	0.849
							Medium Slow	0.939	
							Normal	1.475	1.397
							Medium Fast	1.654	
							Fast	1.878	1.773
E13	61.1	3.41	156	80.8	21.8	36.6	Slow	0.447	1.006
							Medium Slow	0.76	
							Normal	1.118	1.244
							Medium Fast	1.386	
							Fast	1.609	1.589
E14	75	4.62	172	82.8	23.6	42.8	Slow	0.447	1.265
							Medium Slow	0.715	
							Normal	1.028	1.54
							Medium Fast	1.386	
							Fast	1.788	1.7
E15	54.1	3.2	162	76.1	21.5	33.9	Slow	0.447	0.974
							Medium Slow	0.76	
							Normal	1.118	1.194
							Medium Fast	1.341	
							Fast	1.565	1.541
E16	74.7	2.54	167	80.4	24	35.8	Slow	0.447	0.78
							Medium Slow	0.805	
							Normal	1.207	1.158
							Medium Fast	1.475	
							Fast	1.788	1.35

Table 5.1. Participant anthropometrics, stRMR, and average participant walking velocities for the treadmill VO_2 trials and the HMAL trials.

Motion capture markers were placed on each participant at the following landmarks: left and right acromion, greater trochanter, posterior heels, lateral malleoli, and between the second and third metatarsal heads. These were used in post-processing to determine the bitrochanteric width (cm), leg length (cm), and foot length (cm) and to calculate progression velocity (m/s). Stature (m) and participant mass (kg) were measured by the researcher using an inextensible tape measure and a standard scale. Each participant was asked to stand quietly for four minutes while their resting metabolic rate was assessed (stRMR). They then walked on a treadmill and select their preferred Slow, Normal, and Fast velocities. The researchers then calculated Medium Slow and Medium Fast velocities from the midpoint between the Slow and Normal velocities and the Normal and Fast velocities, making five velocity categories. Each participant was fitted with a SensorMedics oxygen analyzer mask. The oxygen analyzer collects VO_2 data by measuring the volumetric rate of inhaled and exhaled oxygen. The electro-galvanic oxygen sensor was calibrated prior to each use. Standing resting metabolic rate (stRMR) was collected prior to testing. Each participant then walked for five minutes at each velocity, with four minutes of quiet standing between each trial. The trial velocities were randomized.

Each participant was then asked to walk along a straight, unobstructed pathway with a force plate (Kistler Instrument Corp., Novi, MI) embedded in the floor at a midpoint. Participants were asked to walk at their preferred Slow, Natural, and Fast velocities across the force plate, but no other control on speed was enforced. Each walking velocity category was repeated ten times (5 trials with the left foot in contact with the force plate and 5 trials with the right) while GRF data and Center of Pressure (CoP) data were recorded. The CoP data were not used in this analysis. Infrared markers were placed on standard anatomical landmarks and marker trajectories were

collected. The trajectory of the acromion marker was used to determine the velocity of each trial for each individual using custom MATLAB (2019a, The Math Works, Natick, MA) code. This project was approved by the Institutional Review Board for the University of Washington.

5.4.2 *DATA PROCESSING*

To address the hypotheses, we isolated the vertical and anteroposterior GRF (vGRF and apGRF, respectively) curves for each participant and each trial using custom MATLAB code. To preserve the integrity of the analysis, we chose not to normalize the GRF or VO_2 data by individuals' mass. Normalization has the potential for negative consequences in the analysis if the relationship between the measured variable and the metric by which it is being normalized is not well understood. If, for example, the true relationship between the variable and the normalizing metric is non-linear, but the variable is normalized linearly, the assumption that the relationship is equally normalized is false. Normalization can also result in spurious correlation if both the covariate and the outcome are normalized by the same metric. Therefore, we did not normalize these data, and chose instead to include normalization metrics, such as participant mass, as covariates in our models.

Oxygen consumption experiment: A plateau in oxygen consumption was obtained for all participants by minute 2 of data collection so the average VO_2 for each minute of minutes 3-5 for each trial were used. From these data, we calculated the metabolic cost of walking for each participant at each velocity as cost of transport (CoT), equation 5.1:

$$\overline{CoT} = \frac{\overline{VO_2\ (\frac{mL}{s})}}{Velocity\ (\frac{m}{s})} \tag{5.2}$$

We then fit a quadratic equation to CoT against velocity for each individual, creating a CoT curve specific to that individual (Figure 5.1). We used these curves to predict VO_2 for each of the self-selected velocities from the GRF trials (described below) for each individual because we could not control overground walking speed. We used CoT to create individual curves as CoT produces a stronger fit for the individual curves. (See Results Table 5.2).

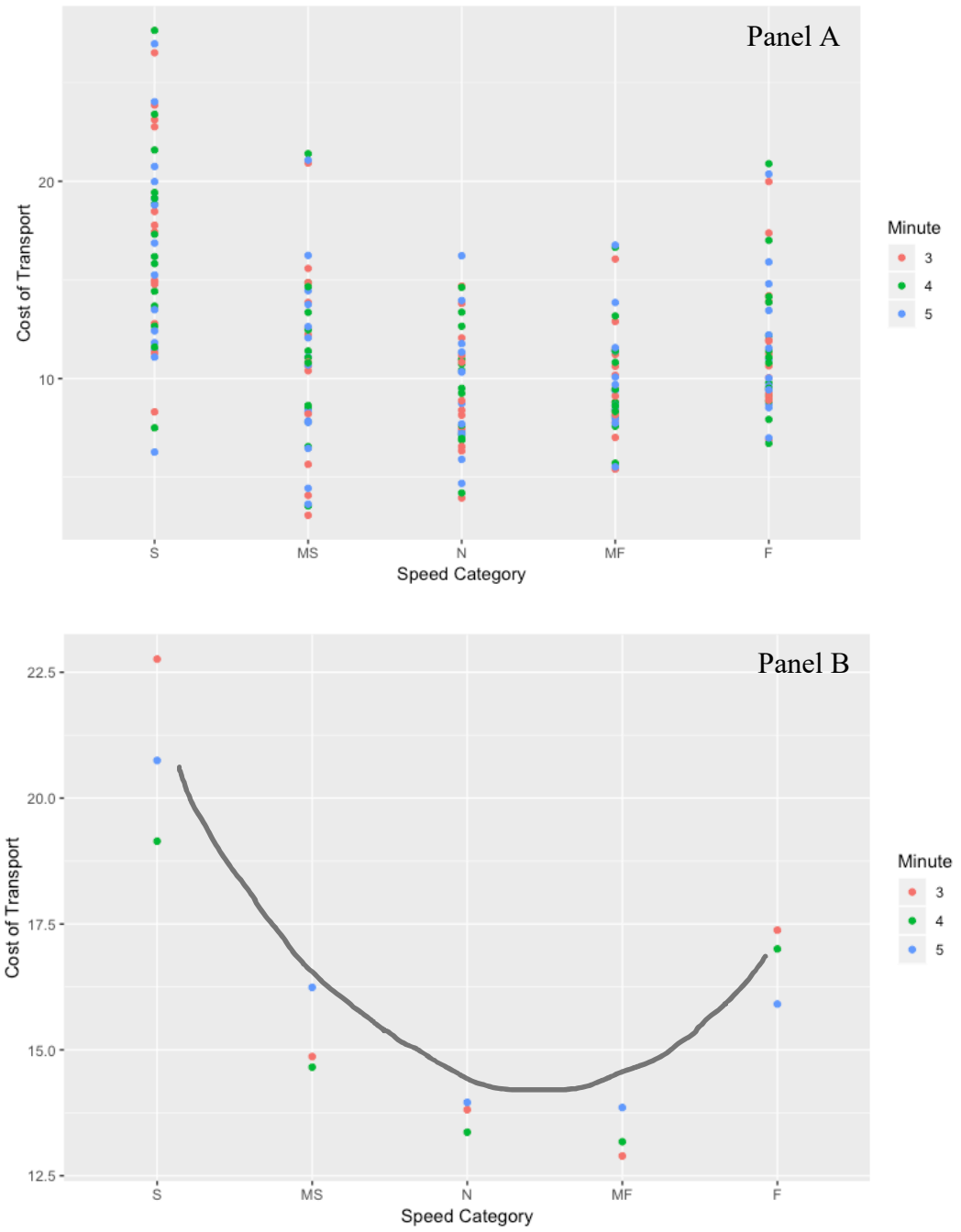

Figure 5.1. Panel A shows the CoT data for minutes 3, 4, and 5 for all trials and all participants at Slow (S), Medium Slow (MS), Normal (N), Medium Fast (MF), and Fast (F) velocities. Panel B shows the CoT data for a single participant at each of these velocities. The quadratic CoT curve was fit for each participant individually.

HMAL experiment: The apGRF and vGRF curves were partitioned into braking and propulsion stages based on the force minima between peak braking vGRF and peak propulsive vGRF: midstance (M) (Figure 5.2).

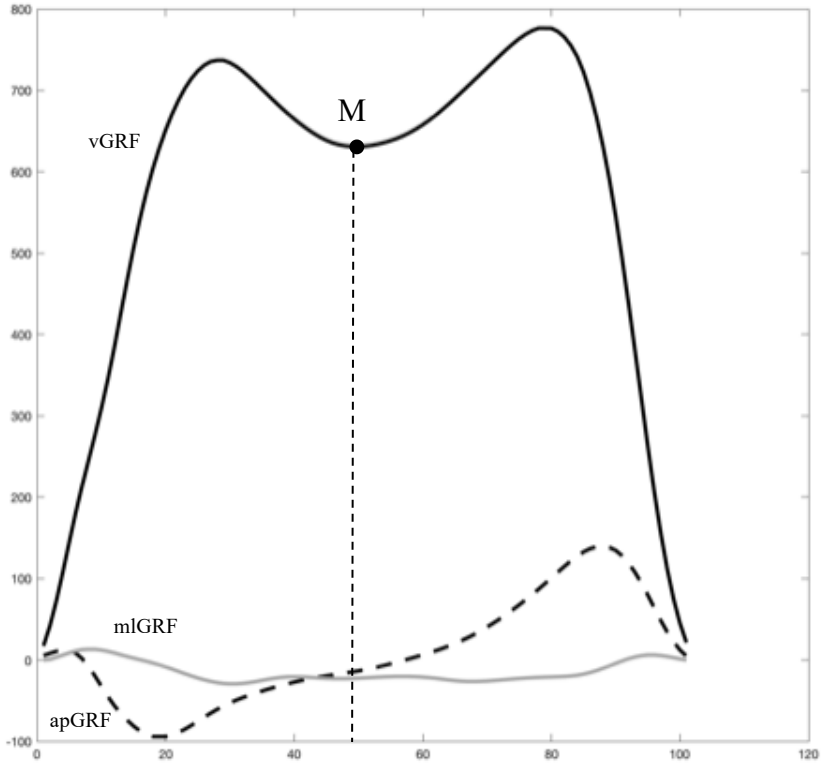

Figure 5.2. Anteroposterior (apGRF), mediolateral (mlGRF), and vertical ground reaction force (vGRF) curves during foot-ground contact. Point M denotes midstance of the gait cycle. We used M to partition the GRF curves into braking and propulsion stages. Mediolateral GRFs were not used in these analyses but are shown for completeness.

GRFs were tared using the average of 20 frames when the force plate was unloaded. From the GRF curves, we calculated the foot-ground contact time for each trial for each participant by subtracting the frame at which the vGRF curve crossed the force threshold of 25N from the frame

at which the vGRF curve fell below the force threshold of 25N and multiplying by the data collection rate (120 frames per second). This threshold was established by visual inspection of the marker data establish heel strike and toe-off and knowledge of the accuracy of the HMAL force plate. We also calculated the average GRF of each individual and trial for braking vGRF and apGRF and propulsion vGRF and apGRF, as well as the average vGRF and apGRF for the full ground-contact cycle. As apGRF changes direction from +X to -X from braking to propulsion, we performed all calculations using the absolute value of apGRF.

5.4.3 *STATISTICAL MODELS*

To interrogate our hypotheses, linear mixed-effects models from the Null model (equation 5.2) using R package 'lmer' (Bates 2015) were developed, with our predicted VO_2 as the dependent variable and accounting for the hierarchical nature of the data by participant.

$$VO_2 \sim 1 + (1 \mid ID)$$

$$VO_{2\,ij} = \beta_o + u_{oj} + e_{ij} \quad (5.2)$$

We developed a baseline linear mixed-effects hierarchical model from our Null model (equation 5.2) and then included the participant covariates of participant mass and stRMR (equation 5.3). Mass and/or stRMR are typically included in energetics models *a priori* to control for physiological variability among participants. The baseline model (equation 5.3) was compared to the corresponding Null model (equation 5.2) using ANOVA. From the baseline model, we added our covariate terms and assessed them against the Null model again using ANOVA. The covariates we considered included: contact time (TC), TC^2 velocity, velocity^2, average total vGRF, average

total apGRF, average braking vGRF, average braking apGRF, average propulsion vGRF, average propulsion apGRF, bitrochanteric breadth (BiTroch), foot length, leg length, and stature.

$$VO_2 \sim \text{mass} + \text{stRMR} + (1 \mid \text{ID})$$

$$VO_{2\,ij} = \beta_o + \beta_1 mass + \beta_2 stRMR + u_{oj} + e_{ij} \qquad (5.3)$$

Statistically significant covariates were added to the model and tested against the prior model. When models were all significantly different from each other in a multiple model ANOVA, we compared the AIC and BIC to determine model strength. Our model development in full can be found in Appendix C.

5.5 RESULTS

The results of our first step to fit a quadratic curve to the cost of transport (CoT) for each velocity by participant in the VO_2 trials are in Table 5.2 and an example curve fit to the CoT versus velocity data for a single participant is illustrated in Figure 5.1 above. Figure 5.3 below shows the calculated CoT versus velocity data for minutes 3, 4, and 5 for each participant that we used to fit the curves in Table 5.2.

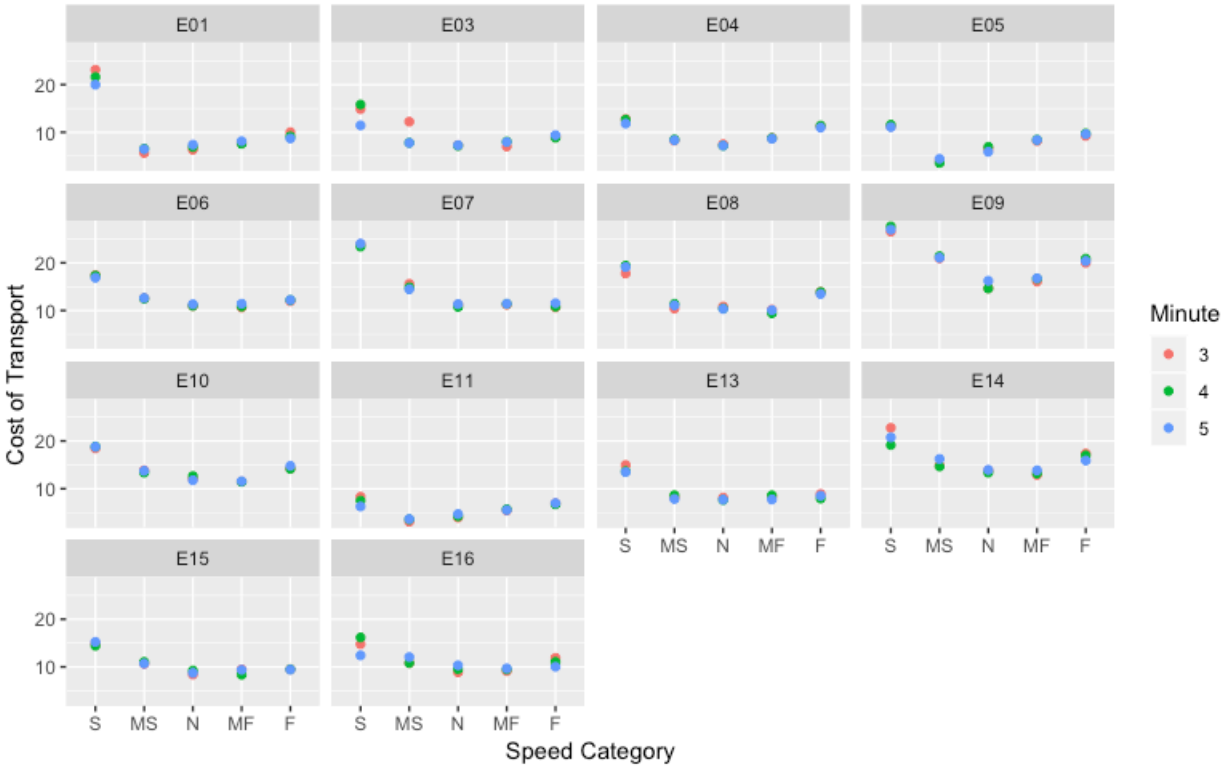

Figure 5.3. The calculated CoT for minutes 3, 4, and 5 for each participant. We then fit a quadratic curve to each of these data (Table 5.2).

Subject	Intercept	Velocity	Velocity^2	R^2
E01	28.497***	-37.185***	15.113***	0.929
E03	21.333***	-21.514***	8.230***	0.781
E04	19.550***	-20.068***	8.242***	0.965
E05	18.325***	-23.235**	10.530**	0.591
E06	29.373***	-29.307***	11.343***	0.968
E07	44.291***	-56.836***	24.193***	0.994
E08	31.008***	-33.969***	13.398***	0.945
E09	49.449***	-52.268***	20.188***	0.892
E10	28.569***	-27.200***	10.747***	0.97
E11	13.491***	-17.323***	7.436***	0.893
E13	23.147***	-26.378***	10.919***	0.876
E14	31.890***	-31.201***	12.756***	0.893
E15	23.475***	-23.667***	9.474***	0.973
E16	21.073***	-17.726***	6.741***	0.811

Table 5.2. Quadratic curve fits for each individual's cost of transport (CoT) vs velocity with corresponding significances (***p<0.001, **p<0.01, *p<0.05) and R^2 values.

An example of our graphical exploration of the covariate contact time versus VO_2 and covariate apGRF and vGRF versus VO_2 are below in Figure 5.4.

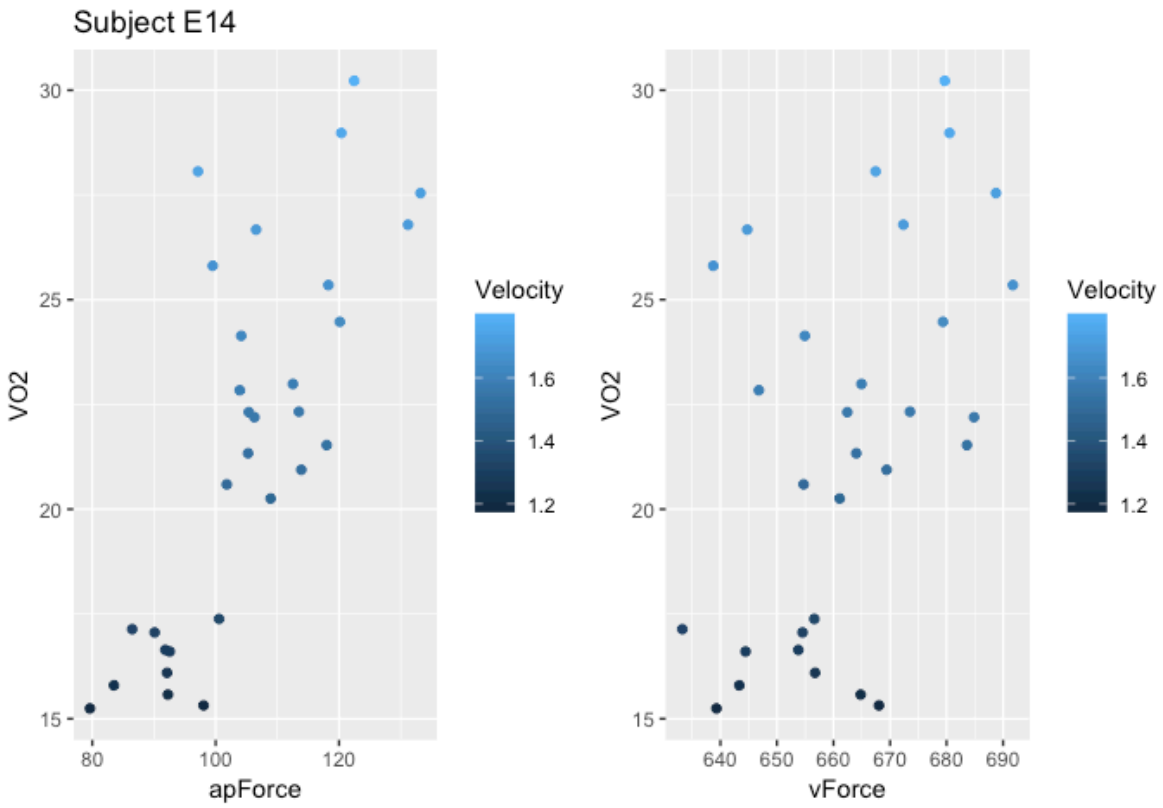

Figure 5.4. An example plot of apGRF and vGRF versus calculated VO_2 for participant E14.

Our baseline linear mixed-effects hierarchical regression model with dependent variable VO_2 and participant covariates mass and stRMR, which were included *a priori*, was significantly different from the corresponding Null model ($p<0.005$). When added our baseline model as a quadratic covariate, TC and TC^2 were significant predictors of VO_2 ($p<0.005$).

$$VO_2 \sim mass + stRMR + TC + TC^2 + (1 \mid ID)$$

$$VO_{2\,ij} = \beta_o + \beta_1 mass + \beta_2 stRMR + \beta_3 TC + \beta_4 TC^2 + u_{oj} + e_{ij} \quad (5.4)$$

From this we added velocity as a quadratic covariate and found that velocity and velocity^2 were significant predictors of VO_2. Equation 5.5 is the built model.

$$VO_2 \sim mass + stRMR + TC + TC^2 + velocity + velocity^2 + (1 \mid ID)$$

$$VO_{2\,ij} = \beta_o + \beta_1 mass + \beta_2 stRMR + \beta_3 TC + \beta_4 TC^2 + \beta_5 velocity + \beta_6 velocity^2 + u_{oj} + e_{ij} \quad (5.5)$$

In parallel, we found that both average total apGRF and vGRF were significant predictors of VO_2 ($p<0.005$ for both). We also found that the average apGRF and vGRF for both the isolated braking and propulsion portions of the ground-contact cycle were significant predictors of VO_2 ($p<0.005$ for all).

After combining our models and testing covariates, the model that best predicted VO_2 was our baseline model with quadratic TC, quadratic velocity, and average full apGRF as covariates (equation 5.6). All vGRF terms were non-significant ($p>0.05$) (Table 5.3).

$$VO_2 \sim mass + stRMR + TC + TC^2 + velocity + velocity^2 + apGRF + (1 \mid ID)$$

$$VO_{2\,ij} = \beta_o + \beta_1 mass + \beta_2 stRMR + \beta_3 TC + \beta_4 TC^2 + \beta_5 velocity + \beta_6 velocity^2 + \beta_6 apGRF + u_{oj} + e_{ij} \quad (5.6)$$

$$VO_2 \sim mass + stRMR + TC + TC^2 + velocity + velocity^2 + apGRF + vGRF + (1 \mid ID) \quad (5.7)$$

$$VO_{2\,ij} = \beta_o + \beta_1 mass + \beta_2 stRMR + \beta_3 TC + \beta_4 TC^2 + \beta_5 velocity + \beta_6 velocity^2 + \beta_6 apGRF + \beta_7 vGRF + u_{oj} + e_{ij}$$

	Null	Baseline	Equation 5.4	Equation 5.5	Equation 5.6	Equation 5.7
Intercept	13.746*** [11.481, 16.011]	-3.138 [-9.491, 3.215]	29.846*** [24.637, 35.040]	-8.368 [-17.941, 1.347]	-2.259 [-11.542, 7.329]	-2.163 [-11.375, 7.366]
Mass		0.010 [-0.001, 0.021]	0.019*** [0.011, 0.026]	0.020** [0.011, 0.029]	0.016** [0.008, 0.024]	0.010 [0.000, 0.021]
stRMR		3.139** [1.741, 4.537]	2.490*** [1.558, 3.421]	2.493** [1.417, 3.569]	2.257** [1.276, 3.237]	2.241** [1.285, 3.198]
Contact time			-77.208*** [-85.467, -68.722]	13.288** [3.744, 22.670]	11.036* [1.704, 20.050]	11.291* [1.980, 20.289]
(Contact time)^2			33.702*** [29.078, 38.177]	-6.649*** [-10.306, -2.970]	-6.323*** [-9.830, -2.747]	-6.449*** [-9.952, -2.880]
Velocity				-25.571*** [-30.890, -20.349]	-29.821*** [-35.237, -24.626]	-30.538*** [-36.033, -25.302]
Velocity^2				15.486*** [13.963, 17.023]	16.021*** [14.550, 17.527]	16.269*** [14.778, 17.810]
apGRF					0.046*** [0.030, 0.062]	0.038*** [0.018, 0.057]
vGRF						0.009 [-0.002, 0.021]

Table 5.3. Linear mixed-effects hierarchical regression model coefficient results and 95% confidence intervals for our two final models (equation 5.4 and equation 5.5) as well as our Null (equation 5.2) and baseline (equation 5.3) models with corresponding significances (***p<0.001, **p<0.01, *p<0.05).

The next best VO_2 predictive model was equation 5.4, our model without the apGRF term (Table 5.4).

Models	AIC	BIC	χ^2	p-value
VO2 ~ 1 + (1 | ID)	2484.3	2496.4	n/a	n/a
VO2 ~ mass + stRMR + (1 | ID)	2467.4	2487.6	20.844	<0.005
VO2 ~ mass + stRMR + TC + TC^2 + velocity + velocity^2 + (1 | ID)	1416	1452.2	1059.435	<0.005
VO2 ~ mass + stRMR + TC + TC^2 + velocity + velocity^2 + apGRF + (1 | ID)	1386.9	1427.1	31.151	<0.005

Table 5.4. ANOVA of our final models against the Null and baseline models. This ANOVA indicates that the model containing the apGRF covariate is more informative than the model without apGRF and both of the final models are significantly more informative than the Null and baseline models.

We found that anthropometric covariates—bitrochanteric breadth (BiTroch), foot length, leg length, and stature—were not significant predictors of VO_2 when added to our models ($p>0.05$ for all).

5.6 DISCUSSION

Our results indicate that our second hypothesis, i.e., that contact time with the ground is predictive of VO_2, is not rejected. Our results for hypothesis one, i.e., the relationship between GRF and VO_2, indicate, however, that apGRF is the stronger predictor of VO_2 consumption, and when participant mass is included in the model, vGRF is non-significant. Our final model (equation 5.6) includes participant mass, stRMR, contact time as a quadratic, velocity as a quadratic, and average total apGRF. As discussed in section 5.2 and in Chapter 2, the purpose of this analysis was to identify quantifiable mechanical proxies to predict metabolic energy consumption. We have found through our analyses that foot-ground contact time, velocity, stRMR, participant mass, and apGRF, when combined in a hierarchical regression model, are predictive of VO_2. Our second-best model, based on ANOVA, was the same model without apGRF as a covariate.

Prior work (e.g. Taylor 1982, Cavagna & Margaria 1966, Kramer 2010 etc.) has supplied evidence of a connection between metabolic energy expenditure and mechanical work of bodies moving through space, but the relationship has been most useful to investigate differences among species (e.g. “mouse to elephant” relationships, Taylor 1980) or among substantially different body morphologies within a species (e.g. Griffin 2004, Saibene 2003). Oxygen consumption varies greatly by individual due to physiological differences and potential variability in everything from the volume of individual muscles (e.g. Charles 2020) to habitual environment (e.g. Hochachka 1985) while individual kinematics (the basis of mechanical metrics) do not (Winter 1988). Consequently, predicting metabolic energy expenditure of level walking from mechanical

parameters other than mass and velocity has been difficult (e.g. Kuo & Donelan 2010). To that end, biomechanists continue to look for mechanical proxies to predict the metabolic cost of locomotion. GRF development over time has been shown to be a predictor of metabolic cost in running, but this relationship had not been previously established for walking. In this analysis we have filled this gap in the literature and established a relationship between several key components of walking and VO_2.

As discussed in Chapter 2, the core motivation for this work was to identify mechanical proxies to predict metabolic energy expenditure during walking. Direct measurement of VO_2 in the laboratory is the most ubiquitous method of determining metabolic cost (Kramer & Sylvester 2011), but laboratories offer their own constraints on what can be studied. For instance, human movement on treadmills is not identical to over-ground walking (Warabi 2005), space constraints limit gradient studies, and, broadly, humans act differently outside of the laboratory (e.g. Wagnild & Wall-Scheffler 2013). Identifying a mechanical proxy for predicting VO_2 consumption without directly measuring VO_2 is one way around this problem.

Prior work using electromyograms (EMGs) has suggested that anteroposterior GRFs constitute up to 50% of the energetic cost of walking based on lower limb muscular activation (Gottschall 2003). Our work supports the suggestion that apGRFs are more predictive of energetic cost than vGRFs. While the majority of the GRF magnitude results from the vertical force of gravity on the body, muscle activation is closely tied to the magnitude of apGRFs (Gottschall 2003), and muscle activation and maintenance of activation over time has a direct metabolic cost (e.g. Ortega 2015, Taylor 1980). This work supports the idea that the GRF component in the direction of progression plays a large role in the energetic cost of that progression. Taylor et. al. did not specify the direction of force or form of locomotion in their 1990 work, postulating that

force development over time is intrinsically tied to metabolic cost of locomotion. Based on our findings, they were correct in their assertation, although we are now able to specify direction of force (anteroposterior) and the component of time (foot-ground contact time) that are predictive of metabolic cost for walking. Our results do not apply to running.

Remote sensing technology has improved dramatically in recent years, specifically in the realm of wireless insole technology. This allows for an alternative to fixed force plates or force sensing treadmills, freeing data collection from the laboratory to some extent. To our knowledge, this technology currently captures vGRFs, center of pressure (CoP), position, and acceleration, but capturing accurate information on apGRFs still poses a challenge. Based on our findings from this analysis, we can predict VO_2 with contact time, velocity, and participant mass, all parameters that can be measured using current wireless insole technology. Participant stRMR is inherently a static variable and can be measured prior to the trials along with other anthropometric variables. While apGRF is an important component to our predictive model, our ANOVA comparison (Table 5.2) of the model with and without apGRF as a covariate showed that their BIC and AIC values were not too dissimilar. This indicates that, while we do lose predictive power without the apGRF term, we can still use this model to predict VO_2, albeit with less precision. Therefore, we should be able to predict VO_2 with some satisfaction using current wireless insole technology, while acknowledging the limitation of the missing apGRF term. Future work should seek to develop the technology to sense apGRF.

Overall, these recent advances in sensing technology open the door to new insights into the mechanics of humans moving freely in their environment, and, with a model containing measurable predictors for VO_2 consumption, we gain the ability to form a more complete picture of human mobility in the environment outside of laboratory conditions. In this chapter, we have

established a relationship between mechanical components of walking in individuals, and oxygen consumption that will facilitate mobility research outside of the laboratory. Future work should assess whether or not the results obtained in this secondary analysis are confirmed and efforts to determine the accuracy of metabolic energy prediction equations that include contact time are necessary. Of particular need is an examination similar to this one but in variable conditions (such as gradients, uneven terrain, and with burdens).

5.7 REFERENCES

Adamczyk PG, Kuo AD. Mechanical and energetic consequences of rolling foot shape in human walking. J Exp Biol. 2013 Jul 15;216(Pt 14):2722-31. doi: 10.1242/jeb.082347. Epub 2013 Apr 11. PMID: 23580717; PMCID: PMC3694099.

Bates D, Maechler M, Bolker B, Walker S. Fitting Linear Mixed-Effects Models Using lme4. Journal of Statistical Software. 2015. 67(1), 1-48. doi:10.18637/jss.v067.i01.

Cavagna GA. The landing-take-off asymmetry in human running. J Exp Biol. 2006 Oct;209(Pt 20):4051-60. doi: 10.1242/jeb.02344. PMID: 17023599.

Cavagna GA, Heglund NC, Taylor CR. Mechanical work in terrestrial locomotion: two basic mechanisms for minimizing energy expenditure. Am J Physiol. 1977 Nov;233(5):R243-61. doi: 10.1152/ajpregu.1977.233.5.R243. PMID: 411381.

Cavagna GA, Margaria R (1966) Mechanics of walking. J Appl Physiol 21:271–278.

Charles JP, Fu FH, Anderst W. Predictions of Anterior Cruciate Ligament Dynamics From Subject-Specific Musculoskeletal Models and Dynamic Biplane Radiography. J Biomech Eng. 2020 Oct 8. doi: 10.1115/1.4048710. Epub ahead of print. PMID: 33030199.

Enoka RM, Duchateau J. Muscle fatigue: what, why and how it influences muscle function. J Physiol. 2008 Jan 1;586(1):11-23. doi: 10.1113/jphysiol.2007.139477. Epub 2007 Aug 16. PMID: 17702815; PMCID: PMC2375565.

Geyer H, Seyfarth A, Blickhan R. Compliant leg behaviour explains basic dynamics of walking and running. Proc Biol Sci. 2006 Nov 22;273(1603):2861-7. doi: 10.1098/rspb.2006.3637. PMID: 17015312; PMCID: PMC1664632.

Gibson MA, Mace R. An energy-saving development initiative increases birth rate and childhood malnutrition in rural Ethiopia. PLoS Med. 2006;3(4):e87. doi:10.1371/journal.pmed.0030087

Gottschall JS, Kram R. Energy cost and muscular activity required for propulsion during walking. J Appl Physiol (1985). 2003 May;94(5):1766-72. doi: 10.1152/japplphysiol.00670.2002. Epub 2002 Dec 27. PMID: 12506042.

Griffin TM, Kram R, Wickler SJ, Hoyt DF. Biomechanical and energetic determinants of the walk-trot transition in horses. J Exp Biol. 2004 Nov;207(Pt 24):4215-23. doi: 10.1242/jeb.01277. PMID: 15531642.

Hochachka PW, Stanley C, Matheson GO, McKenzie DC, Allen PS, Parkhouse WS. Metabolic and work efficiencies during exercise in Andean natives. J Appl Physiol (1985). 1991 Apr;70(4):1720-30. doi: 10.1152/jappl.1991.70.4.1720. PMID: 2055851.

Howland HC. Optimal strategies for predator avoidance: the relative importance of speed and manoeuvrability. J Theor Biol. 1974;47(2):333-350. doi:10.1016/0022-5193(74)90202-1

Jung Y, Jung M, Lee K, Koo S. Ground reaction force estimation using an insole-type pressure mat and joint kinematics during walking. J Biomech. 2014;47(11):2693-2699. doi:10.1016/j.jbiomech.2014.05.007

Kram R, Taylor CR. Energetics of running: a new perspective. Nature. 1990 Jul 19;346(6281):265-7. doi: 10.1038/346265a0. PMID: 2374590.

Kramer PA. The costs of human locomotion: maternal investment in child transport. Am J Phys Anthropol. 1998;107(1):71-85. doi:10.1002/(SICI)1096-8644(199809)107:1<71::AID-AJPA6>3.0.CO;2-G

Kramer PA, The effect on energy expenditure of walking on gradients or carrying burdens, Am. J. Hum. Biol. 22 (2010) 497–507. https://doi.org/10.1002/ajhb.21027.

Kramer PA, Sylvester AD. The energetic cost of walking: a comparison of predictive methods. PLoS One. 2011. 6:e21290.

Kuo AD, Donelan JM. Dynamic principles of gait and their clinical implications. Phys Ther. 2010 Feb;90(2):157-74. doi: 10.2522/ptj.20090125. Epub 2009 Dec 18. PMID: 20023002; PMCID: PMC2816028.

Nilsson J, & Thorstensson A. Ground reaction forces at different speeds of human walking and running. Acta Physiologica Scandinavica, (1989) 136(2), 217–227. https://doi.org/10.1111/j.1748-1716.1989.tb08655.x

Ortega JO, Lindstedt SL, Nelson FE, Jubrias SA, Kushmerick MJ, Conley KE. Muscle force, work and cost: a novel technique to revisit the Fenn effect. J Exp Biol. 2015 Jul;218(Pt 13):2075-82. doi: 10.1242/jeb.114512. Epub 2015 May 11. PMID: 25964423; PMCID: PMC6514452.

Rebula JR, Kuo AD. The cost of leg forces in bipedal locomotion: a simple optimization study. PLoS One. 2015 Feb 23;10(2):e0117384. doi: 10.1371/journal.pone.0117384. PMID: 25707000; PMCID: PMC4338056.

Ross CT, Winterhalder B. Sit-and-wait versus active-search hunting: A behavioral ecological model of optimal search mode. J Theor Biol. 2015;387:76-87. doi:10.1016/j.jtbi.2015.09.022

Saibene F, Minetti AE. Biomechanical and physiological aspects of legged locomotion in humans. Eur J Appl Physiol. 2003 Jan;88(4-5):297-316. doi: 10.1007/s00421-002-0654-9. Epub 2002 Nov 13. PMID: 12527959.

Taylor CR. Force development during sustained locomotion: a determinant of gait, speed and metabolic power. J Exp Biol. 1985;115:253-262.

Taylor CR, Heglund NC. Energetics and mechanics of terrestrial locomotion. Annu Rev Physiol. 1982. 44: 97–107

Taylor CR, Heglund NC, McMahon TA, Looney TR. Energetic cost of generating muscular force during running: a comparison of large and small animals. Journal of Experimental Biology. 1980 Jun 1;86(1):9-18.

Wagnild J, Wall-Scheffler CM. Energetic consequences of human sociality: walking speed choices among friendly dyads. PLoS One. 2013 Oct 23;8(10):e76576. doi: 10.1371/journal.pone.0076576. PMID: 24194840; PMCID: PMC3806777.

Wang AB, Perreault EJ, Royston TJ, Lee SSM. Changes in shear wave propagation within skeletal muscle during active and passive force generation. J Biomech. 2019 Sep 20;94:115-122. doi: 10.1016/j.jbiomech.2019.07.019. Epub 2019 Jul 25. PMID: 31376979; PMCID: PMC6736689.

Warabi T, Kato M, Kiriyama K, Yoshida T, Kobayashi N. Treadmill walking and overground walking of human subjects compared by recording sole-floor reaction force, Neurosci. Res. 53 (2005) 343–348. https://doi.org/10.1016/j.neures.2005.08.005.

Winter DA, The Biomechanics and Motor Control of Human Gait, 1988. https://doi.org/10.1016/s0031-9406(10)63713-3.

Chapter 6. CONCLUSIONS & FUTURE WORK

6.1 CONCLUSIONS

This dissertation work sought to develop further understanding of one of the most fundamental aspects of bipedal walking; the interaction of the foot with the ground. While one of the most ubiquitous occurrences of daily living, the mechanics and repercussions of this interaction on the body as a system both physically and physiologically are still not well understood. This dissertation research highlights the need for further biomechanics research outside of the laboratory, as surface conditions, velocities, and gradients result in changes in ground reaction forces (GRFs) magnitudes as well as changes to the locations of peak forces on the foot during walking. My research also highlights the importance of examining multiple, contiguous steps outside of the laboratory to ensure the data are robust and add insight as to consistency, or lack thereof, in human movement patterns. Finally, I showed that the duration of the foot-ground interaction and anteroposterior GRFs (apGRFs) when included with velocity, are mechanical proxies for the metabolic cost of walking.

As stated several times throughout this dissertation, bipedal locomotion, and particularly walking, is a complex structural problem. While biomechanists, clinicians, and anthropologists all have their own motivations for attempting to disentangle the complexities of bipedal walking, at the most basic level, if we understand walking we understand one of the most foundational aspects of the human experience. Bipedal walking can be distilled into two main components: 1.) mechanics and 2.) energy expenditure. The mechanics of walking can be approximated using various simplified models, such as the pendulum model, the inverted pendulum model, and the dampened spring model (e.g. Cavagna 1977, Geyer 2006, Rebula & Kuo 2015, etc.), but these models neglect the mechanics, and, subsequently, the forces occurring at the interaction between

the foot and the ground. The energetics of walking is a complex relationship between metabolic energy requirements of muscle activation and mechanical energy requirements as the body propels itself through space.

Feet are a direct interface between the body and the environment and so are critical for understanding mobility. The forces that occur during walking impact everything, from evolution of the musculoskeletal system to patient recovery and rehabilitation after injury to the lower limb. Humans encounter a wide variety of surfaces and obstacles as they navigate through their daily activities, and yet, most gait research has been restricted to data collection in laboratories using embedded force plates or on tracks using motion-capture. Naturally occurring variation in terrain influences the mechanics and energetics of walking, but most biomechanical studies have been constrained to laboratory protocols that cannot fully capture adaptations to terrain over multiple connected gait cycles. This dissertation work highlights the necessity of extending research outside of the laboratory and the importance of capturing gait data across multiple, contiguous steps. I showed that peak GRFs are variable across different surfaces and along gradients and that treadmill walking is distinct from over-ground walking over multiple gait cycles. I also showed that the locations of these peak GRFs on the foot are inconsistent during braking, but highly consistent during propulsion, which was contrary to my expectations. Finally, I showed that anteroposterior GRFs, velocity, and contact time between the foot and the ground during walking are predictive mechanical proxies for metabolic energy expenditure.

Because GRFs that occur between the foot and the surface directly influence joint moments throughout the body and, consequently, the counteracting muscular forces, GRFs and their locations are directly tied to both morphology and energetics of bipedal movement. Mobility is a non-trivial portion of the daily activity budget, and, in turn, influences the nutritional requirements

for survival and reproduction (e.g. Ross & Winterhalder 2015, Howland 1974, Gibson & Mace 2006, Kramer 1998). The derived morphology of the modern human foot is one of the more substantial differences between the anatomy of modern humans and extant nonhuman primates, and this morphology is associated with bipedalism. The changes to the foot in response to bipedalism are part of the morphological adjustments of the musculoskeletal system that are a result of changes to the locations and magnitudes of the applied forces. As with any dynamic system, repeated loading patterns play an important part in system design to ensure durability, i.e., these systems are designed for fatigue loading. It is crucial, therefore, that we understand where the peak forces occur on the foot, not just over one loading cycle, but over many loading cycles to fully grasp the system dynamics as a whole and what it implies for human bipedal mobility. The environmental pressures that led to the transition from quadrupedalism to bipedalism are still subjects of speculation (e.g. Sylvester & Kramer 2008, Bramble & Lieberman 2004, Rosenberg & DeSilva 2017, etc.) and understanding the mechanical interaction of the foot with the ground and its influence on the bipedal body as a system during the most habitual human locomotion, i.e. walking, helps to inform our view of bipedal evolution.

6.2 FUTURE WORK

My dissertation work originated with an interest in measuring the shear forces associated with movement – in other words, apGRFs – outside of the confines of the laboratory. As discussed in some detail in Chapter 2 of this dissertation, bone is strain sensitive and responds to applied forces, although the mechanism and further details regarding this response is not well understood (e.g. Frost 2003, Kivell 2016, Currey 2003). In the engineering materials realm, strain has several forms, one of which is shear strain, or the deformation of a material in response to an applied shear force.

It is generally accepted that bony morphology is heavily influenced by these applied forces (e.g. Lovejoy 2005, Ruff 2017), so it only followed to track down the forces responsible for these changes.

Humans move differently in their environment than in the laboratory (e.g. Yao 2019 and Lim & Lee 2018), and the surfaces, gradients, and obstacles they encounter are difficult to recreate in a laboratory, but are potentially crucial to understanding the true forces of bipedal locomotion. Current wireless sensing technology is limited to only capturing vertical GRFs (vGRFs), so I was not able to investigate apGRFs outside of the laboratory and across multiple, contiguous steps. As I have shown in this dissertation, apGRFs are predictive of metabolic energy expenditure, so the necessity for gathering apGRF data is twofold; 1.) to accurately predict energy expenditure and 2.) to inform our understanding of the shear forces applied to the bony system. In future work I will use alternatives to force sensors, IMUs capturing acceleration and displacement, outside of the laboratory and use the data from these devices to calculate apGRFs and vGRFs, until wireless force-sensing technology is capable of measuring apGRFs.

Since we now know that contact time is predictive of energetic cost, future work should utilize the wireless insoles to measure contact time outside of the laboratory and, therefore, energy expenditure. Future work should also expand the participant sample from the energetic study. I performed a secondary analysis on data that was collected from 2010-2013 on individuals selected to be relatively homogeneous in body shape and size. To further validate my findings, the sample size and range of body types should be increased. Across all three studies, the range of velocities and surface types should be expanded, and a wider range of gradients should be explored.

6.3 REFERENCES

Bramble DM, Lieberman DE. Endurance running and the evolution of Homo. Nature. 2004 Nov 18;432(7015):345-52. doi: 10.1038/nature03052. PMID: 15549097.

Cavagna GA, Heglund NC, Taylor CR. Mechanical work in terrestrial locomotion: two basic mechanisms for minimizing energy expenditure. Am J Physiol. 1977 Nov;233(5):R243-61. doi: 10.1152/ajpregu.1977.233.5.R243. PMID: 411381.

Currey JD. The many adaptations of bone. J Biomech. 2003 Oct;36(10):1487-95. doi: 10.1016/s0021-9290(03)00124-6. PMID: 14499297.

Frost HM. A 2003 update of bone physiology and Wolff's Law for clinicians. Angle Orthod. 2004 Feb;74(1):3-15. doi: 10.1043/0003-3219(2004)074<0003:AUOBPA>2.0.CO;2. PMID: 15038485.

Geyer H, Seyfarth A, Blickhan R. Compliant leg behaviour explains basic dynamics of walking and running. Proc Biol Sci. 2006 Nov 22;273(1603):2861-7. doi: 10.1098/rspb.2006.3637. PMID: 17015312; PMCID: PMC1664632.

Gibson MA, Mace R. An energy-saving development initiative increases birth rate and childhood malnutrition in rural Ethiopia. PLoS Med. 2006;3(4):e87. doi:10.1371/journal.pmed.0030087

Howland HC. Optimal strategies for predator avoidance: the relative importance of speed and manoeuvrability. J Theor Biol. 1974;47(2):333-350. doi:10.1016/0022-5193(74)90202-1

Kivell TL. A review of trabecular bone functional adaptation: what have we learned from trabecular analyses in extant hominoids and what can we apply to fossils? J Anat. 2016 Apr;228(4):569-94. doi: 10.1111/joa.12446. Epub 2016 Feb 16. PMID: 26879841; PMCID: PMC4804137.

Kramer PA. The costs of human locomotion: maternal investment in child transport. Am J Phys Anthropol. 1998;107(1):71-85. doi:10.1002/(SICI)1096-8644(199809)107:1<71::AID-AJPA6>3.0.CO;2-G

Lim SY, Lee WH. Effects of pelvic range of motion and lower limb muscle activation pattern on over-ground and treadmill walking at the identical speed in healthy adults. J Phys Ther Sci. 2018;30(4):619-624. doi:10.1589/jpts.30.619

Lovejoy CO. The natural history of human gait and posture. Parts 1-3. Gait Posture. 2005;21(1):113-124. doi:10.1016/j.gaitpost.2004.06.010

Rebula JR, Kuo AD. The cost of leg forces in bipedal locomotion: a simple optimization study. PLoS One. 2015 Feb 23;10(2):e0117384. doi: 10.1371/journal.pone.0117384. PMID: 25707000; PMCID: PMC4338056.

Rosenberg KR, DeSilva JM. Evolution of the Human Pelvis. Anat Rec (Hoboken). 2017 May;300(5):789-797. doi: 10.1002/ar.23580. PMID: 28406563.

Ross CT, Winterhalder B. Sit-and-wait versus active-search hunting: A behavioral ecological model of optimal search mode. J Theor Biol. 2015;387:76-87. doi:10.1016/j.jtbi.2015.09.022

Ruff C. Mechanical Constraints on the Hominin Pelvis and the "Obstetrical Dilemma". Anat Rec (Hoboken). 2017;300(5):946-955. doi:10.1002/ar.23539

Sylvester AD, Kramer PA. Brief Communication: Stand and shuffle: when does it make energetic sense? Am J Phys Anthropol. 2008 Apr;135(4):484-8. doi: 10.1002/ajpa.20752. PMID: 18000893.

Yao J, Guo N, Xiao Y, Li Z, Li Y, Pu F, Fan Y. Lower limb joint motion and muscle force in treadmill and over-ground exercise. Biomed Eng Online. 2019;18(1):89. Published 2019 Aug 22. doi:10.1186/s12938-019-0708-4

APPENDIX A

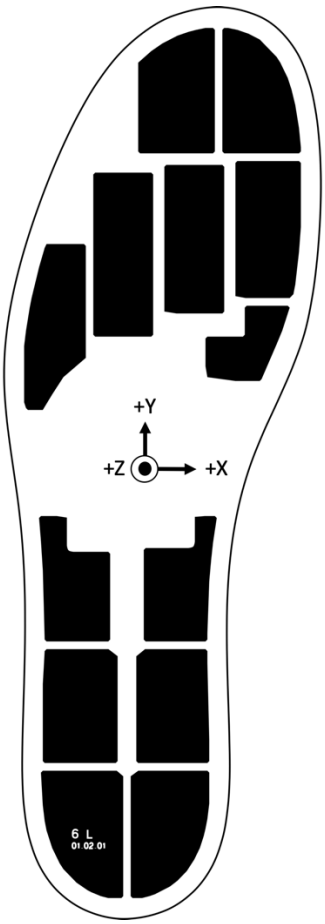

Supplementary Figure 1 – Moticon GmbH pressure-sensing insole sensor arrangement.

Participant	Age	Mass (kg)	Neutral Standing Force (N)	Insole Size	Arch Index
X1	26	70.2	868.0	8/9	0.244
X3	29	86.4	819.0	9.5/10.5	0.182
X4	20	120.0	1176.0	11/12	0.424
X5	21	70.7	692.9	8/9	0.235
X6	28	52.0	509.6	6.5/7.5	0.252
X7	42	86.0	842.8	9.5/10.5	0.249
X9	29	55.0	539.0	6.5/7.5	0.128
X10	20	48.9	479.2	6.5/7.5	0.089
X11	32	72.9	714.4	8/9	0.162
X12	21	54.6	535.1	6.5/7.5	0.159
X13	32	66.5	651.7	8/9	0.349

Supplementary Table 1 – Participant Data

Trial	Steps Analyzed
Slow Treadmill	572
Moderate Treadmill	1183
Fast Treadmill	1218
Incline Treadmill	680
Hallway	1130
Downhill	973
Uphill	955

Supplementary Table 2 – Number of isolated steps with a clear braking and propulsive peak per trial. A total of 6711 steps were analyzed.

Participant	Hallway (m/s)	Downhill (m/s)	Uphill (m/s)
X1	1.43	1.52	1.51
X3	1.24	1.50	1.56
X4	1.29	1.49	1.36
X5	1.20	1.43	1.52
X6	1.15	1.32	1.46
X7	1.24	1.41	1.39
X9	1.12	1.28	1.34
X10	1.11	1.50	1.33
X11	1.15	1.34	1.24
X12	1.24	1.39	1.47
X13	1.23	1.47	1.52

Supplementary Table 3 – Participant velocities for self-selected velocity trials.

Correlation Matrix	Peak Braking Force	Peak Propulsive Force
Mass	0.648	0.690
Neutral Stance	0.703	0.576
Velocity	0.256	-0.0913
Arch Index	0.353	0.407

Supplementary Table 4 – Correlation matrix for participant-level variable and peak braking and peak propulsive forces.

APPENDIX B

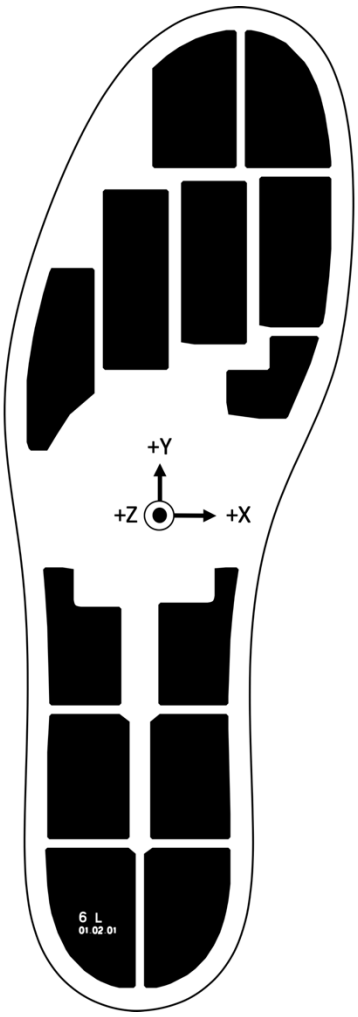

Supplementary Figure 1 - A schematic of the Moticon ReGo wireless insole pressure sensor array.

Trial	Steps Analyzed
Slow Treadmill	572
Moderate Treadmill	1183
Fast Treadmill	1218
Incline Treadmill	680
Hallway	1130
Downhill	973
Uphill	955

Supplementary Table 1 – Number of isolated steps with a clear braking and propulsive peak per trial. A total of 6711 steps were analyzed.

Braking	Slow Treadmill	Moderate Treadmill	Fast Treadmill	Incline Treadmill	Hallway	Downhill	Uphill
Slow Treadmill							
Moderate Treadmill	For d > 0.01m						
Fast Treadmill	For d > 0.01m	NS					
Incline Treadmill	NS	For d > 0.03m	For d > 0.03m				
Hallway	For all d	NS	NS	For d > 0.02m			
Downhill	For all d	For all d	For all d	For all d	For d > 0.01m		
Uphill	For all d	NS	NS	For all d	NS	For all d	

Propulsion	Slow Treadmill	Moderate Treadmill	Fast Treadmill	Incline Treadmill	Hallway	Downhill	Uphill
Slow Treadmill							
Moderate Treadmill	For all d						
Fast Treadmill	For all d	NS					
Incline Treadmill	NS	For all d	For all d				
Hallway	For all d	NS	NS	For all d			
Downhill	For all d	NS	NS	For all d	NS		
Uphill	For all d	NS	NS	For all d	NS	NS	

Supplementary Table 2 – Statistical results for all pairwise trial comparisons of K(d) for braking and propulsion. Significance based on Monte Carlo acceptance envelopes. Results are for d in meters.

APPENDIX C

Paper #3 of AGH Dissertation
Finding a Mechanical Proxy for Energy Expenditure
Impulse Edition

```{r, echo=FALSE}
library(dplyr)
library(uwIntroStats)
library(tidyr)
library(lme4)
library(pander)
library(nlme)
library(lmerTest)
library(readxl)
library(ggplot2)
```

Overview

Pull in E-series data from PAK files. I have brought all the individual subject data into one excel sheet.
Each participant was asked to walk on a treadmill and select their preferred Slow, Normal, and Fast velocities. The researchers then calculated Medium Slow and Medium Fast velocities from the midpoint between the Slow and Normal velocities and the Normal and Fast velocities. Each participant was fitted with a SensorMedics oxygen analyzer mask. Standing resting metabolic rate (stRMR) was collected prior to testing. Each participant then walked for five minutes at each velocity, with four minutes of quiet standing between each trial. The trial velocities were randomized.

Data structure notes:

E-Series: 16 females

Treadmill velocities (CoTs):
Slow
Medium Slow
Natural
Medium Fast
Fast

Force plate velocities GRFs (5 trials on left, 5 trials on right):
Slow
Natural
Fast

Plan:
1. Calculate Impulse for each GRF curve
  a.) "Tare" each trial by averaging frames 10-100 (there is always some offset)
  b.) Assign y-axes cutoff for vertical (50N?) and ant-post (?) -- Thresholding
  c.) Find: start point, end point for each step
  d.) Use "findpeaks" to find: braking and propulsion vert peaks, |abs| for ap peaks
  e.) Define midstance point as 50% between start and end points
  f.) Use trapz() in MATLAB to calculate Impulse for each step **do not normalize**

2. Calculate CoT for each participant at each velocity
  a.) Pull in excel sheet with CoT calculated for each minute
  b.) Use minutes 3, 4, 5 individually **do not average across minutes**
  c.) Fit quadratic curve (CoT~velocity) for each individual

First, CoT by individual

```{r, echo=FALSE}
#import dataset
library(readxl)

Eall <- read_excel("~/Documents/Paper #3/Eall.xlsx")
View(Eall)

#JUST REALIZED AVG COT IN EXCEL SHEET IS BY MPH NOT M/S
#ALSO AVG VO2 IS BY L/MIN, CONVERT TO ML/S BEFORE CALCULATING COT
```
```{r}
set.seed(456)

names(Eall)[10] <- "avgCoTmph"
names(Eall)[8] <- "avgVO2Lpermin"

Eall$time <- as.factor(Eall$time)
Eall$velocity <- as.numeric(Eall$velocity)
Eall$'avgCoTmph' <- as.numeric(Eall$'avgCoTmph')

Eall$speedcat <- factor(Eall$condition, levels=c("S","MS","N","MF","F"))

```

The average CoT in the excel sheet was caluclated by using mph
Recalculate using m/s

```{r}
#Make sure you have avgCoT as m/s and numeric
```

```
Eall$avgCoT <- as.numeric(Eall$avgCoT)

#Add a column for net CoT ((avgVO2 - stRMR)/velocity)
Eall$netCoT <- ((Eall$avgVO2 - Eall$stRMR)/Eall$velocity)
```

ggplot2 is being a POS

```{r}
Eall %>%
  filter(Subject == "E01") %>%
  ggplot(aes(x=speedcat, y=avgCoT, colour=time)) +
  geom_point()

Eall %>%
  filter(Subject == "E02") %>%
  ggplot(aes(x=speedcat, y=avgCoT, colour=time)) +
  geom_point()

Eall %>%
  filter(Subject == "E03") %>%
  ggplot(aes(x=speedcat, y=avgCoT, colour=time)) +
  geom_point()

Eall %>%
  filter(Subject == "E04") %>%
  ggplot(aes(x=speedcat, y=avgCoT, colour=time)) +
  geom_point()

Eall %>%
  filter(Subject == "E05") %>%
  ggplot(aes(x=speedcat, y=avgCoT, colour=time)) +
  geom_point()

Eall %>%
  filter(Subject == "E06") %>%
  ggplot(aes(x=speedcat, y=avgCoT, colour=time)) +
  geom_point()

Eall %>%
  filter(Subject == "E07") %>%
  ggplot(aes(x=speedcat, y=avgCoT, colour=time)) +
  geom_point()

Eall %>%
```

```
  filter(Subject == "E08") %>%
  ggplot(aes(x=speedcat, y=avgCoT, colour=time)) +
  geom_point()

Eall %>%
  filter(Subject == "E09") %>%
  ggplot(aes(x=speedcat, y=avgCoT, colour=time)) +
  geom_point()

Eall %>%
  filter(Subject == "E10") %>%
  ggplot(aes(x=speedcat, y=avgCoT, colour=time)) +
  geom_point()

Eall %>%
  filter(Subject == "E11") %>%
  ggplot(aes(x=speedcat, y=avgCoT, colour=time)) +
  geom_point()

Eall %>%
  filter(Subject == "E12") %>%
  ggplot(aes(x=speedcat, y=avgCoT, colour=time)) +
  geom_point()

Eall %>%
  filter(Subject == "E13") %>%
  ggplot(aes(x=speedcat, y=avgCoT, colour=time)) +
  geom_point()

Eall %>%
  filter(Subject == "E14") %>%
  ggplot(aes(x=speedcat, y=avgCoT, colour=time)) +
  geom_point()

Eall %>%
  filter(Subject == "E15") %>%
  ggplot(aes(x=speedcat, y=avgCoT, colour=time)) +
  geom_point()

Eall %>%
  filter(Subject == "E16") %>%
  ggplot(aes(x=speedcat, y=avgCoT, colour=time)) +
  geom_point()

```
```{r}
```

```
Eall %>%
  #filter(Subject == "E01") %>%
  ggplot(aes(x=speedcat, y=avgCoT, colour=time)) +
  geom_point()

Eall %>%
  filter(!time %in% c('1', '2')) %>%
  filter(!Subject %in% c('E02', 'E12')) %>%
  ggplot(aes(x=speedcat, y=avgCoT, colour=time)) +
  xlab("Speed Category") +
  ylab("Cost of Transport (mL/m)") +
  labs(color = "Minute") +
  geom_point(alpha=0.7, size=4)

Eall %>%
  filter(!time %in% c('1', '2')) %>%
  filter(Subject=="E14") %>%
  ggplot(aes(x=speedcat, y=avgCoT, colour=time)) +
  xlab("Speed Category") +
  ylab("Cost of Transport (mL/m)") +
  labs(color = "Minute") +
  geom_point(alpha=1, size=4)

Eall %>%
  #filter(Subject == "E01") %>%
  ggplot(aes(x=speedcat, y=netCoT, colour=time)) +
  geom_point()
```

Subset the data into a new dataframe with just minutes 3, 4, and 5.

```{r}
E345 <- Eall %>%
  filter(!time %in% c('1', '2'))
View(E345)
```

```{r}
#velocity as continuous

E345curveE01 <- lm(formula = avgCoT[Subject=='E01'] ~
                poly(velocity[Subject=='E01'],2,raw=TRUE),
                data=E345)
summary(E345curveE01)

E345curveE02 <- lm(formula = avgCoT[Subject=='E02'] ~
                poly(velocity[Subject=='E02'],2,raw=TRUE),
               data=E345)
```

```
summary(E345curveE02)

E345curveE03 <- lm(formula = avgCoT[Subject=='E03'] ~
             poly(velocity[Subject=='E03'],2,raw=TRUE),
           data=E345)
summary(E345curveE03)

E345curveE04 <- lm(formula = avgCoT[Subject=='E04'] ~
             poly(velocity[Subject=='E04'],2,raw=TRUE), data=E345)
summary(E345curveE04)

E345curveE05 <- lm(formula = avgCoT[Subject=='E05'] ~
             poly(velocity[Subject=='E05'],2,raw=TRUE), data=E345)
summary(E345curveE05)

E345curveE06 <- lm(formula = avgCoT[Subject=='E06'] ~
             poly(velocity[Subject=='E06'],2,raw=TRUE), data=E345)
summary(E345curveE06)

E345curveE07 <- lm(formula = avgCoT[Subject=='E07'] ~
             poly(velocity[Subject=='E07'],2,raw=TRUE), data=E345)
summary(E345curveE07)

E345curveE08 <- lm(formula = avgCoT[Subject=='E08'] ~
             poly(velocity[Subject=='E08'],2,raw=TRUE), data=E345)
summary(E345curveE08)

E345curveE09 <- lm(formula = avgCoT[Subject=='E09'] ~
             poly(velocity[Subject=='E09'],2,raw=TRUE), data=E345)
summary(E345curveE09)

E345curveE10 <- lm(formula = avgCoT[Subject=='E10'] ~
             poly(velocity[Subject=='E10'],2,raw=TRUE), data=E345)
summary(E345curveE10)


E345curveE11 <- lm(formula = avgCoT[Subject=='E11'] ~
             poly(velocity[Subject=='E11'],2,raw=TRUE), data=E345)
summary(E345curveE11)

E345curveE12 <- lm(formula = avgCoT[Subject=='E12'] ~
             poly(velocity[Subject=='E12'],2,raw=TRUE), data=E345)
summary(E345curveE12)

E345curveE13 <- lm(formula = avgCoT[Subject=='E13'] ~
             poly(velocity[Subject=='E13'],2,raw=TRUE), data=E345)
```

```
summary(E345curveE13)

E345curveE14 <- lm(formula = avgCoT[Subject=='E14'] ~
            poly(velocity[Subject=='E14'],2,raw=TRUE), data=E345)
summary(E345curveE14)

E345curveE15 <- lm(formula = avgCoT[Subject=='E15'] ~
            poly(velocity[Subject=='E15'],2,raw=TRUE), data=E345)
summary(E345curveE15)

E345curveE16 <- lm(formula = avgCoT[Subject=='E16'] ~
            poly(velocity[Subject=='E16'],2,raw=TRUE), data=E345)
summary(E345curveE16)
```

Put the CoT fitted curve coefficients for each individual into a table.
Columns: ID, Intercept (Bo), B1, B2, p-value, R^2

```{r}
columnnames <- c("ID", "Intercept", "B1", "B2")
short.coeff.frame <- data.frame(ID=c("1", "2", "3", "4", "5", "6", "7",
                          "8", "9", "10", "11", "12", "13", "14",
                          "15", "16"),
                    Bo=c(E345curveE01$coefficients[1],
                        E345curveE02$coefficients[1],
                        E345curveE03$coefficients[1],
                        E345curveE04$coefficients[1],
                        E345curveE05$coefficients[1],
                        E345curveE06$coefficients[1],
                        E345curveE07$coefficients[1],
                        E345curveE08$coefficients[1],
                        E345curveE09$coefficients[1],
                        E345curveE10$coefficients[1],
                        E345curveE11$coefficients[1],
                        E345curveE12$coefficients[1],
                        E345curveE13$coefficients[1],
                        E345curveE14$coefficients[1],
                        E345curveE15$coefficients[1],
                        E345curveE16$coefficients[1]),
                    B1=c(E345curveE01$coefficients[2],
                        E345curveE02$coefficients[2],
                        E345curveE03$coefficients[2],
                        E345curveE04$coefficients[2],
                        E345curveE05$coefficients[2],
                        E345curveE06$coefficients[2],
                        E345curveE07$coefficients[2],
```

```
                    E345curveE08$coefficients[2],
                    E345curveE09$coefficients[2],
                    E345curveE10$coefficients[2],
                    E345curveE11$coefficients[2],
                    E345curveE12$coefficients[2],
                    E345curveE13$coefficients[2],
                    E345curveE14$coefficients[2],
                    E345curveE15$coefficients[2],
                    E345curveE16$coefficients[2]),
                B2=c(E345curveE01$coefficients[3],
                    E345curveE02$coefficients[3],
                    E345curveE03$coefficients[3],
                    E345curveE04$coefficients[3],
                    E345curveE05$coefficients[3],
                    E345curveE06$coefficients[3],
                    E345curveE07$coefficients[3],
                    E345curveE08$coefficients[3],
                    E345curveE09$coefficients[3],
                    E345curveE10$coefficients[3],
                    E345curveE11$coefficients[3],
                    E345curveE12$coefficients[3],
                    E345curveE13$coefficients[3],
                    E345curveE14$coefficients[3],
                    E345curveE15$coefficients[3],
                    E345curveE16$coefficients[3]))
coeff.frame <- short.coeff.frame %>%
  slice(rep(1:n(), each = 3))
View(coeff.frame)
```

VO2 Analysis

```{r}
E345 %>%
  ggplot(aes(x=velocity, y=avgVO2, colour=condition)) +
  geom_point() +
  facet_wrap(~id)
```

```{r}
E345VOcurveE01 <- lm(formula = avgVO2[Subject=='E01'] ~
              poly(velocity[Subject=='E01'],2,raw=TRUE),
              data=E345)
summary(E345VOcurveE01)

E345VOcurveE02 <- lm(formula = avgVO2[Subject=='E02'] ~
              poly(velocity[Subject=='E02'],2,raw=TRUE),
             data=E345)
```

```
summary(E345VOcurveE02)

E345VOcurveE03 <- lm(formula = avgVO2[Subject=='E03'] ~
              poly(velocity[Subject=='E03'],2,raw=TRUE),
            data=E345)
summary(E345VOcurveE03)

E345VOcurveE04 <- lm(formula = avgVO2[Subject=='E04'] ~
              poly(velocity[Subject=='E04'],2,raw=TRUE), data=E345)
summary(E345VOcurveE04)

E345VOcurveE05 <- lm(formula = avgVO2[Subject=='E05'] ~
              poly(velocity[Subject=='E05'],2,raw=TRUE), data=E345)
summary(E345VOcurveE05)

E345VOcurveE06 <- lm(formula = avgVO2[Subject=='E06'] ~
              poly(velocity[Subject=='E06'],2,raw=TRUE), data=E345)
summary(E345VOcurveE06)

E345VOcurveE07 <- lm(formula = avgVO2[Subject=='E07'] ~
              poly(velocity[Subject=='E07'],2,raw=TRUE), data=E345)
summary(E345VOcurveE07)

E345VOcurveE08 <- lm(formula = avgVO2[Subject=='E08'] ~
              poly(velocity[Subject=='E08'],2,raw=TRUE), data=E345)
summary(E345VOcurveE08)

E345VOcurveE09 <- lm(formula = avgVO2[Subject=='E09'] ~
              poly(velocity[Subject=='E09'],2,raw=TRUE), data=E345)
summary(E345VOcurveE09)

E345VOcurveE10 <- lm(formula = avgVO2[Subject=='E10'] ~
              poly(velocity[Subject=='E10'],2,raw=TRUE), data=E345)
summary(E345VOcurveE10)


E345VOcurveE11 <- lm(formula = avgVO2[Subject=='E11'] ~
              poly(velocity[Subject=='E11'],2,raw=TRUE), data=E345)
summary(E345VOcurveE11)

E345VOcurveE12 <- lm(formula = avgVO2[Subject=='E12'] ~
              poly(velocity[Subject=='E12'],2,raw=TRUE), data=E345)
summary(E345VOcurveE12)

E345VOcurveE13 <- lm(formula = avgVO2[Subject=='E13'] ~
              poly(velocity[Subject=='E13'],2,raw=TRUE), data=E345)
```

```
summary(E345VOcurveE13)

E345VOcurveE14 <- lm(formula = avgVO2[Subject=='E14'] ~
            poly(velocity[Subject=='E14'],2,raw=TRUE), data=E345)
summary(E345VOcurveE14)

E345VOcurveE15 <- lm(formula = avgVO2[Subject=='E15'] ~
            poly(velocity[Subject=='E15'],2,raw=TRUE), data=E345)
summary(E345VOcurveE15)

E345VOcurveE16 <- lm(formula = avgVO2[Subject=='E16'] ~
            poly(velocity[Subject=='E16'],2,raw=TRUE), data=E345)
summary(E345VOcurveE16)
```
```{r}
write.table(E345, "~/Documents/Paper #3/E345.txt", sep="/")
write.table(Eall, "~/Documents/Paper #3/ESeriesVO2.txt", sep="/")
```

Combining CoT and Impulse (CoT from EnergeticsCode rmd)

```{r, echo=FALSE}
library(dplyr)
library(uwIntroStats)
library(tidyr)
library(lme4)
library(pander)
library(nlme)
library(lmerTest)
library(readxl)
library(ggplot2)


set.seed(456)
```

Data structure notes:

E-Series: 16 females

Treadmill velocities (CoTs):
Slow
Medium Slow
Natural
Medium Fast

Fast

Force plate velocities GRFs (5 trials on left, 5 trials on right):
Slow
Natural
Fast

```{r, echo=FALSE}
#import dataset
library(readxl)

# updated Imps file
EImps <- read_excel("~/Documents/Paper #3/Eseries_PAK_AGH.xlsx")
View(EImps)

#Energetics file
Eall <- read_excel("~/Documents/Paper #3/Eall.xlsx")
View(Eall) #THE EXCEL SHEET AVERAGE COT IS BY MPH
```
Make sure CoT data is clean:

```{r}
names(Eall)[10] <- "avgCoTmph"
names(Eall)[8] <- "avgVO2Lpermin"

Eall$time <- as.factor(Eall$time)
Eall$velocity <- as.numeric(Eall$velocity)
Eall$'avgCoTmph' <- as.numeric(Eall$'avgCoTmph')

Eall$speedcat <- factor(Eall$condition, levels=c("S","MS","N","MF","F"))

#Make sure you have avgCoT as m/s and numeric
Eall$avgCoT <- as.numeric(Eall$avgCoT)

#Add a column for net CoT ((avgVO2 - stRMR)/velocity)
Eall$netCoT <- ((Eall$avgVO2 - Eall$stRMR)/Eall$velocity)

E345 <- Eall %>%
  filter(!time %in% c('1', '2'))
View(E345)

E345$id <- as.factor(E345$id)

```

Need to assign velocities to trial numbers on the GRF data.

1-10: Slow
11-20: Normal
21-30: Fast

```{r}
#Now assign Slow Natural Fast to trial numbers
EImps$speed <-
  ifelse(EImps$Trial == 1, 'Slow',
         ifelse(EImps$Trial == 2, 'Slow',
          ifelse(EImps$Trial == 3, 'Slow',
          ifelse(EImps$Trial == 4, 'Slow',
          ifelse(EImps$Trial == 5, 'Slow',
          ifelse(EImps$Trial == 6, 'Slow',
          ifelse(EImps$Trial == 7, 'Slow',
          ifelse(EImps$Trial == 8, 'Slow',
          ifelse(EImps$Trial == 9, 'Slow',
          ifelse(EImps$Trial == 10, 'Slow',
          ifelse(EImps$Trial == 11, 'Normal',
          ifelse(EImps$Trial == 12, 'Normal',
          ifelse(EImps$Trial == 13, 'Normal',
          ifelse(EImps$Trial == 14, 'Normal',
          ifelse(EImps$Trial == 15, 'Normal',
          ifelse(EImps$Trial == 16, 'Normal',
          ifelse(EImps$Trial == 17, 'Normal',
          ifelse(EImps$Trial == 18, 'Normal',
          ifelse(EImps$Trial == 19, 'Normal',
          ifelse(EImps$Trial == 20, 'Normal',
          ifelse(EImps$Trial == 21, 'Fast',
          ifelse(EImps$Trial == 22, 'Fast',
          ifelse(EImps$Trial == 23, 'Fast',
          ifelse(EImps$Trial == 24, 'Fast',
          ifelse(EImps$Trial == 25, 'Fast',
          ifelse(EImps$Trial == 26, 'Fast',
          ifelse(EImps$Trial == 27, 'Fast',
          ifelse(EImps$Trial == 28, 'Fast',
          ifelse(EImps$Trial == 29, 'Fast',
          ifelse(EImps$Trial == 30, 'Fast', NA
              ))))))))))))))))))))))))))))))

#First, make ID and Trial categorical
#Imps$ID <- as.factor(Imps$ID)
#Imps$Trial <- as.factor(Imps$Trial)

EImps$ID <- as.factor(EImps$ID)
EImps$Trial <- as.factor(EImps$Trial)
```

```
EImps$acrovel <- EImps$acromionvelocity/1000
EImps$Nmass <- EImps$mass*9.8

EImps$NormvImp1 <- EImps$vImp1/EImps$Nmass
EImps$NormvImp6 <- EImps$vImp6/EImps$Nmass
EImps$NormvImp7 <- EImps$vImp7/EImps$Nmass

#Assign levels
#Imps$speed <- factor(Imps$speed, levels=c("Slow","Normal","Fast"))
EImps$speed <- factor(EImps$speed, levels=c("Slow","Normal","Fast"))
```

Back out average force as a new variable from impulses

```{r}
EImps$vForce <- (EImps$vImp1)/EImps$contact
EImps$apForce <- (EImps$apImp1)/EImps$contact

EImps$vBForce <- (EImps$vImp6)/(EImps$contact)
EImps$vPForce <- (EImps$vImp7)/(EImps$contact)

EImps$apBForce <- (EImps$apImp6)/(EImps$contact)
EImps$apPForce <- (EImps$apImp7)/(EImps$contact)
```

```{r}
#Imps %>%
  #filter(!time %in% c('1', '2')) %>%
#  ggplot(aes(x=speed, y=apImp1, colour=speed)) +
#  geom_point() +
#  facet_wrap(~ID)

#Imps %>%
  #filter(!time %in% c('1', '2')) %>%
#  ggplot(aes(x=speed, y=vImp1, colour=speed)) +
#  geom_point() +
#  facet_wrap(~ID)

EImps %>%
  #filter(!time %in% c('1', '2')) %>%
  ggplot(aes(x=acrovel, y=apImp1, colour=speed)) +
  geom_point() +
  facet_wrap(~ID)

EImps %>%
  #filter(!time %in% c('1', '2')) %>%
```

```
  ggplot(aes(x=acrovel, y=vImp1, colour=speed)) +
  geom_point() +
  facet_wrap(~ID)
```

```{r}
#Imps %>%
#  filter(ID==10) %>%
#  ggplot(aes(x=speed, y=vImp1, colour=speed)) +
#  geom_point()
  #facet_wrap(~ID)

#Imps %>%
#  filter(ID==10) %>%
#  ggplot(aes(x=speed, y=apImp1, colour=speed)) +
#  geom_point()
  #facet_wrap(~ID)

EImps %>%
  filter(ID==10) %>%
  ggplot(aes(x=acrovel, y=vImp1, colour=speed)) +
  geom_point()
  #facet_wrap(~ID)

EImps %>%
  filter(ID==10) %>%
  ggplot(aes(x=acrovel, y=apImp1, colour=speed)) +
  geom_point()
  #facet_wrap(~ID)

EImps %>%
  filter(ID==10) %>%
  ggplot(aes(x=vImp1, y=apImp1, colour=speed)) +
  geom_point()
  #facet_wrap(~ID)

EImps %>%
  #filter(ID==10) %>%
  ggplot(aes(x=acrovel, y=apImp1, colour=speed)) +
  geom_point()
  #facet_wrap(~ID)

EImps %>%
  #filter(ID==10) %>%
  ggplot(aes(x=acrovel, y=vImp1, colour=speed)) +
  geom_point()
  #facet_wrap(~ID)
```

```
```{r}
EImps %>%
  #filter(ID==10) %>%
  ggplot(aes(x=acrovel, y=NormvImp1, colour=speed)) +
  geom_point() +
  facet_wrap(~ID)

EImps %>%
  #filter(ID==10) %>%
  ggplot(aes(x=acrovel, y=NormvImp6, colour=speed)) +
  geom_point() +
  facet_wrap(~ID)

EImps %>%
  #filter(ID==10) %>%
  ggplot(aes(x=acrovel, y=NormvImp7, colour=speed)) +
  geom_point() +
  facet_wrap(~ID)
```
Model exploration.

```{r}
#Run full apImp and vImp vs acrovel, taking into account ID heirarchial structuring
summary(lmer(apImp1~acrovel + (1 | ID), data=EImps, na.rm=TRUE))
summary(lmer(vImp1~acrovel + (1 | ID), data=EImps, na.rm=TRUE))

#library(geepack)
#regress("mean", apImp1 ~ acrovel, id="ID", data=EImps)

#Check quadratic
summary(lmer(apImp1~acrovel + I(acrovel^2) + (1 | ID), data=EImps, na.rm=TRUE))
summary(lmer(vImp1~acrovel + I(acrovel^2) + (1 | ID), data=EImps, na.rm=TRUE))

summary(lmer(formula=apImp1~poly(acrovel,2) + (1 | ID), data=EImps, na.rm=TRUE))
summary(lmer(formula=vImp1~poly(acrovel,2) + (1 | ID), data=EImps, na.rm=TRUE))
#Not quadratic

```

Stick to linear rather than quadradic.

```{r}
EImps %>%
  #filter(!time %in% c('1', '2')) %>%
  ggplot(aes(x=acrovel, y=apImp6, colour=ID)) +
```
```

```
  geom_point()
  #facet_wrap(~ID)

EImps %>%
  #filter(!time %in% c('1', '2')) %>%
  ggplot(aes(x=acrovel, y=vImp6, colour=ID)) +
  geom_point()
  #facet_wrap(~ID)

EImps %>%
  #filter(!time %in% c('1', '2')) %>%
  ggplot(aes(x=acrovel, y=apImp7, colour=ID)) +
  geom_point()
  #facet_wrap(~ID)

EImps %>%
  #filter(!time %in% c('1', '2')) %>%
  ggplot(aes(x=acrovel, y=vImp7, colour=ID)) +
  geom_point()
  #facet_wrap(~ID)

```
```{r}
EImps %>%
  #filter(!time %in% c('1', '2')) %>%
  ggplot(aes(x=acrovel, y=apImp6, colour=speed)) +
  geom_point() +
  facet_wrap(~ID)

EImps %>%
  #filter(!time %in% c('1', '2')) %>%
  ggplot(aes(x=acrovel, y=vImp6, colour=speed)) +
  geom_point() +
  facet_wrap(~ID)

EImps %>%
  #filter(!time %in% c('1', '2')) %>%
  ggplot(aes(x=acrovel, y=apImp7, colour=speed)) +
  geom_point() +
  facet_wrap(~ID)

EImps %>%
  #filter(!time %in% c('1', '2')) %>%
  ggplot(aes(x=acrovel, y=vImp7, colour=speed)) +
  geom_point() +
  facet_wrap(~ID)
```

```
#Imps are not relevant

##Moving on to combining the CoT data and the GRF data

Output a table of averaged acromion velocities for the GRF trials for each participant.

avg(Slow)
avg(Normal)
avg(Fast)

```{r}
acroveltable <- EImps %>%
   group_by(ID, speed) %>%
   summarise(mean = mean(acrovel), stdev = sd(acrovel), n = n())
View(acroveltable)
write.table(acroveltable, "~/Documents/Paper #3/acroveltable.txt", sep="/")
```

Combine the model coefficients from the energetic trials with the acromion velocities.

```{r}
#First, pull in coeff.frame from energetics code and combine with acrovel
calcCoT <- cbind(coeff.frame, acroveltable$speed, acroveltable$mean, acroveltable$stdev)
calcCoT <- calcCoT %>%
  rename(speedcat=`acroveltable$speed`,
        meanVel=`acroveltable$mean`,
        sdVel=`acroveltable$stdev`)
calcCoT$speedcat <- as.factor(calcCoT$speedcat)
calcCoT$speedcat <- factor(calcCoT$speedcat, levels=c("Slow","Normal","Fast"))
View(calcCoT)
```

Now calculate CoT for the GRF data based on the curves calculated for each individual.

```{r}
calcCoT$CoT <- (calcCoT$Bo +
                (calcCoT$B1*calcCoT$meanVel) +
                (calcCoT$B2*(calcCoT$meanVel^2)))
```

Now graph them and see if they make sense. Note: These are averaged. CoTs will be calculated for all velocities, not just averaged velocities below.

```{r}
```
```

```
calcCoT %>%
  #filter(!time %in% c('1', '2')) %>%
  ggplot(aes(x=meanVel, y=CoT, colour=speedcat)) +
  geom_point() +
  facet_wrap(~ID)
```

```{r}
write.table(calcCoT, "~/Documents/Paper #3/calcCoT.txt", sep="/")
```

Now, we need to average the impulses and combine with the calculated CoTs.
Create a new dataframe for this.

```{r}
CoTImps <- EImps %>%
    group_by(ID, speed) %>%
    summarise(avgImp1ap = mean(apImp1),
              avgImp6ap = mean(apImp6),
              avgImp7ap = mean(apImp7),
              avgImp1v = mean(vImp1),
              avgImp6v = mean(vImp6),
              avgImp7v = mean(vImp7),
              avgacrovel = mean(acrovel),
              Nmass = mean(Nmass),
              stRMR = mean(stRMR),
              stature = mean(stature))
CoTImps$calcCoT <- calcCoT$CoT
View(CoTImps)

EImps <- left_join(EImps, short.coeff.frame, "ID")

EImps$calcCoT <- (EImps$Bo +
                  (EImps$B1*EImps$acrovel) +
                  (EImps$B2*(EImps$acrovel^2)))

EImps <- EImps %>%
    rename(avgleg=`average leg length`)

#EImps$crural <- ((EImps$avgleg-EImps$BiTroch)/EImps$BiTroch) #get help with this
```

Check the quadratic curve fit for non-averaged calculated CoTs for each participant.

```{r}
#velocity as continuous
```

```
calccurveE01 <- lm(formula = calcCoT[ID=='1'] ~
              poly(acrovel[ID=='1'],2,raw=TRUE),
              data=EImps)
summary(calccurveE01)

calccurveE02 <- lm(formula = calcCoT[ID=='2'] ~
              poly(acrovel[ID=='2'],2,raw=TRUE),
             data=EImps)
summary(calccurveE02)

calccurveE03 <- lm(formula = calcCoT[ID=='3'] ~
              poly(acrovel[ID=='3'],2,raw=TRUE),
            data=EImps)
summary(calccurveE03)

calccurveE04 <- lm(formula = calcCoT[ID=='4'] ~
              poly(acrovel[ID=='4'],2,raw=TRUE), data=EImps)
summary(calccurveE04)

calccurveE05 <- lm(formula = calcCoT[ID=='5'] ~
              poly(acrovel[ID=='5'],2,raw=TRUE), data=EImps)
summary(calccurveE05)

calccurveE06 <- lm(formula = calcCoT[ID=='6'] ~
              poly(acrovel[ID=='6'],2,raw=TRUE), data=EImps)
summary(calccurveE06)

calccurveE07 <- lm(formula = calcCoT[ID=='7'] ~
              poly(acrovel[ID=='7'],2,raw=TRUE), data=EImps)
summary(calccurveE07)

calccurveE08 <- lm(formula = calcCoT[ID=='8'] ~
              poly(acrovel[ID=='8'],2,raw=TRUE), data=EImps)
summary(calccurveE08)

calccurveE09 <- lm(formula = calcCoT[ID=='9'] ~
              poly(acrovel[ID=='9'],2,raw=TRUE), data=EImps)
summary(calccurveE09)

calccurveE10 <- lm(formula = calcCoT[ID=='10'] ~
              poly(acrovel[ID=='10'],2,raw=TRUE), data=EImps)
summary(calccurveE10)


calccurveE11 <- lm(formula = calcCoT[ID=='11'] ~
              poly(acrovel[ID=='11'],2,raw=TRUE), data=EImps)
```

```
summary(calccurveE11)

calccurveE12 <- lm(formula = calcCoT[ID=='12'] ~
            poly(acrovel[ID=='12'],2,raw=TRUE), data=EImps)
summary(calccurveE12)

calccurveE13 <- lm(formula = calcCoT[ID=='13'] ~
            poly(acrovel[ID=='13'],2,raw=TRUE), data=EImps)
summary(calccurveE13)

calccurveE14 <- lm(formula = calcCoT[ID=='14'] ~
            poly(acrovel[ID=='14'],2,raw=TRUE), data=EImps)
summary(calccurveE14)

calccurveE15 <- lm(formula = calcCoT[ID=='15'] ~
            poly(acrovel[ID=='15'],2,raw=TRUE), data=EImps)
summary(calccurveE15)

calccurveE16 <- lm(formula = calcCoT[ID=='16'] ~
            poly(acrovel[ID=='16'],2,raw=TRUE), data=EImps)
summary(calccurveE16)
```

All calculated CoT curves are sig quadratic. Good.

Now graph to explore.

```{r}
CoTImps %>%
  ggplot(aes(x=calcCoT, y=avgImp1ap, colour=speed)) +
  geom_point() +
  facet_wrap(~ID)

CoTImps %>%
  ggplot(aes(x=avgImp1ap, y=calcCoT, colour=speed)) +
  geom_point() +
  facet_wrap(~ID)

EImps %>%
  ggplot(aes(x=calcCoT, y=apImp1, colour=speed)) +
  geom_point() +
  facet_wrap(~ID)

EImps %>%
  ggplot(aes(x=apImp1, y=calcCoT, colour=speed)) +
  geom_point() +
```

```
  facet_wrap(~ID)
```

Now into the models.
CoT ~ Impulse | ID

```{r}
#Full Imps
summary(lmer(calcCoT~apImp1 + (1 | ID), data=subset(EImps, ID!='12'), na.rm=TRUE))
I1m2ap <- lmer(calcCoT~apImp1 + (1 | ID), data=subset(EImps, ID!='12'), na.rm=TRUE)
summary(lmer(calcCoT~vImp1 + (1 | ID), data=subset(EImps, ID!='12'), na.rm=TRUE))
I1m2v <- lmer(calcCoT~apImp1 + (1 | ID), data=subset(EImps, ID!='12'), na.rm=TRUE)

#Braking Imps
summary(lmer(calcCoT~apImp6 + (1 | ID), data=subset(EImps, ID!='12'), na.rm=TRUE))
summary(lmer(calcCoT~vImp6 + (1 | ID), data=subset(EImps, ID!='12'), na.rm=TRUE))

#Propulsive Imps
summary(lmer(calcCoT~apImp7 + (1 | ID), data=subset(EImps, ID!='12'), na.rm=TRUE))
summary(lmer(calcCoT~vImp7 + (1 | ID), data=subset(EImps, ID!='12'), na.rm=TRUE))
```

```{r}
#Full Imps
#summary(lmer(calcCoT~apImp1 + (1 | ID), data=EImps, na.rm=TRUE))
summary(lmer(calcCoT~NormvImp1 + (1 | ID), data=EImps, na.rm=TRUE))

#Braking Imps
#summary(lmer(calcCoT~apImp6 + (1 | ID), data=EImps, na.rm=TRUE))
summary(lmer(calcCoT~NormvImp6 + (1 | ID), data=EImps, na.rm=TRUE))

#Propulsive Imps
#summary(lmer(calcCoT~apImp7 + (1 | ID), data=EImps, na.rm=TRUE))
summary(lmer(calcCoT~NormvImp7 + (1 | ID), data=EImps, na.rm=TRUE))
```

Check quadratic

```{r}
#Full Imps
summary(lmer(calcCoT~apImp1 + I(apImp1^2) + (1 | ID),
        data=subset(EImps, ID!='12'), na.rm=TRUE))
summary(lmer(calcCoT~vImp1 + I(vImp1^2) + (1 | ID),
        data=subset(EImps, ID!='12'), na.rm=TRUE))
```

```
#Braking Imps
summary(lmer(calcCoT~apImp6 + I(apImp6^2) + (1 | ID),
        data=subset(EImps, ID!='12'), na.rm=TRUE))
summary(lmer(calcCoT~vImp6 + I(vImp6^2) + (1 | ID),
        data=subset(EImps, ID!='12'), na.rm=TRUE))

#Propulsive Imps
summary(lmer(calcCoT~apImp7 + I(apImp7^2) + (1 | ID),
        data=subset(EImps, ID!='12'), na.rm=TRUE))
summary(lmer(calcCoT~vImp7 + I(vImp7^2) + (1 | ID),
        data=subset(EImps, ID!='12'), na.rm=TRUE))
```

vImp fits quadratic. Maybe due to contact time?

```{r}
#Full Imps
summary(lmer(calcCoT~apImp1 + acrovel + (1 | ID), data=subset(EImps, ID!='12'),
na.rm=TRUE))
summary(lmer(calcCoT~vImp1 + acrovel + (1 | ID), data=subset(EImps, ID!='12'),
na.rm=TRUE))

#Braking Imps
summary(lmer(calcCoT~apImp6 + acrovel + (1 | ID), data=subset(EImps, ID!='12'),
na.rm=TRUE))
summary(lmer(calcCoT~vImp6 + acrovel + (1 | ID), data=subset(EImps, ID!='12'),
na.rm=TRUE))

#Propulsive Imps
summary(lmer(calcCoT~apImp7 + acrovel + (1 | ID), data=subset(EImps, ID!='12'),
na.rm=TRUE))
summary(lmer(calcCoT~vImp7 + acrovel + (1 | ID), data=subset(EImps, ID!='12'),
na.rm=TRUE))
```

Check the relationship between contact time and CoT first, then combine Imp and contact time.

```{r}
summary(lmer(calcCoT~contact + I(contact^2) + (1 | ID),
        data=subset(EImps, ID!='12'), na.rm=TRUE))

summary(lmer(calcCoT~contact + I(contact^2) + acrovel + (1 | ID),
        data=subset(EImps, ID!='12'), na.rm=TRUE))

summary(lmer(calcCoT~contact + I(contact^2) + Nmass + (1 | ID),
        data=subset(EImps, ID!='12'), na.rm=TRUE))
```

```
summary(lmer(calcCoT~contact + I(contact^2) + stRMR + (1 | ID),
        data=subset(EImps, ID!='12'), na.rm=TRUE))

summary(lmer(calcCoT~contact + I(contact^2) + vImp1 + (1 | ID),
        data=subset(EImps, ID!='12'), na.rm=TRUE))

summary(lmer(calcCoT~contact + I(contact^2) + apImp1 + (1 | ID),
        data=subset(EImps, ID!='12'), na.rm=TRUE))
```

Dig a bit more into Imps and CoT and contact time based on Gottschall's propulsion observations.

```{r}
summary(lmer(calcCoT~contact + I(contact^2)
        + apImp6
        + (1 | ID),
        data=subset(EImps, ID!='12'), na.rm=TRUE))

summary(lmer(calcCoT~contact + I(contact^2)
        + vImp6
        + (1 | ID),
        data=subset(EImps, ID!='12'), na.rm=TRUE))

summary(lmer(calcCoT~contact + I(contact^2)
        + apImp6
        + vImp6
        + (1 | ID),
        data=subset(EImps, ID!='12'), na.rm=TRUE))

summary(lmer(calcCoT~contact + I(contact^2)
        + apImp7
        + (1 | ID),
        data=subset(EImps, ID!='12'), na.rm=TRUE))

summary(lmer(calcCoT~contact + I(contact^2)
        + vImp7
        + (1 | ID),
        data=subset(EImps, ID!='12'), na.rm=TRUE))

summary(lmer(calcCoT~contact + I(contact^2)
        + apImp7
        + vImp7
        + (1 | ID),
```

```
        data=subset(EImps, ID!='12'), na.rm=TRUE))

summary(lmer(calcCoT~contact + I(contact^2)
        + vImp6
        + apImp7
        + (1 | ID),
        data=subset(EImps, ID!='12'), na.rm=TRUE))
```

```{r}
summary(lmer(calcCoT~contact + I(contact^2)
        + acrovel
        + Nmass
        + (1 | ID),
        data=subset(EImps, ID!='12'), na.rm=TRUE))

summary(lmer(calcCoT~contact + I(contact^2)
        + acrovel
        + vImp6
        + apImp7
        + (1 | ID),
        data=subset(EImps, ID!='12'), na.rm=TRUE))

summary(lmer(calcCoT~contact + I(contact^2)
        + stRMR
        + vImp6
        + apImp7
        + (1 | ID),
        data=subset(EImps, ID!='12'), na.rm=TRUE))

summary(lmer(calcCoT~contact + I(contact^2)
        + acrovel
        + stRMR
        + (1 | ID),
        data=subset(EImps, ID!='12'), na.rm=TRUE))

summary(lmer(calcCoT~contact + I(contact^2)
        + acrovel
        + stRMR
        + Nmass
        + (1 | ID),
        data=subset(EImps, ID!='12'), na.rm=TRUE))
```

Need to adjust anthropometric units:

```{r}
#Check units for anthropometrics
summary(lmer(calcCoT~contact + I(contact^2)
        + acrovel
        + stRMR
        + avgleg
        + (1 | ID),
        data=EImps, na.rm=TRUE))

summary(lmer(calcCoT~contact + I(contact^2)
        + acrovel
        + stRMR
        + Rfoot
        + (1 | ID),
        data=EImps, na.rm=TRUE))

summary(lmer(calcCoT~contact + I(contact^2)
        + acrovel
        + stRMR
        + BiASIS
        + (1 | ID),
        data=EImps, na.rm=TRUE))

summary(lmer(calcCoT~contact + I(contact^2)
        + acrovel
        + stRMR
        + BiTroch
        + (1 | ID),
        data=EImps, na.rm=TRUE))

summary(lmer(calcCoT~contact + I(contact^2)
        + acrovel
        #+ stRMR
        + BiTroch
        + (1 | ID),
        data=EImps, na.rm=TRUE))

summary(lmer(calcCoT~contact + I(contact^2)
        + acrovel
        #+ stRMR
        + BiASIS
        + (1 | ID),
        data=EImps, na.rm=TRUE))
```

```{r}
#Full Imps
summary(lmer(calcCoT~apImp1 + Nmass + (1 | ID), data=subset(EImps, ID!='12'),
na.rm=TRUE))
I1m3ap <- lmer(calcCoT~apImp1 + Nmass + (1 | ID), data=subset(EImps, ID!='12'),
na.rm=TRUE)
summary(lmer(calcCoT~vImp1 + Nmass + (1 | ID), data=subset(EImps, ID!='12'),
na.rm=TRUE))
I1m3v <- lmer(calcCoT~apImp1 + Nmass + (1 | ID), data=subset(EImps, ID!='12'),
na.rm=TRUE)

#Braking Imps
summary(lmer(calcCoT~apImp6 + Nmass + (1 | ID), data=subset(EImps, ID!='12'),
na.rm=TRUE))
summary(lmer(calcCoT~vImp6 + Nmass + (1 | ID), data=subset(EImps, ID!='12'),
na.rm=TRUE))

#Propulsive Imps
summary(lmer(calcCoT~apImp7 + Nmass + (1 | ID), data=subset(EImps, ID!='12'),
na.rm=TRUE))
summary(lmer(calcCoT~vImp7 + Nmass + (1 | ID), data=subset(EImps, ID!='12'),
na.rm=TRUE))
```

Just for kicks, try using VO2 instead of CoT?
Since CoT = VO2/velocity, back calculate VO2=CoT*velocity
(unsure if this is legitimate but just throw it in for now)

```{r}
EImps$VO2 <- (EImps$calcCoT*EImps$acrovel)
```

```{r}
EImps %>%
  ggplot(aes(x=acrovel, y=VO2, colour=speed)) +
  geom_point() +
  facet_wrap(~ID)

EImps %>%
  ggplot(aes(x=acrovel, y=calcCoT, colour=speed)) +
  geom_point() +
  facet_wrap(~ID)
```

```
EImps %>%
  ggplot(aes(x=VO2, y=calcCoT, colour=speed)) +
  geom_point() +
  facet_wrap(~ID)

EImps %>%
  ggplot(aes(x=Nmass, y=calcCoT, colour=ID)) +
  geom_point()

EImps %>%
  ggplot(aes(x=Nmass, y=VO2, colour=ID)) +
  geom_point()
```

```{r}
EImps %>%
  ggplot(aes(x=apImp1, y=VO2, colour=speed)) +
  geom_point() +
  facet_wrap(~ID)

EImps %>%
  ggplot(aes(x=vImp1, y=VO2, colour=speed)) +
  geom_point() +
  facet_wrap(~ID)
```
```{r}
#Full Imps
summary(lmer(VO2~apImp1 + (1 | ID), data=subset(EImps, ID!='12'), na.rm=TRUE))
summary(lmer(VO2~vImp1 + (1 | ID), data=subset(EImps, ID!='12'), na.rm=TRUE))

#Braking Imps
summary(lmer(VO2~apImp6 + (1 | ID), data=subset(EImps, ID!='12'), na.rm=TRUE))
summary(lmer(VO2~vImp6 + (1 | ID), data=subset(EImps, ID!='12'), na.rm=TRUE))

#Propulsive Imps
summary(lmer(VO2~apImp7 + (1 | ID), data=subset(EImps, ID!='12'), na.rm=TRUE))
summary(lmer(VO2~vImp7 + (1 | ID), data=subset(EImps, ID!='12'), na.rm=TRUE))
```



```{r}
EImps$acrovel2 <- (EImps$acrovel)^2

summary(lmer(VO2~acrovel + (1 | ID), data=subset(EImps, ID!='12'), na.rm=TRUE))
summary(lmer(VO2~acrovel + I(acrovel^2) + (1 | ID), data=subset(EImps, ID!='12'),
na.rm=TRUE))
```

```
summary(lmer(VO2~contact + (1 | ID), data=subset(EImps, ID!='12'), na.rm=TRUE))
summary(lmer(VO2~contact + I(contact^2) + (1 | ID), data=subset(EImps, ID!='12'),
na.rm=TRUE))

summary(lmer(VO2~contact + I(contact^2)
        + acrovel + (1 | ID), data=subset(EImps, ID!='12'), na.rm=TRUE))
summary(lmer(VO2~contact + I(contact^2)
        + acrovel + I(acrovel^2) + (1 | ID), data=subset(EImps, ID!='12'), na.rm=TRUE))

#lmer(VO2~contact + I(contact^2)
#           + acrovel + I(acrovel^2) + (1 | ID), data=EImps, na.rm=TRUE)
```

Model robusticity check:

```{r}
summary(lmer(VO2~acrovel + acrovel2 + (1 | ID), data=subset(EImps, ID!='12'),
na.rm=TRUE))
summary(glm(VO2~acrovel + acrovel2, data=subset(EImps, ID!='12')))
summary(glmer(VO2~acrovel + acrovel2 + (1 | ID), data=subset(EImps, ID!='12'),
na.rm=TRUE))

summary(lmer(VO2~acrovel + acrovel2 + (1 | ID), data=subset(EImps, ID!='12'& ID!='2'),
na.rm=TRUE))
summary(glm(VO2~acrovel + acrovel2, data=subset(EImps, ID!='12'& ID!='2')))
summary(glmer(VO2~acrovel + acrovel2 + (1 | ID), data=subset(EImps, ID!='12'& ID!='2'),
na.rm=TRUE))
```

Check with vs without E12:

```{r}
summary(lmer(VO2~contact + I(contact^2)
        + acrovel + I(acrovel^2) + (1 | ID), data=EImps, na.rm=TRUE))
summary(lmer(VO2~contact + I(contact^2)
        + acrovel + I(acrovel^2) + (1 | ID), data=subset(EImps, ID!='12'), na.rm=TRUE))

summary(lmer(VO2~contact + I(contact^2)
        + acrovel + I(acrovel^2)
        + Nmass + stRMR
        + (1 | ID), data=EImps, na.rm=TRUE))
summary(lmer(VO2~contact + I(contact^2)
        + acrovel + I(acrovel^2)
```

```
        + Nmass + stRMR
        + (1 | ID), data=subset(EImps, ID!='12'), na.rm=TRUE))
```

Exclude E12 due to sensor issues during force plate data collection. Tare values are off, lack of confidence in contact time measurement accuracy.

Assess outliers in E02, trials 26-30.

```{r}
#Without E02 Trials 26-30 removed (rows 55-58), E12 removed entirely (rows 322-351)
summary(lmer(VO2~contact + I(contact^2)
        + acrovel + I(acrovel^2)
        + Nmass + stRMR
        + (1 | ID), data=EImps[-c(322:351),], na.rm=TRUE))

#With E02 trials 26-30 removed
summary(lmer(VO2~contact + I(contact^2)
        + acrovel + I(acrovel^2)
        + Nmass + stRMR
        + (1 | ID), data=EImps[-c(55:58, 322:351),], na.rm=TRUE))
```

E02's information was reviewed. Participant had scoliosis and did not disclose this to the researchers. We must remove E02 as a participant.

```{r}
summary(lmer(VO2~acrovel + I(acrovel^2) + (1 | ID),
        data=subset(EImps, ID!='12' & ID!='2'),
        na.rm=TRUE))

summary(lmer(VO2~contact + I(contact^2)
        + (1 | ID),
        data=subset(EImps, ID!='12' & ID!='2'),
        na.rm=TRUE))

summary(lmer(VO2~contact + I(contact^2)
        + acrovel + (1 | ID),
        data=subset(EImps, ID!='12' & ID!='2'),
        na.rm=TRUE))

summary(lmer(VO2~contact + I(contact^2)
        + acrovel + I(acrovel^2) + (1 | ID),
        data=subset(EImps, ID!='12' & ID!='2'),
        na.rm=TRUE))
```

```
summary(lmer(VO2~contact + I(contact^2)
        + acrovel + I(acrovel^2)
        + Nmass + (1 | ID), data=subset(EImps, ID!='12' & ID!='2'), na.rm=TRUE))

summary(lmer(VO2~contact + I(contact^2)
        + acrovel + I(acrovel^2)
        + stRMR + (1 | ID), data=subset(EImps, ID!='12' & ID!='2'), na.rm=TRUE))

summary(lmer(VO2~contact + I(contact^2)
        + acrovel + I(acrovel^2)
        + stRMR + Nmass + (1 | ID),
        data=subset(EImps, ID!='12' & ID!='2'), na.rm=TRUE))

summary(lmer(VO2~contact + I(contact^2)
        + acrovel + I(acrovel^2)
        + apImp1 + (1 | ID), data=subset(EImps, ID!='12' & ID!='2'), na.rm=TRUE))

summary(lmer(VO2~contact + I(contact^2)
        + acrovel + I(acrovel^2)
        + vImp1 + (1 | ID), data=subset(EImps, ID!='12' & ID!='2'), na.rm=TRUE))
```

```{r}
summary(lmer(VO2~contact + I(contact^2)
        + acrovel + I(acrovel^2)
        + stRMR + Nmass + stature + (1 | ID),
        data=subset(EImps, ID!='12' & ID!='2'), na.rm=TRUE))

summary(lmer(VO2~contact + I(contact^2)
        + acrovel + I(acrovel^2)
        + stRMR + Nmass + BiTroch + (1 | ID),
        data=subset(EImps, ID!='12' & ID!='2'), na.rm=TRUE))

summary(lmer(VO2~contact + I(contact^2)
        + acrovel + I(acrovel^2)
        + stRMR + Nmass + BiASIS + (1 | ID),
        data=subset(EImps, ID!='12' & ID!='2'), na.rm=TRUE))

summary(lmer(VO2~contact + I(contact^2)
        + acrovel + I(acrovel^2)
        + stRMR + Nmass + avgleg + (1 | ID),
        data=subset(EImps, ID!='12' & ID!='2'), na.rm=TRUE))

summary(lmer(VO2~contact + I(contact^2)
        + acrovel + I(acrovel^2)
        + stRMR + Nmass + Lfoot + (1 | ID),
```

```
        data=subset(EImps, ID!='12' & ID!='2'), na.rm=TRUE))
```

```{r}
modNull <- (lmer(VO2~1
        + (1 | ID), data=subset(EImps, ID!='12' & ID!='2'), na.rm=TRUE))

modBase <- (lmer(VO2~stRMR + Nmass
        + (1 | ID), data=subset(EImps, ID!='12' & ID!='2'), na.rm=TRUE))

mod0 <- (lmer(VO2~contact + I(contact^2)
        + acrovel + I(acrovel^2)
        + stRMR + Nmass
        + (1 | ID), data=subset(EImps, ID!='12' & ID!='2'), na.rm=TRUE))

#vmod0 <- (lmer(VO2~contact + I(contact^2)
#          + acrovel + I(acrovel^2)
#          + stRMR + Nmass
#          + (1 | ID), data=subset(EImps, ID!='12' & ID!='2'), na.rm=TRUE))

apmod1 <- (lmer(VO2~contact + I(contact^2)
        + acrovel + I(acrovel^2)
        + stRMR + Nmass
        + apForce + (1 | ID), data=subset(EImps, ID!='12' & ID!='2'), na.rm=TRUE))

vmod1 <- (lmer(VO2~contact + I(contact^2)
        + acrovel + I(acrovel^2)
        + stRMR + Nmass
        + vForce + (1 | ID), data=subset(EImps, ID!='12' & ID!='2'), na.rm=TRUE))

apmod2 <- (lmer(VO2~contact + I(contact^2)
        + acrovel + I(acrovel^2)
        + stRMR + Nmass
        + apBForce + (1 | ID), data=subset(EImps, ID!='12' & ID!='2'), na.rm=TRUE))

vmod2 <- (lmer(VO2~contact + I(contact^2)
        + acrovel + I(acrovel^2)
        + stRMR + Nmass
        + vBForce + (1 | ID), data=subset(EImps, ID!='12' & ID!='2'), na.rm=TRUE))

apmod3 <- (lmer(VO2~contact + I(contact^2)
        + acrovel + I(acrovel^2)
        + stRMR + Nmass
        + apPForce + (1 | ID), data=subset(EImps, ID!='12' & ID!='2'), na.rm=TRUE))
```

```
vmod3 <- (lmer(VO2~contact + I(contact^2)
        + acrovel + I(acrovel^2)
        + stRMR + Nmass
        + vPForce + (1 | ID), data=subset(EImps, ID!='12' & ID!='2'), na.rm=TRUE))
```

```{r}
anova(modNull, modBase, mod0)
anova(modNull, modBase, mod0, apmod1, vmod1, apmod2, vmod2, apmod3, vmod3)
```
```{r}
CoTmodNull <- (lmer(calcCoT~1
        + (1 | ID), data=subset(EImps, ID!='12' & ID!='2'), na.rm=TRUE))

CoTmodBase <- (lmer(calcCoT~stRMR + Nmass
        + (1 | ID), data=subset(EImps, ID!='12' & ID!='2'), na.rm=TRUE))
```

```{r}
anova(CoTmodNull, CoTmodBase)
```
```{r}
summary(lmer(calcCoT~contact + stRMR + Nmass
        + (1 | ID), data=subset(EImps, ID!='12' & ID!='2'), na.rm=TRUE))

summary(lmer(calcCoT~contact + I(contact^2)
        + stRMR + Nmass
        + (1 | ID), data=subset(EImps, ID!='12' & ID!='2'), na.rm=TRUE))
```
```{r}
modBase.1 <- (lmer(VO2~contact + stRMR + Nmass
        + (1 | ID), data=subset(EImps, ID!='12' & ID!='2'), na.rm=TRUE))

modBase.2 <- (lmer(VO2~contact + I(contact^2)
        + stRMR + Nmass
        + (1 | ID), data=subset(EImps, ID!='12' & ID!='2'), na.rm=TRUE))

modBase.3 <- (lmer(VO2~contact + I(contact^2)
        + acrovel
        + stRMR + Nmass
        + (1 | ID), data=subset(EImps, ID!='12' & ID!='2'), na.rm=TRUE))

modBase.4 <- (lmer(VO2~contact + I(contact^2)
        + acrovel + I(acrovel^2)
        + stRMR + Nmass
        + (1 | ID), data=subset(EImps, ID!='12' & ID!='2'), na.rm=TRUE))
```

```

```{r}
summary(modBase.1)
summary(modBase.2)
summary(modBase.3)
summary(modBase.4)
```
```{r}
anova(modBase, modBase.1, modBase.2, modBase.3, modBase.4)
```
```{r}
summary(modBase.2)
confint(modBase.2)
```
```{r}
summary(lmer(calcCoT~contact + I(contact^2)
        + acrovel + I(acrovel^2) + (1 | ID),
        data=subset(EImps, ID!='12' & ID!='2'),
        na.rm=TRUE))

summary(lmer(calcCoT~contact + I(contact^2)
        + acrovel + I(acrovel^2)
        + Nmass + (1 | ID), data=subset(EImps, ID!='12' & ID!='2'), na.rm=TRUE))

summary(lmer(calcCoT~contact + I(contact^2)
        + acrovel + I(acrovel^2)
        + stRMR + (1 | ID), data=subset(EImps, ID!='12' & ID!='2'), na.rm=TRUE))

summary(lmer(calcCoT~contact + I(contact^2)
        + acrovel + I(acrovel^2)
        + stRMR + Nmass + (1 | ID), data=subset(EImps, ID!='12' & ID!='2'), na.rm=TRUE))

summary(lmer(calcCoT~contact + I(contact^2)
        + acrovel + I(acrovel^2)
        + apImp1 + (1 | ID), data=subset(EImps, ID!='12' & ID!='2'), na.rm=TRUE))

summary(lmer(calcCoT~contact + I(contact^2)
        + acrovel + I(acrovel^2)
        + vImp1 + (1 | ID), data=subset(EImps, ID!='12' & ID!='2'), na.rm=TRUE))
```
```{r}
summary(lmer(VO2~stRMR + Nmass
        + apForce + (1 | ID), data=subset(EImps, ID!='12' & ID!='2'), na.rm=TRUE))

summary(lmer(VO2~stRMR + Nmass

```
        + vForce + (1 | ID), data=subset(EImps, ID!='12' & ID!='2'), na.rm=TRUE))

###
summary(lmer(VO2~stRMR + Nmass
        + apForce + vForce + (1 | ID),
        data=subset(EImps, ID!='12' & ID!='2'), na.rm=TRUE))
###

summary(lmer(VO2~stRMR + Nmass
        + apBForce + (1 | ID), data=subset(EImps, ID!='12' & ID!='2'), na.rm=TRUE))

summary(lmer(VO2~stRMR + Nmass
        + vBForce + (1 | ID), data=subset(EImps, ID!='12' & ID!='2'), na.rm=TRUE))

summary(lmer(VO2~stRMR + Nmass
        + apPForce + (1 | ID), data=subset(EImps, ID!='12' & ID!='2'), na.rm=TRUE))

summary(lmer(VO2~stRMR + Nmass
        + vPForce + (1 | ID), data=subset(EImps, ID!='12' & ID!='2'), na.rm=TRUE))
```

```{r}
contactmod <- (lmer(VO2~stRMR + Nmass
        + contact + (1 | ID),
        data=subset(EImps, ID!='12' & ID!='2'), na.rm=TRUE))

contactmod2 <- (lmer(VO2~stRMR + Nmass
        + contact + I(contact^2) + (1 | ID),
        data=subset(EImps, ID!='12' & ID!='2'), na.rm=TRUE))
```

```{r}
summary(lmer(VO2~contact + I(contact^2)
        + acrovel + I(acrovel^2)
        + stRMR + Nmass
        + apForce + (1 | ID), data=subset(EImps, ID!='12' & ID!='2'), na.rm=TRUE))

summary(lmer(VO2~contact + I(contact^2)
        + acrovel + I(acrovel^2)
        + stRMR + Nmass
        + vForce + (1 | ID), data=subset(EImps, ID!='12' & ID!='2'), na.rm=TRUE))

summary(lmer(VO2~contact + I(contact^2)
        + acrovel + I(acrovel^2)
```

```
        + stRMR + Nmass
        + apBForce + (1 | ID), data=subset(EImps, ID!='12' & ID!='2'), na.rm=TRUE))

summary(lmer(VO2~contact + I(contact^2)
        + acrovel + I(acrovel^2)
        + stRMR + Nmass
        + vBForce + (1 | ID), data=subset(EImps, ID!='12' & ID!='2'), na.rm=TRUE))

summary(lmer(VO2~contact + I(contact^2)
        + acrovel + I(acrovel^2)
        + stRMR + Nmass
        + apPForce + (1 | ID), data=subset(EImps, ID!='12' & ID!='2'), na.rm=TRUE))

summary(lmer(VO2~contact + I(contact^2)
        + acrovel + I(acrovel^2)
        + stRMR + Nmass
        + vPForce + (1 | ID), data=subset(EImps, ID!='12' & ID!='2'), na.rm=TRUE))
```

```{r}
apmod <- (lmer(VO2~contact + I(contact^2)
        + acrovel + I(acrovel^2)
        + stRMR + Nmass
        + apForce + (1 | ID), data=subset(EImps, ID!='12' & ID!='2'), na.rm=TRUE))

vmod <- (lmer(VO2~contact + I(contact^2)
        + acrovel + I(acrovel^2)
        + stRMR + Nmass
        + vForce + (1 | ID), data=subset(EImps, ID!='12' & ID!='2'), na.rm=TRUE))

apBmod <- (lmer(VO2~contact + I(contact^2)
        + acrovel + I(acrovel^2)
        + stRMR + Nmass
        + apBForce + (1 | ID), data=subset(EImps, ID!='12' & ID!='2'), na.rm=TRUE))

vBmod <- (lmer(VO2~contact + I(contact^2)
        + acrovel + I(acrovel^2)
        + stRMR + Nmass
        + vBForce + (1 | ID), data=subset(EImps, ID!='12' & ID!='2'), na.rm=TRUE))

apPmod <- (lmer(VO2~contact + I(contact^2)
        + acrovel + I(acrovel^2)
        + stRMR + Nmass
        + apPForce + (1 | ID), data=subset(EImps, ID!='12' & ID!='2'), na.rm=TRUE))

vPmod <- (lmer(VO2~contact + I(contact^2)
```

```
        + acrovel + I(acrovel^2)
        + stRMR + Nmass
        + vPForce + (1 | ID), data=subset(EImps, ID!='12' & ID!='2'), na.rm=TRUE))

apvmod <- (lmer(VO2~contact + I(contact^2)
        + acrovel + I(acrovel^2)
        + stRMR + Nmass
        + apForce + vForce + (1 | ID),
        data=subset(EImps, ID!='12' & ID!='2'), na.rm=TRUE))
```

```{r}
summary(modNull)
confint(modNull, level=0.95)

summary(modBase)
confint(modBase)

summary(modBase.4)
confint(modBase.4)

summary(apmod)
confint(apmod)

summary(vmod)
confint(vmod)

summary(apvmod)
confint(apvmod)
```
```{r}
anova(modBase, modBase.4, apmod, vmod, apBmod, vBmod, apPmod, vPmod)
anova(modBase, modBase.4, apmod, apPmod)
anova(modNull, modBase, modBase.4, apmod)
```
```{r}
#Output EImps for PAK
write.table(EImps, "~/Documents/Paper #3/EImps_calcCoT.txt", sep="/")
```

Run each model by individual?

```{r}
summary(lm(calcCoT~contact, data=subset(EImps, ID=='1'), na.rm=TRUE))
summary(lm(calcCoT~contact + I(contact^2), data=subset(EImps, ID=='1'), na.rm=TRUE))
```

```
summary(lm(calcCoT~contact + I(contact^2)
           + acrovel,
           data=subset(EImps, ID=='1'), na.rm=TRUE))
summary(lm(calcCoT~contact + I(contact^2)
           + acrovel + I(acrovel^2),
           data=subset(EImps, ID=='1'), na.rm=TRUE))

##Can't use VO2 with velocity? calculated it from CoT*vel
#summary(lm(VO2~contact, data=subset(EImps, ID=='1'), na.rm=TRUE))
#summary(lm(VO2~contact + I(contact^2), data=subset(EImps, ID=='1'), na.rm=TRUE))

#summary(lm(VO2~contact + I(contact^2)
#           + acrovel,
#           data=subset(EImps, ID=='1'), na.rm=TRUE))
#summary(lm(VO2~contact + I(contact^2)
#           + acrovel + I(acrovel^2),
#           data=subset(EImps, ID=='1'), na.rm=TRUE))
```

Check each participant for outliers etc.

```{r}
EImps %>%
   group_by(ID, speed) %>%
   summarise(mean = mean(acrovel), stdev = sd(acrovel), n = n())

EImps %>%
   group_by(ID, speed) %>%
   summarise(mean = mean(calcCoT), stdev = sd(calcCoT))

#need to examine E12 and E2 further
EImps %>%
  filter(ID=='12') %>%
  group_by(Trial) %>%
  summarise(meanCoT=mean(calcCoT), meanVel=mean(acrovel),
          Bo=mean(Bo), B1=mean(B1), B2=mean(B2))
E345 %>%
  filter(id=='12') %>%
  group_by(speedcat) %>%
  summarise(meanVO2=mean(avgVO2), stdevV02=sd(avgVO2),
          meanVel=mean(velocity),
          meanCoT=mean(avgCoT))
```

```{r}
library(patchwork)
```

```{r}
plot1 <- ggplot(aes(x=acrovel, y=calcCoT, colour=ID), data=EImps) +
  geom_point() +
  labs(x="acrovel", y="calcCoT")
plot2 <- ggplot(aes(x=velocity, y=avgCoT, colour=id), data=E345) +
  geom_point() +
  labs(x="velocity", y="real CoT")
plot1 + plot2 + plot_layout()

ggplot(aes(x=acrovel, y=calcCoT, colour=ID), data=EImps) +
  geom_point() +
  labs(x="acrovel", y="calcCoT") +
  ggplot(aes(x=velocity, y=avgCoT, colour=id), data=E345) +
  geom_point() +
  labs(x="velocity", y="real CoT") +
  plot_layout()

ggplot(aes(x=acrovel, y=calcCoT, colour=speed), data=subset(EImps, ID!='12')) +
  geom_point() +
  labs(x="acrovel", y="calcCoT", title="All Participants") +
  lims(y=c(0,25), x=c(0,2.3)) +
  ggplot(aes(x=velocity, y=avgCoT, colour=id), data=subset(E345, id!='12')) +
  geom_point() +
  labs(x="velocity", y="real CoT") +
  lims(y=c(0,25), x=c(0,2.3)) +
  plot_layout()

ggplot(aes(x=acrovel, y=calcCoT, colour=speed), data=subset(EImps, ID=='1')) +
  geom_point() +
  labs(x="acrovel", y="calcCoT", title="E01") +
  lims(y=c(0,25), x=c(0,2.3)) +
  ggplot(aes(x=velocity, y=avgCoT, colour=speedcat), data=subset(E345, id=='1')) +
  geom_point() +
  labs(x="velocity", y="real CoT") +
  lims(y=c(0,25), x=c(0,2.3)) +
  plot_layout()
```
```{r}
ggplot(aes(x=acrovel, y=calcCoT, colour=speed), data=subset(EImps, ID=='2')) +
  geom_point() +
  labs(x="acrovel", y="calcCoT", title="E02") +
  lims(y=c(0,25), x=c(0,2.3)) +
  ggplot(aes(x=velocity, y=avgCoT, colour=speedcat), data=subset(E345, id=='2')) +
  geom_point() +
  labs(x="velocity", y="real CoT") +
```

```
  lims(y=c(0,25), x=c(0,2.3)) +
  plot_layout()

ggplot(aes(x=acrovel, y=calcCoT, colour=speed), data=subset(EImps, ID=='3')) +
  geom_point() +
  labs(x="acrovel", y="calcCoT", title="E03") +
  lims(y=c(0,25), x=c(0,2.3)) +
  ggplot(aes(x=velocity, y=avgCoT, colour=speedcat), data=subset(E345, id=='3')) +
  geom_point() +
  labs(x="velocity", y="real CoT") +
  lims(y=c(0,25), x=c(0,2.3)) +
  plot_layout()

ggplot(aes(x=acrovel, y=calcCoT, colour=speed), data=subset(EImps, ID=='4')) +
  geom_point() +
  labs(x="acrovel", y="calcCoT", title="E04") +
  lims(y=c(0,25), x=c(0,2.3)) +
  ggplot(aes(x=velocity, y=avgCoT, colour=speedcat), data=subset(E345, id=='4')) +
  geom_point() +
  labs(x="velocity", y="real CoT") +
  lims(y=c(0,25), x=c(0,2.3)) +
  plot_layout()

ggplot(aes(x=acrovel, y=calcCoT, colour=speed), data=subset(EImps, ID=='5')) +
  geom_point() +
  labs(x="acrovel", y="calcCoT", title="E05") +
  lims(y=c(0,25), x=c(0,2.3)) +
  ggplot(aes(x=velocity, y=avgCoT, colour=speedcat), data=subset(E345, id=='5')) +
  geom_point() +
  labs(x="velocity", y="real CoT") +
  lims(y=c(0,25), x=c(0,2.3)) +
  plot_layout()

ggplot(aes(x=acrovel, y=calcCoT, colour=speed), data=subset(EImps, ID=='6')) +
  geom_point() +
  labs(x="acrovel", y="calcCoT", title="E06") +
  lims(y=c(0,25), x=c(0,2.3)) +
  ggplot(aes(x=velocity, y=avgCoT, colour=speedcat), data=subset(E345, id=='6')) +
  geom_point() +
  labs(x="velocity", y="real CoT") +
  lims(y=c(0,25), x=c(0,2.3)) +
  plot_layout()

ggplot(aes(x=acrovel, y=calcCoT, colour=speed), data=subset(EImps, ID=='7')) +
  geom_point() +
  labs(x="acrovel", y="calcCoT", title="E07") +
```

```
  lims(y=c(0,25), x=c(0,2.3)) +
  ggplot(aes(x=velocity, y=avgCoT, colour=speedcat), data=subset(E345, id=='7')) +
  geom_point() +
  labs(x="velocity", y="real CoT") +
  lims(y=c(0,25), x=c(0,2.3)) +
  plot_layout()

ggplot(aes(x=acrovel, y=calcCoT, colour=speed), data=subset(EImps, ID=='8')) +
  geom_point() +
  labs(x="acrovel", y="calcCoT", title="E08") +
  lims(y=c(0,25), x=c(0,2.3)) +
  ggplot(aes(x=velocity, y=avgCoT, colour=speedcat), data=subset(E345, id=='8')) +
  geom_point() +
  labs(x="velocity", y="real CoT") +
  lims(y=c(0,25), x=c(0,2.3)) +
  plot_layout()

ggplot(aes(x=acrovel, y=calcCoT, colour=speed), data=subset(EImps, ID=='9')) +
  geom_point() +
  labs(x="acrovel", y="calcCoT", title="E09") +
  lims(y=c(0,25), x=c(0,2.3)) +
  ggplot(aes(x=velocity, y=avgCoT, colour=speedcat), data=subset(E345, id=='9')) +
  geom_point() +
  labs(x="velocity", y="real CoT") +
  lims(y=c(0,25), x=c(0,2.3)) +
  plot_layout()

ggplot(aes(x=acrovel, y=calcCoT, colour=speed), data=subset(EImps, ID=='10')) +
  geom_point() +
  labs(x="acrovel", y="calcCoT", title="E10") +
  lims(y=c(0,25), x=c(0,2.3)) +
  ggplot(aes(x=velocity, y=avgCoT, colour=speedcat), data=subset(E345, id=='10')) +
  geom_point() +
  labs(x="velocity", y="real CoT") +
  lims(y=c(0,25), x=c(0,2.3)) +
  plot_layout()

ggplot(aes(x=acrovel, y=calcCoT, colour=speed), data=subset(EImps, ID=='11')) +
  geom_point() +
  labs(x="acrovel", y="calcCoT", title="E11") +
  lims(y=c(0,25), x=c(0,2.3)) +
  ggplot(aes(x=velocity, y=avgCoT, colour=speedcat), data=subset(E345, id=='11')) +
  geom_point() +
  labs(x="velocity", y="real CoT") +
  lims(y=c(0,25), x=c(0,2.3)) +
  plot_layout()
```

```
ggplot(aes(x=acrovel, y=calcCoT, colour=speed), data=subset(EImps, ID=='12')) +
  geom_point() +
  labs(x="acrovel", y="calcCoT", title="E12") +
  lims(y=c(0,25), x=c(0,2.3)) +
  ggplot(aes(x=velocity, y=avgCoT, colour=speedcat), data=subset(E345, id=='12')) +
  geom_point() +
  labs(x="velocity", y="real CoT") +
  lims(y=c(0,25), x=c(0,2.3)) +
  plot_layout()

ggplot(aes(x=acrovel, y=calcCoT, colour=speed), data=subset(EImps, ID=='13')) +
  geom_point() +
  labs(x="acrovel", y="calcCoT", title="E13") +
  lims(y=c(0,25), x=c(0,2.3)) +
  ggplot(aes(x=velocity, y=avgCoT, colour=speedcat), data=subset(E345, id=='13')) +
  geom_point() +
  labs(x="velocity", y="real CoT") +
  lims(y=c(0,25), x=c(0,2.3)) +
  plot_layout()

ggplot(aes(x=acrovel, y=calcCoT, colour=speed), data=subset(EImps, ID=='14')) +
  geom_point() +
  labs(x="acrovel", y="calcCoT", title="E14") +
  lims(y=c(0,25), x=c(0,2.3)) +
  ggplot(aes(x=velocity, y=avgCoT, colour=speedcat), data=subset(E345, id=='14')) +
  geom_point() +
  labs(x="velocity", y="real CoT") +
  lims(y=c(0,25), x=c(0,2.3)) +
  plot_layout()


ggplot(aes(x=acrovel, y=calcCoT, colour=speed), data=subset(EImps, ID=='15')) +
  geom_point() +
  labs(x="acrovel", y="calcCoT", title="E15") +
  lims(y=c(0,25), x=c(0,2.3)) +
  ggplot(aes(x=velocity, y=avgCoT, colour=speedcat), data=subset(E345, id=='15')) +
  geom_point() +
  labs(x="velocity", y="real CoT") +
  lims(y=c(0,25), x=c(0,2.3)) +
  plot_layout()

ggplot(aes(x=acrovel, y=calcCoT, colour=speed), data=subset(EImps, ID=='16')) +
  geom_point() +
  labs(x="acrovel", y="calcCoT", title="E16") +
  lims(y=c(0,25), x=c(0,2.3)) +
```

```
  ggplot(aes(x=velocity, y=avgCoT, colour=speedcat), data=subset(E345, id=='16')) +
  geom_point() +
  labs(x="velocity", y="real CoT") +
  lims(y=c(0,25), x=c(0,2.3)) +
  plot_layout()

```
```{r}
ggplot(aes(x=acrovel, y=VO2, colour=speed), data=subset(EImps, ID=='1')) +
  geom_point() +
  labs(x="acrovel", y="calcVO2", title="E01") +
  lims(y=c(0,25), x=c(0,2.3)) +
  ggplot(aes(x=velocity, y=avgVO2, colour=speedcat), data=subset(E345, id=='1')) +
  geom_point() +
  labs(x="velocity", y="real VO2") +
  lims(y=c(0,25), x=c(0,2.3)) +
  plot_layout()

ggplot(aes(x=acrovel, y=VO2, colour=speed), data=subset(EImps, ID=='2')) +
  geom_point() +
  labs(x="acrovel", y="calcVO2", title="E02") +
  lims(y=c(0,25), x=c(0,2.3)) +
  ggplot(aes(x=velocity, y=avgVO2, colour=speedcat), data=subset(E345, id=='2')) +
  geom_point() +
  labs(x="velocity", y="real VO2") +
  lims(y=c(0,25), x=c(0,2.3)) +
  plot_layout()

ggplot(aes(x=acrovel, y=VO2, colour=speed), data=subset(EImps, ID=='3')) +
  geom_point() +
  labs(x="acrovel", y="calcVO2", title="E03") +
  lims(y=c(0,25), x=c(0,2.3)) +
  ggplot(aes(x=velocity, y=avgVO2, colour=speedcat), data=subset(E345, id=='3')) +
  geom_point() +
  labs(x="velocity", y="real VO2") +
  lims(y=c(0,25), x=c(0,2.3)) +
  plot_layout()

ggplot(aes(x=acrovel, y=VO2, colour=speed), data=subset(EImps, ID=='4')) +
  geom_point() +
  labs(x="acrovel", y="calc VO2", title="E04") +
  lims(y=c(0,25), x=c(0,2.3)) +
  ggplot(aes(x=velocity, y=avgVO2, colour=speedcat), data=subset(E345, id=='4')) +
  geom_point() +
  labs(x="velocity", y="real VO2") +
  lims(y=c(0,25), x=c(0,2.3)) +
```

```
  plot_layout()

ggplot(aes(x=acrovel, y=VO2, colour=speed), data=subset(EImps, ID=='5')) +
  geom_point() +
  labs(x="acrovel", y="calc VO2", title="E05") +
  lims(y=c(0,25), x=c(0,2.3)) +
  ggplot(aes(x=velocity, y=avgVO2, colour=speedcat), data=subset(E345, id=='5')) +
  geom_point() +
  labs(x="velocity", y="real VO2") +
  lims(y=c(0,25), x=c(0,2.3)) +
  plot_layout()

ggplot(aes(x=acrovel, y=VO2, colour=speed), data=subset(EImps, ID=='6')) +
  geom_point() +
  labs(x="acrovel", y="calc VO2", title="E06") +
  lims(y=c(0,25), x=c(0,2.3)) +
  ggplot(aes(x=velocity, y=avgVO2, colour=speedcat), data=subset(E345, id=='6')) +
  geom_point() +
  labs(x="velocity", y="real VO2") +
  lims(y=c(0,25), x=c(0,2.3)) +
  plot_layout()

ggplot(aes(x=acrovel, y=VO2, colour=speed), data=subset(EImps, ID=='7')) +
  geom_point() +
  labs(x="acrovel", y="calc VO2", title="E07") +
  lims(y=c(0,25), x=c(0,2.3)) +
  ggplot(aes(x=velocity, y=avgVO2, colour=speedcat), data=subset(E345, id=='7')) +
  geom_point() +
  labs(x="velocity", y="real VO2") +
  lims(y=c(0,25), x=c(0,2.3)) +
  plot_layout()

ggplot(aes(x=acrovel, y=VO2, colour=speed), data=subset(EImps, ID=='8')) +
  geom_point() +
  labs(x="acrovel", y="calc VO2", title="E08") +
  lims(y=c(0,25), x=c(0,2.3)) +
  ggplot(aes(x=velocity, y=avgVO2, colour=speedcat), data=subset(E345, id=='8')) +
  geom_point() +
  labs(x="velocity", y="real VO2") +
  lims(y=c(0,25), x=c(0,2.3)) +
  plot_layout()

ggplot(aes(x=acrovel, y=VO2, colour=speed), data=subset(EImps, ID=='9')) +
  geom_point() +
  labs(x="acrovel", y="calc VO2", title="E09") +
  lims(y=c(0,25), x=c(0,2.3)) +
```

```
  ggplot(aes(x=velocity, y=avgVO2, colour=speedcat), data=subset(E345, id=='9')) +
  geom_point() +
  labs(x="velocity", y="real VO2") +
  lims(y=c(0,25), x=c(0,2.3)) +
  plot_layout()

ggplot(aes(x=acrovel, y=VO2, colour=speed), data=subset(EImps, ID=='10')) +
  geom_point() +
  labs(x="acrovel", y="calcVO2", title="E10") +
  lims(y=c(0,25), x=c(0,2.3)) +
  ggplot(aes(x=velocity, y=avgVO2, colour=speedcat), data=subset(E345, id=='10')) +
  geom_point() +
  labs(x="velocity", y="real VO2") +
  lims(y=c(0,25), x=c(0,2.3)) +
  plot_layout()

ggplot(aes(x=acrovel, y=VO2, colour=speed), data=subset(EImps, ID=='11')) +
  geom_point() +
  labs(x="acrovel", y="calc VO2", title="E11") +
  lims(y=c(0,25), x=c(0,2.3)) +
  ggplot(aes(x=velocity, y=avgVO2, colour=speedcat), data=subset(E345, id=='11')) +
  geom_point() +
  labs(x="velocity", y="real VO2") +
  lims(y=c(0,25), x=c(0,2.3)) +
  plot_layout()

ggplot(aes(x=acrovel, y=VO2, colour=speed), data=subset(EImps, ID=='12')) +
  geom_point() +
  labs(x="acrovel", y="calc VO2", title="E12") +
  lims(y=c(0,25), x=c(0,2.3)) +
  ggplot(aes(x=velocity, y=avgVO2, colour=speedcat), data=subset(E345, id=='12')) +
  geom_point() +
  labs(x="velocity", y="real VO2") +
  lims(y=c(0,25), x=c(0,2.3)) +
  plot_layout()

ggplot(aes(x=acrovel, y=VO2, colour=speed), data=subset(EImps, ID=='13')) +
  geom_point() +
  labs(x="acrovel", y="calc VO2", title="E13") +
  lims(y=c(0,25), x=c(0,2.3)) +
  ggplot(aes(x=velocity, y=avgVO2, colour=speedcat), data=subset(E345, id=='13')) +
  geom_point() +
  labs(x="velocity", y="real VO2") +
  lims(y=c(0,25), x=c(0,2.3)) +
  plot_layout()
```

```
ggplot(aes(x=acrovel, y=VO2, colour=speed), data=subset(EImps, ID=='14')) +
  geom_point() +
  labs(x="acrovel", y="calc VO2", title="E14") +
  lims(y=c(0,25), x=c(0,2.3)) +
  ggplot(aes(x=velocity, y=avgVO2, colour=speedcat), data=subset(E345, id=='14')) +
  geom_point() +
  labs(x="velocity", y="real VO2") +
  lims(y=c(0,25), x=c(0,2.3)) +
  plot_layout()


ggplot(aes(x=acrovel, y=VO2, colour=speed), data=subset(EImps, ID=='15')) +
  geom_point() +
  labs(x="acrovel", y="calc VO2", title="E15") +
  lims(y=c(0,25), x=c(0,2.3)) +
  ggplot(aes(x=velocity, y=avgVO2, colour=speedcat), data=subset(E345, id=='15')) +
  geom_point() +
  labs(x="velocity", y="real VO2") +
  lims(y=c(0,25), x=c(0,2.3)) +
  plot_layout()

ggplot(aes(x=acrovel, y=VO2, colour=speed), data=subset(EImps, ID=='16')) +
  geom_point() +
  labs(x="acrovel", y="calc VO2", title="E16") +
  lims(y=c(0,25), x=c(0,2.3)) +
  ggplot(aes(x=velocity, y=avgVO2, colour=speedcat), data=subset(E345, id=='16')) +
  geom_point() +
  labs(x="velocity", y="real VO2") +
  lims(y=c(0,25), x=c(0,2.3)) +
  plot_layout()

```
```{r}
ggplot(aes(x=acrovel, y=contact, colour=speed), data=subset(EImps, ID=='1')) +
  geom_point() +
  labs(x="acrovel", y="contact", title="E01") +
  #lims(y=c(0,25), x=c(0,2.3)) +
  ggplot(aes(x=velocity, y=avgVO2, colour=speedcat), data=subset(E345, id=='1')) +
  geom_point() +
  labs(x="velocity", y="real VO2") +
  lims(y=c(0,25), x=c(0,2.3)) +
  plot_layout()

ggplot(aes(x=acrovel, y=contact, colour=speed), data=subset(EImps, ID=='2')) +
  geom_point() +
  labs(x="acrovel", y="contact", title="E02") +
```

```
  #lims(y=c(0,25), x=c(0,2.3)) +
  ggplot(aes(x=velocity, y=avgVO2, colour=speedcat), data=subset(E345, id=='2')) +
  geom_point() +
  labs(x="velocity", y="real VO2") +
  lims(y=c(0,25), x=c(0,2.3)) +
  plot_layout()

ggplot(aes(x=acrovel, y=contact, colour=speed), data=subset(EImps, ID=='3')) +
  geom_point() +
  labs(x="acrovel", y="contact", title="E03") +
  #lims(y=c(0,25), x=c(0,2.3)) +
  ggplot(aes(x=velocity, y=avgVO2, colour=speedcat), data=subset(E345, id=='3')) +
  geom_point() +
  labs(x="velocity", y="real VO2") +
  lims(y=c(0,25), x=c(0,2.3)) +
  plot_layout()

ggplot(aes(x=acrovel, y=contact, colour=speed), data=subset(EImps, ID=='4')) +
  geom_point() +
  labs(x="acrovel", y="contact", title="E04") +
  #lims(y=c(0,25), x=c(0,2.3)) +
  ggplot(aes(x=velocity, y=avgVO2, colour=speedcat), data=subset(E345, id=='4')) +
  geom_point() +
  labs(x="velocity", y="real VO2") +
  lims(y=c(0,25), x=c(0,2.3)) +
  plot_layout()

ggplot(aes(x=acrovel, y=contact, colour=speed), data=subset(EImps, ID=='5')) +
  geom_point() +
  labs(x="acrovel", y="contact", title="E05") +
  #lims(y=c(0,25), x=c(0,2.3)) +
  ggplot(aes(x=velocity, y=avgVO2, colour=speedcat), data=subset(E345, id=='5')) +
  geom_point() +
  labs(x="velocity", y="real VO2") +
  lims(y=c(0,25), x=c(0,2.3)) +
  plot_layout()

ggplot(aes(x=acrovel, y=contact, colour=speed), data=subset(EImps, ID=='6')) +
  geom_point() +
  labs(x="acrovel", y="contact", title="E06") +
  #lims(y=c(0,25), x=c(0,2.3)) +
  ggplot(aes(x=velocity, y=avgVO2, colour=speedcat), data=subset(E345, id=='6')) +
  geom_point() +
  labs(x="velocity", y="real VO2") +
  lims(y=c(0,25), x=c(0,2.3)) +
  plot_layout()
```

```
ggplot(aes(x=acrovel, y=contact, colour=speed), data=subset(EImps, ID=='7')) +
  geom_point() +
  labs(x="acrovel", y="contact", title="E07") +
  #lims(y=c(0,25), x=c(0,2.3)) +
  ggplot(aes(x=velocity, y=avgVO2, colour=speedcat), data=subset(E345, id=='7')) +
  geom_point() +
  labs(x="velocity", y="real VO2") +
  lims(y=c(0,25), x=c(0,2.3)) +
  plot_layout()

ggplot(aes(x=acrovel, y=contact, colour=speed), data=subset(EImps, ID=='8')) +
  geom_point() +
  labs(x="acrovel", y="contact", title="E08") +
  #lims(y=c(0,25), x=c(0,2.3)) +
  ggplot(aes(x=velocity, y=avgVO2, colour=speedcat), data=subset(E345, id=='8')) +
  geom_point() +
  labs(x="velocity", y="real VO2") +
  lims(y=c(0,25), x=c(0,2.3)) +
  plot_layout()

ggplot(aes(x=acrovel, y=contact, colour=speed), data=subset(EImps, ID=='9')) +
  geom_point() +
  labs(x="acrovel", y="contact", title="E09") +
  #lims(y=c(0,25), x=c(0,2.3)) +
  ggplot(aes(x=velocity, y=avgVO2, colour=speedcat), data=subset(E345, id=='9')) +
  geom_point() +
  labs(x="velocity", y="real VO2") +
  lims(y=c(0,25), x=c(0,2.3)) +
  plot_layout()

ggplot(aes(x=acrovel, y=contact, colour=speed), data=subset(EImps, ID=='10')) +
  geom_point() +
  labs(x="acrovel", y="contact", title="E10") +
  #lims(y=c(0,25), x=c(0,2.3)) +
  ggplot(aes(x=velocity, y=avgVO2, colour=speedcat), data=subset(E345, id=='10')) +
  geom_point() +
  labs(x="velocity", y="real VO2") +
  lims(y=c(0,25), x=c(0,2.3)) +
  plot_layout()

ggplot(aes(x=acrovel, y=contact, colour=speed), data=subset(EImps, ID=='11')) +
  geom_point() +
  labs(x="acrovel", y="contact", title="E11") +
  #lims(y=c(0,25), x=c(0,2.3)) +
  ggplot(aes(x=velocity, y=avgVO2, colour=speedcat), data=subset(E345, id=='11')) +
```

```
  geom_point() +
  labs(x="velocity", y="real VO2") +
  lims(y=c(0,25), x=c(0,2.3)) +
  plot_layout()

ggplot(aes(x=acrovel, y=contact, colour=speed), data=subset(EImps, ID=='12')) +
  geom_point() +
  labs(x="acrovel", y="contact", title="E12") +
  #lims(y=c(0,25), x=c(0,2.3)) +
  ggplot(aes(x=velocity, y=avgVO2, colour=speedcat), data=subset(E345, id=='12')) +
  geom_point() +
  labs(x="velocity", y="real VO2") +
  lims(y=c(0,25), x=c(0,2.3)) +
  plot_layout()

ggplot(aes(x=acrovel, y=contact, colour=speed), data=subset(EImps, ID=='13')) +
  geom_point() +
  labs(x="acrovel", y="contact", title="E13") +
  #lims(y=c(0,25), x=c(0,2.3)) +
  ggplot(aes(x=velocity, y=avgVO2, colour=speedcat), data=subset(E345, id=='13')) +
  geom_point() +
  labs(x="velocity", y="real VO2") +
  lims(y=c(0,25), x=c(0,2.3)) +
  plot_layout()

ggplot(aes(x=acrovel, y=contact, colour=speed), data=subset(EImps, ID=='14')) +
  geom_point() +
  labs(x="acrovel", y="contact", title="E14") +
  #lims(y=c(0,25), x=c(0,2.3)) +
  ggplot(aes(x=velocity, y=avgVO2, colour=speedcat), data=subset(E345, id=='14')) +
  geom_point() +
  labs(x="velocity", y="real VO2") +
  lims(y=c(0,25), x=c(0,2.3)) +
  plot_layout()


ggplot(aes(x=acrovel, y=contact, colour=speed), data=subset(EImps, ID=='15')) +
  geom_point() +
  labs(x="acrovel", y="contact", title="E15") +
  #lims(y=c(0,25), x=c(0,2.3)) +
  ggplot(aes(x=velocity, y=avgVO2, colour=speedcat), data=subset(E345, id=='15')) +
  geom_point() +
  labs(x="velocity", y="real VO2") +
  lims(y=c(0,25), x=c(0,2.3)) +
  plot_layout()
```

```
ggplot(aes(x=acrovel, y=contact, colour=speed), data=subset(EImps, ID=='16')) +
  geom_point() +
  labs(x="acrovel", y="contact", title="E16") +
  #lims(y=c(0,25), x=c(0,2.3)) +
  ggplot(aes(x=velocity, y=avgVO2, colour=speedcat), data=subset(E345, id=='16')) +
  geom_point() +
  labs(x="velocity", y="real VO2") +
  lims(y=c(0,25), x=c(0,2.3)) +
  plot_layout()
```

```{r}
ggplot(aes(x=acrovel, y=contact, colour=speed), data=subset(EImps, ID=='14')) +
  geom_point() +
  labs(x="velocity", y="contact time", title="E14") +
  #lims(y=c(0,25), x=c(0,2.3)) +
  xlab("Velocity (m/s)") +
  ylab("Contact Time (s)") +
  labs(color = "Speed") +
  geom_point(alpha=1, size=4)
  ggplot(aes(x=acrovel, y=VO2, colour=speed), data=subset(EImps, ID=='14')) +
  geom_point(alpha=1, size=4) +
  xlab("Velocity (m/s)") +
  ylab("VO2 (mL/s)") +
  labs(color = "Speed") +
  #lims(y=c(0,25), x=c(0,2.3)) +
  plot_layout()

ggplot(aes(x=acrovel, y=contact, colour=speed), data=subset(EImps, !ID=='12')) +
  labs(x="velocity", y="contact time") +
  #lims(y=c(0,25), x=c(0,2.3)) +
  xlab("Velocity (m/s)") +
  ylab("Contact Time (s)") +
  labs(color = "Speed") +
  geom_point(alpha=0.5, size=2) +
  ggplot(aes(x=acrovel, y=VO2, colour=speed), data=subset(EImps, !ID=='12')) +
  geom_point(alpha=0.5, size=2) +
  xlab("Velocity (m/s)") +
  ylab("VO2 (mL/s)") +
  labs(color = "Speed") +
  #lims(y=c(0,25), x=c(0,2.3)) +
  plot_layout()

ggplot(aes(x=acrovel, y=apForce, colour=speed), data=subset(EImps, !ID=='12')) +
  #labs(x="velocity", y="contact time") +
  #lims(y=c(0,25), x=c(0,2.3)) +
  xlab("Velocity (m/s)") +
```

```
  ylab("apGRF (N)") +
  labs(color = "Speed") +
  geom_point(alpha=0.5, size=2) +
  ggplot(aes(x=acrovel, y=VO2, colour=speed), data=subset(EImps, !ID=='12')) +
  geom_point(alpha=0.5, size=2) +
  xlab("Velocity (m/s)") +
  ylab("VO2 (mL/s)") +
  labs(color = "Speed") +
  #lims(y=c(0,25), x=c(0,2.3)) +
  plot_layout()

ggplot(aes(x=acrovel, y=vForce, colour=speed), data=subset(EImps, !ID=='12')) +
  #labs(x="velocity", y="contact time") +
  #lims(y=c(0,25), x=c(0,2.3)) +
  xlab("Velocity (m/s)") +
  ylab("vGRF (N)") +
  labs(color = "Speed") +
  geom_point(alpha=0.5, size=2)

ggplot(aes(x=acrovel, y=contact, colour=speed), data=subset(EImps, ID=='14')) +
  geom_point(alpha=1, size=4) +
  labs(x="velocity", y="contact time", title="E14")

ggplot(aes(x=acrovel, y=VO2, colour=speed), data=subset(EImps, ID=='14')) +
  geom_point(alpha=1, size=4) +
  labs(x="velocity", y="Predicted VO2")

ggplot(aes(x=acrovel, y=calcCoT, colour=speed), data=subset(EImps, ID=='14')) +
  geom_point(alpha=1, size=4) +
  labs(x="velocity", y="Predicted CoT")

ggplot(aes(x=velocity, y=avgVO2, colour=speedcat), data=subset(E345, id=='14')) +
  geom_point(alpha=1, size=4) +
  labs(x="velocity", y="Real VO2")

ggplot(aes(x=velocity, y=avgCoT, colour=speedcat), data=subset(E345, id=='14')) +
  geom_point(alpha=1, size=4) +
  labs(x="velocity", y="Real CoT")
```

```{r}
ggplot(aes(x=apForce, y=VO2, colour=speed), data=subset(EImps, !ID=='12')) +
  #labs(x="velocity", y="contact time") +
  #lims(y=c(0,25), x=c(0,2.3)) +
  xlab("apGRF (N)") +
  ylab("VO2 (mL/s)") +
  labs(color = "Speed") +
```

```
  geom_point(alpha=0.5, size=3)

ggplot(aes(x=vForce, y=VO2, colour=speed), data=subset(EImps, !ID=='12')) +
  #labs(x="velocity", y="contact time") +
  #lims(y=c(0,25), x=c(0,2.3)) +
  xlab("vGRF (N)") +
  ylab("VO2 (mL/s)") +
  labs(color = "Speed") +
  geom_point(alpha=0.5, size=3)

ggplot(aes(x=contact, y=VO2, colour=speed), data=subset(EImps, !ID=='12')) +
  #labs(x="velocity", y="contact time") +
  #lims(y=c(0,25), x=c(0,2.3)) +
  xlab("Contact Time (s)") +
  ylab("VO2 (mL/s)") +
  labs(color = "Speed") +
  geom_point(alpha=0.5, size=3)

ggplot(aes(x=contact, y=apForce, colour=speed), data=subset(EImps, !ID=='12')) +
  #labs(x="velocity", y="contact time") +
  #lims(y=c(0,25), x=c(0,2.3)) +
  xlab("Contact Time (s)") +
  ylab("apGRF (N)") +
  labs(color = "Speed") +
  geom_point(alpha=0.5, size=3)

ggplot(aes(x=contact, y=VO2, colour=speed), data=subset(EImps, !ID=='12')) +
  #labs(x="velocity", y="contact time") +
  #lims(y=c(0,25), x=c(0,2.3)) +
  xlab("Contact Time (s)") +
  ylab("VO2 (mL/s)") +
  labs(color = "Speed") +
  geom_point(alpha=0.5, size=2) +
  ggplot(aes(x=apForce, y=VO2, colour=speed), data=subset(EImps, !ID=='12')) +
  #labs(x="velocity", y="contact time") +
  #lims(y=c(0,25), x=c(0,2.3)) +
  xlab("apGRF (N)") +
  ylab("VO2 (mL/s)") +
  labs(color = "Speed") +
  geom_point(alpha=0.5, size=2)
```
```{r}
ggplot(aes(x=acrovel, y=contact, colour=speed), data=subset(EImps, ID=='14')) +
  geom_point() +
  labs(x="Velocity", y="Contact Time", title="Subject E14")
```

```
ggplot(aes(x=apForce, y=VO2, colour=acrovel), data=subset(EImps, ID=='14')) +
  geom_point() +
  labs(x="apForce", y="VO2", title="Subject E14") +
  labs(color="Velocity") +
  #lims(y=c(0,25), x=c(0,2.3)) +
  ggplot(aes(x=vForce, y=VO2, colour=acrovel), data=subset(EImps, ID=='14')) +
  geom_point() +
  labs(x="vForce", y="VO2") +
  #lims(y=c(0,25), x=c(0,2.3)) +
  labs(color="Velocity") +
  plot_layout()

ggplot(aes(x=acrovel, y=contact, colour=speed), data=subset(EImps, ID=='14')) +
  geom_point() +
  labs(x="acrovel", y="contact", title="E14") +
  #lims(y=c(0,25), x=c(0,2.3)) +
  ggplot(aes(x=velocity, y=avgVO2, colour=speedcat), data=subset(E345, id=='14')) +
  geom_point() +
  labs(x="velocity", y="real VO2") +
  lims(y=c(0,25), x=c(0,2.3)) +
  plot_layout()
```

```{r}
EImps %>%
  group_by(ID, speed) %>%
  summarise(vel=mean(acrovel))

Eall %>%
  group_by(Subject, speedcat) %>%
  summarise(vel=mean(velocity))

EImps %>%
  group_by(ID) %>%
  summarise(stRMR=mean(stRMR))
```

VITA

Alexandra G. Hammerberg holds a Bachelor of Science in Materials Science & Engineering and a minor in Architecture from Columbia University in the City of New York. She then worked as an engineer for several years prior to joining Dr. Patricia Ann Kramer's Primate Evolutionary Biomechanics Laboratory at the University of Washington to pursue her doctorate.